
Decoherence as a Resource for Quantum Information

Dissertation
zur Erlangung des Grades
des Doktors der Naturwissenschaften
der Naturwissenschaftlich - Technischen Fakultät
der Universität des Saarlandes

von

Peter Ken Schuhmacher

Saarbrücken

2021

Tag des Kolloquiums: 11. August 2021

Dekan: Prof. Dr. Jörn Erik Walter

Berichterstatter: Prof. Dr. Frank K. Wilhelm-Mauch
Prof. Dr. Sergej Rjasanow

Vorsitz: Prof. Dr. Christoph Becher

Akad. Mitglied: Dr. Stephan Kucera

“Wisdom comes from experience. Experience is often a result of lack of wisdom.”

Terry Pratchett

Abstract

The field of quantum information develops rapidly as it promises to solve various computational problems that are intractable for classical computers. However, building a functional quantum computer turns out to be a challenging task as its performance suffers from unavoidable decoherence. Decoherence removes the quantum nature of matter and hence the source of the quantum advantage over classical computing. However, for specific applications, some carefully engineered decoherence assisting the unitary quantum evolution can be beneficial. In this thesis, I discuss two such examples: Quantum stochastic walks (QSWs) and hybrid quantum-classical annealing (HQCA). QSWs generalize the concept of unitary quantum walks to additional non-unitary evolution. This gives rise to directed walks. QSWs can either be continuous-time or discrete-time. In the first part of this work, I present two algorithms to simulate specific QSWs on a coherent quantum computer. The first one applies to continuous-time QSWs and the second one applies to discrete-time QSWs. In the second part of this work, I present a method called hybrid quantum-classical annealing to improve the performance of adiabatic quantum computing (AQC), which is supposed to find the ground state of some target Hamiltonian. HQCA is supposed to increase the final ground state probability by coupling the qubit system to an engineered heat bath. The performance of HQCA is numerically tested for a single qubit and for two qubits.

Kurzzusammenfassung

Die Quanteninformationstheorie entwickelt sich rapide, da sie verspricht verschiedene Rechenaufgaben zu lösen, die für klassische Rechner nicht handhabbar sind. Doch ist es eine Herausforderung einen Quantenrechner zu bauen, weil dessen Performanz von unvermeidbarer Dekohärenz eingeschränkt wird. Durch diese verliert Materie ihre quantenmechanischen Eigenschaften und damit die Quelle der Vorteile eines Quantenrechners. Für bestimmte Anwendungen kann gesteuerte, die unitären Zeitentwicklung begleitende Dekohärenz allerdings von Vorteil sein. In dieser Arbeit diskutiere ich zwei solcher Fälle: stochastische Quanten-Walks (QSWs) und hybrides quanten-klassisches Ausglühen (HQCA). QSWs sind eine Verallgemeinerung der Quanten-Walks auf zusätzliche nicht-unitäre Zeitentwicklung. Damit ermöglichen sie gerichtete Walks. Wie ihre unitären Analoga können QSWs sowohl stetig als auch diskret in der Zeit sein. Im ersten Teil dieser Arbeit präsentiere ich zwei Algorithmen, die QSWs auf einem Quantenrechner simulieren. Der erste Algorithmus simuliert stetige und der zweite diskrete QSWs. Im zweiten Teil dieser Arbeit präsentiere ich eine Methode, die wir vorgeschlagen haben um adiabatisches Quantencomputing (AQC) zu verbessern. Das Ziel von AQC ist es den Grundzustand eines gewünschten Hamiltonoperators zu finden. HQCA soll die Grundzustandsbesetzung erhöhen, indem man die Qubits an ein künstliches Wärmebad ankoppelt. Der Effekt von HQCA wird numerisch für ein und für zwei Qubits getestet.

Publication List

Published

- L. C. G. Govia, B. G. Taketani, P. K. Schuhmacher and F. K. Wilhelm
Quantum Simulation of a Quantum Stochastic Walk
Quantum Science and Technology (2017)

Submitted

- L. S. Theis, P. K. Schuhmacher, M. Marthaler and Frank K. Wilhelm
Gap-independent cooling and hybrid quantum-classical annealing
arXiv:1808.09873 (2018)
- P. K. Schuhmacher, L. C. G. Govia, B. G. Taketani and Frank K. Wilhelm
Quantum Simulation of a Discrete-Time Quantum Stochastic Walk
arXiv:2004.06151 (2020)

Previous Publications

- F. K. Wilhelm, R. Steinwandt, B. Langenberg, P. J. Liebermann, A. Messinger,
P. K. Schuhmacher and A. Misra-Spieldenner
Entwicklungsstand Quantencomputer
BSI Project Number 283 (2018)

Acknowledgements

First and foremost I thank Prof. Frank Wilhelm-Mauch who has given me the chance to work in his research group. His scientific supervision has been outstandingly well throughout my time there.

I would also like to thank all the people I worked with during the process of this thesis, especially Dr. Luke Govia, Dr. Bruno Taketani and Dr. Salil Bedkihal who have been the perfect collaborators guiding me through the challenges of my research goals. Also I would like to thank Aditi Misra-Spieldenner, Dr. Lukas Theis, Dr. Per Liebermann, Dr. David Bruschi and all the other group members I had the chance to work and to become friends with.

Additionally I would like to thank all my family and friends, it would not have been possible to achieve the completion of this thesis without your love and support.

Finally I thank all people who contributed to this thesis in some way and who supported me throughout the writing of this thesis, including Dr. Marius Schöndorf, Andrii Sokolov, Matthias Kreis, Lukas Wettmann, Tina Rohrbacher and Andreas Buchheit who helped with proofreading. I also thank Prof. Sergej Rjasanow to volunteer as my second examiner.

Contents

Acknowledgements	xi
I Introduction	1
1 Development of Modern Computers	3
2 Quantum Information	5
2.1 Postulates of Quantum Mechanics	5
2.2 Entanglement	7
2.3 Qubits and Quantum Gates	7
2.4 Quantum Algorithms	9
2.5 DiVincenzo Criteria	9
3 Open Quantum Systems	10
3.1 Preliminaries	10
3.2 Density Matrices and Partial Trace	11
3.3 Entropy	13
3.4 Quantum Channels	13
3.5 Quantum Dynamical Maps	14
3.6 The Lindblad Master Equation	15
3.7 The Redfield Master Equation	18
3.8 Bath Correlation Functions	19
3.9 Quantum Adiabatic Markovian Master Equations	20
3.10 The Secular Approximation	29
3.11 Comparison of Master Equations	30
3.12 Harmonic Baths	31
3.13 The Quasi-Adiabatic Propagator Path Integral Method	34
4 Summary	37
II Quantum Simulations of Quantum Stochastic Walks	39
4 Introduction to Quantum Stochastic Walks (QSWs)	41
4.1 Continuous-Time Quantum Stochastic Walks	41
4.2 Discrete-Time Quantum Stochastic Walks	42
5 Quantum Simulation of a Continuous-Time QSW	43
5.1 Quantum Trajectories on a Classical Computer	44
5.2 Quantum Trajectories on a Quantum Computer	44
5.3 QTQC of a Quantum Stochastic Walk	46
5.4 Conclusion	51
6 Quantum Simulation of a Discrete-Time QSW	52
6.1 Quantum Simulation of a Kraus Map	52
6.2 Protocol	53
6.3 Simulating a Continuous-Time QSW by a Discrete-Time QSW	57
6.4 Conclusion	59
Appendices	61
A.a Graph Restriction due to Commutation of \hat{K}_{SE} and \hat{H}_{SE}	61
A.b Simulating Nonphysical Evolution	61

A.c	Measurement Operators	63
III	Hybrid Quantum-Classical Annealing	65
8	Introduction to Adiabatic Quantum Computing	67
8.1	3-SAT	67
8.2	Solving 3-SAT by Exploiting Physics	67
8.3	Adiabatic Quantum Computing	69
9	Hybrid Quantum-Classical Annealing of a Single Qubit	72
9.1	Model and Equations of Motion	72
9.2	Environmental Engineering	75
9.3	Conclusion	78
10	On the Scaling to Larger Qubit Numbers	78
10.1	Cooling Operator Candidates	78
10.2	Defining the Toy Model	82
10.3	Methods	83
10.4	The Cooling Operator Championship	83
10.5	Conclusion and Outlook	86
Appendices	87
A.d	Derivation of the quantum master equations	87
A.e	Numerical verification of relaxation and cooling	89
	Conclusion and Outlook	91

List of Figures

1.1 Bloch sphere	8
1.2 Commutative diagram	15
2.1 Sample graph	47
2.2 QTQC Protocol	49
2.3 Two vertex graph	53
2.4 Protocol to simulate discrete-time QSWs	54
3.1 Landau-Zener physics as a toy model for AQC	71
3.2 Hybrid quantum-classical annealing	73
3.3 Flux qubit coupled to coplanar waveguide	75
3.4 Numerical results on cooling	77
3.5 Robustness	79
3.6 Cooling throughout the sweep	84
3.7 Cooling after gap	85
3.8 Ground state population	90

Für meine Familie

Chapter I

Introduction

In this first part of the thesis I discuss the scientific context which is needed to understand this work. First, I give a brief overview of the historical development of computers and explain how quantum effects influence the further development in section 1. This interplay between computers and quantum physics culminates in the today's strongly expanding research field of quantum information which we introduce in section 2. Last but not least, I briefly review the theory of open quantum systems which sets up the physical background to engineer real-life quantum devices in section 3.

1 Development of Modern Computers

Creating physical devices that are able to perform difficult computations remains an active research discipline, although the first examples of such devices like the abacus were invented in ancient times. Abaci have been used over centuries to add or multiply numbers and for more complex operations such as calculating square roots. However, the potential of such devices is obviously limited, and hence, people tried to develop other machines.

The starting shot of modern computer science goes back to Alan Turing. In 1936, he proposed an abstract version of a programmable computer, which is nowadays known as the Turing machine [1]. In his remarkable article, he proved that any algorithm implemented on any deterministic device can also be implemented on the Turing machine. This fundamental property is called universality.

Although the Turing machine serves an useful model for theoretical studies, its direct physical implementation would be inefficient as the runtime for computations scales terribly. However, one could build a computer out of any physical device, as long as one can mathematically map the Turing machine on it. For instance, a famous trading card game has been shown to be Turing-complete [2]. Obviously, this result is a useless fact from a practical perspective. However, it shows that computers can be designed in various ways.

Inspired by Turing's work, the development of modern computers made a remarkable progress all over the world. In 1941, Konrad Zuse presented the Z3, the first functional, fully automatic and programmable computing device using floating point numbers in binary representation. In 1945, the United States Army's Ballistic Research Laboratory completed the first electronic version of a Turing-complete computing device called ENIAC (Electronic Numerical Integrator and Computer). It is still under debate which of these two machines counts as the first modern computer.

The main issue of these first machines was their large physical size and their error-proneness which limited the calculations to small-scale problems. This changed dramatically with the invention of the transistor in 1947 by W. B. Shockley, J. Bardeen, and W. H. Brattain who have been awarded with the Nobel price in 1956 [3] for their joint work. The transistor is an error-robust physical key building block of universal electronic computers and it turned out to be enormously scalable by using integrated circuits and miniaturizing them. The further development of integrated circuits has been honored with a Nobel price for Jack S. Kilby in 2010 [4]. As predicted by Moore in the 1960s, the computer power doubled every year since then, a circumstance referred to as Moore's law [5].

It is somehow surprising, how many years Moore's phenomenological prediction has been come true¹. However, it slowly starts to saturate as quantum effects become more and more relevant in the miniaturizing procedure [6]. Particularly, the quantum mechanical tunnel effect, which is the basic ingredient to make a transistor work, becomes too dominant at small scales and hence, it causes the transistor to behave like a cable. In other words, the quantum mechanical tunnel effect is crucial for building transistors but it also limits the minimal size of such a device fundamentally.

In conclusion, the strategy to build better computers by miniaturizing hardware is reaching its fundamental limits. However, there exist computational problems which probably will never be efficiently solvable on standard-type computers independent of even optimized hardware [7]. Standard examples are the traveling-salesman-problem or 3-SAT. These kind of problems scale at least exponentially in their run-time, their

¹Actually, Moore's prediction became a self-fulfilling prophecy: It defined roadmaps and everyone tried to satisfy them.

memory, or both. Hence, the resources to solve these problems exceed the overall resources available on our finite planet even for rather small problem sizes.

Another exponential hard problem for standard-type computers, which I from now on refer as *classical* computers, is the simulation of quantum mechanical systems. The hardness in this case results from the exponential growth of its Hilbert space dimension with system size [8]. Hence, quantum mechanics plays an important role regarding the hardware limitations and in addition, its simulation represents a computationally hard problem itself. This observation leads to the idea that a computer that satisfies the laws of quantum mechanics itself (particularly using its exponential Hilbert space dimension as a computing *resource*) could circumvent the fundamental restrictions of classical computers. This idea goes back to Paul Benioff in 1980 and Richard Feynman in 1981 [9, 10] and can be treated as the child birth of *quantum information theory*.

There is no unique way how to exploit quantum mechanics for computational tasks. Today's main research direction is the so-called *gate-based model* [8]. It is similar to classical computing: A *quantum algorithm* is performed via *quantum gates* on a universal *quantum computer* where *quantum bits* replace the classical bit. The gate-based model is strongly pushed by academic research but also by commercial companies like IBM, Google, Microsoft and various new startup companies like Rigetti Computing. However, even if we would focus only on the gate-based model, it is not clear yet which kind of physical platform like *ion traps*, *superconducting circuits* or *quantum dots* will be used to construct the first useful gate-based quantum computer. An overview of the different platforms with their respective advantages and disadvantages, as well as a list of international competitors in the field can be found in Ref. [11], a study about the state of development of quantum computers with focus on their impact on cryptanalysis.

The most prominent alternative to the gate-based model is *adiabatic quantum computation* or *quantum annealing* [12]. Here, the solution of an optimization problem is encoded in the ground state of a Hamiltonian. Calculating its eigenspectrum is intractable for classical computers. Instead, one initializes the quantum annealer in the ground state of some initial Hamiltonian and then transforms it adiabatically to the target Hamiltonian. The *adiabatic theorem* guarantees then ending in the desired ground state. Although shown to be equivalent to the gate-based model, quantum annealing is far less developed. However, the Canadian company D-Wave Systems works on such devices and did already sell some prototypes to customers.

Another way to think about quantum algorithms is given by the concept of *quantum walks* [13]. A quantum walk is the quantum mechanical analogue to the ubiquitous classical random walk on a graph. They can either be continuous-time [14] or discrete-time [15, 16] and both types have been shown to be universal for quantum computation [17, 18]. However, quantum walks currently play a minor role in the context of building a universal quantum computer as the underlying graph typically needs an exponential number of nodes to show an asymptotical quantum advantage [19]. Nevertheless, quantum walks can be thought of as *quantum simulation* of quantum transport. Purposefully built quantum simulators [20] are not universal but found application in a range of fields like quantum chemistry [21, 22]. Hence, quantum simulators might solve the first real-life problems before the ability to construct an error-robust and universal quantum computer is reached [23, 24, 25].

All the different strategies have a common obstacle to overcome: *Decoherence* arising from the unavoidable disturbance of any quantum system to its environment [26]. Decoherence causes the transition between quantum and classical behavior of a physical system. The time this takes limits the time a quantum computer performs correctly in a fundamental way. However, in special cases, purposefully engineered

decoherence could *enhance* the performance of a quantum device, as it will be shown in this thesis.

In this work, I do not only regard decoherence as a real-life phenomenon physicists have to deal with. Instead, I outline the potential of some amount of *engineered* decoherence as a *resource* to improve the performance of specific quantum information applications. Prima facie, this ansatz appears counter-intuitive as decoherence is the main enemy of quantum computing, because it destroys the quantum nature of the computation and hence the source of the advantage over classical computing. However, in very special cases, some engineered decoherence assisting the quantum evolution can indeed be beneficial. I discuss two such examples in this thesis: In chapter II, it is shown how to simulate so-called *quantum stochastic walks* on a quantum computer. In this case, engineered decoherence provides the option of directional walks. Here, it is implemented via a special measurement and feed-forward scheme. In chapter III, I outline *hybrid quantum-classical annealing*. Here, the ansatz is to engineer decoherence on top of standard ground state quantum annealing to increase the probability to find the ground state of the target Hamiltonian.

2 Quantum Information

As mentioned in the previous section, the development of a functional quantum computer is a central research goal these days. In this section, I review the basics of quantum mechanics needed to understand the working principle of a quantum computer [8]. Afterwards, I outline the general concepts like quantum bits (qubits) and quantum gates for quantum information. Finally, I review the DiVincenzo criteria for scalable quantum computing [27].

2.1 Postulates of Quantum Mechanics

The paradigms of quantum mechanics can be found in many textbooks [28, 29]. Here, I review the basic terms and postulates.

The *quantum state* of a quantum system is described by a complex vector $|\psi\rangle \in \mathcal{H}$ of unit norm in a Hilbert space $\mathcal{H} = \mathbb{C}^d$ and $d \in \mathbb{N} \cup \{\infty\}$ covering all the possible states of the quantum system¹. The adjoint $|\psi\rangle^\dagger$ is denoted by $\langle\psi|$ and as the vector has unit norm $\langle\psi|\psi\rangle = 1$. Let $|\xi\rangle \in \mathcal{H}$ be another quantum state, then the square of the absolute value of the scalar product $|\langle\xi|\psi\rangle|^2$ describes the probability to find the quantum system in state $|\xi\rangle$ given a state $|\psi\rangle$. Note that the scalar product $\langle\cdot|\cdot\rangle$ in physics is defined as linear in the second argument and antilinear in the first argument.

An observable in quantum mechanics is represented by a Hermitian operator \hat{O} acting on the Hilbert space \mathcal{H} . If \mathcal{H} is finite dimensional, this implies $\hat{O} = \hat{O}^\dagger$. This property guarantees the eigenvalues of \hat{O} are real and hence, we refer these eigenvalues as the possible measurement results if one measures \hat{O} . The most important operator in this context is the *Hamiltonian* \hat{H} . It represents the energy of the quantum system and generates its time-evolution according to Schrödinger's equation

$$i\hbar \frac{\partial}{\partial t} |\psi(t)\rangle = \hat{H} |\psi(t)\rangle \quad (1.1)$$

¹In quantum information theory, the Hilbert space dimensions are typically finite.

with Planck's constant $\hbar = h/2\pi$. Note that \hat{H} can itself be time-dependent. The formal solution of equation (1.1) reads

$$|\psi(t)\rangle = \hat{\mathcal{T}} \exp\left(-\frac{i}{\hbar} \int_0^t \hat{H}(s) ds\right) |\psi(0)\rangle =: \hat{U}(t, 0) |\psi(0)\rangle. \quad (1.2)$$

Here, the operator $\hat{\mathcal{T}}$ denotes time-ordering to ensure causality. The operator $\hat{U}(t, 0)$ is called the *propagator* of the quantum system. It is a unitary operator and therefore, it satisfies $\hat{U}^\dagger \hat{U} = \hat{\mathbb{I}}$ with the identity $\hat{\mathbb{I}}$.

If we couple a quantum system described by Hilbert space \mathcal{H}_1 to another described by \mathcal{H}_2 , the Hilbert space describing the combined system is given by the product space $\mathcal{H} = \mathcal{H}_1 \otimes \mathcal{H}_2$. Its dimension equals

$$\dim(\mathcal{H}) = \dim(\mathcal{H}_1) \cdot \dim(\mathcal{H}_2). \quad (1.3)$$

Hence, if we couple N identical d -dimensional quantum systems to each other, the joint Hilbert space dimension then equals d^N . As pointed out in section 1, this exponential growth of the Hilbert space dimension with the number of coupled quantum systems is the resource to exploit in quantum computers.

Equation (1.1) describes the evolution of a *closed* quantum system. Therefore, it is only truly valid if the quantum system of interest is completely decoupled from its environment. However, this will never be the case in a real-life laboratory as the quantum system has at least to couple to its measurement apparatus. Therefore, the unitary time-evolution (1.2) is only true for the combined system of the quantum system under interest and its environment. Hence, the time-evolution of the quantum subsystem only will not be unitary in general. We are going to discuss the theory of *open quantum systems* in section 3.

The quantum measurement represents an important example for open quantum system evolution as measurements are made by a controlled coupling between the quantum system and its measurement apparatus. Therefore, measurements break the unitary time-evolution in general. Nevertheless, the founders of quantum mechanics included measurements in the closed quantum system description via the concept of *projective measurements* [30]. In this context, every measurement is described by a set of measurement operators $\{\hat{M}_k\}$ which satisfy the completeness relation

$$\sum_k \hat{M}_k^\dagger \hat{M}_k = \hat{\mathbb{I}}. \quad (1.4)$$

These measurement operators are projective and act on the Hilbert space of the system being measured. The possible measurement results are represented by the index k . Let $|\psi\rangle$ be the current state of the quantum system. The probability $P(k)$ to observe the result k is then given by

$$P(k) = \langle \psi | \hat{M}_k^\dagger \hat{M}_k | \psi \rangle. \quad (1.5)$$

If k is measured, the state vector after the measurement equals

$$\frac{\hat{M}_k |\psi\rangle}{\sqrt{\langle \psi | \hat{M}_k^\dagger \hat{M}_k | \psi \rangle}} \quad (1.6)$$

where the scaling factor guarantees that the resulting state vector has unit norm.

2.2 Entanglement

Entanglement is one of the most counter-intuitive concepts of quantum mechanics. Even Albert Einstein was struggling with it [31]. Nevertheless, the existence of entanglement has been shown many times by violating Bell's inequalities [32, 33, 34, 35]. In the context of quantum information, entanglement is treated as one of main ingredients to reach a quantum advantage over classical computers, although there is no proof yet that entanglement is necessary for it.

To define entanglement it is convenient to define its opposite first. Let $\mathcal{H} = \mathcal{H}_A \otimes \mathcal{H}_B$ be the Hilbert space of a composite quantum system consisting of subsystems A and B. A quantum state $|\psi\rangle$ is called a *product state* if and only if it can be written as $|\psi\rangle = |\psi\rangle_A \otimes |\psi\rangle_B$ where $|\psi\rangle_A \in \mathcal{H}_A$ and $|\psi\rangle_B \in \mathcal{H}_B$. If this is not possible, then $|\psi\rangle$ is called *entangled*.

For example, we consider two coupled spin- $\frac{1}{2}$ particles. Each of the particles has two natural eigenstates "spin up" $|\uparrow\rangle_{1/2}$ and "spin down" $|\downarrow\rangle_{1/2}$. Therefore, the Hilbert space describing the two spin- $\frac{1}{2}$ particles is spanned by the four basic states $|\uparrow\uparrow\rangle, |\uparrow\downarrow\rangle, |\downarrow\uparrow\rangle$ and $|\downarrow\downarrow\rangle$. Here, we used the short notation $|ss'\rangle := |s\rangle_1 \otimes |s'\rangle_2$ for $s, s' \in \{\uparrow, \downarrow\}$. The symmetric superposition of all the four basis states is not entangled as it can be written as a product state

$$\frac{1}{2} (|\uparrow\uparrow\rangle + |\uparrow\downarrow\rangle + |\downarrow\uparrow\rangle + |\downarrow\downarrow\rangle) = \left(\frac{1}{\sqrt{2}} (|\uparrow\rangle_1 + |\downarrow\rangle_1) \right) \otimes \left(\frac{1}{\sqrt{2}} (|\uparrow\rangle_2 + |\downarrow\rangle_2) \right). \quad (1.7)$$

In contrast, the quantum state

$$\frac{1}{\sqrt{2}} (|\uparrow\uparrow\rangle + |\downarrow\downarrow\rangle) \quad (1.8)$$

is entangled. The state (1.8) is one of the famous *Bell states*.

2.3 Qubits and Quantum Gates

The basic abstract building block of a classical computer is the bit. It takes either the values "0" or "1". A bit is typically realized by a transistor, which can be switched between conductive or non-conductive. In a quantum computer, the bit is replaced by a quantum bit (*qubit*) [8]. In contrast to its classical counterpart, the qubit has two *basis states* $|0\rangle$ and $|1\rangle$ which span a two-dimensional Hilbert space \mathcal{H} . Hence, an arbitrary quantum state of the qubit can be written in the form

$$|\psi\rangle = \alpha|0\rangle + \beta|1\rangle \quad (1.9)$$

with coefficients $\alpha, \beta \in \mathbb{C}$ such that $|\alpha|^2 + |\beta|^2 = 1$ due to normalization. In polar coordinates, equation (1.9) can be rewritten as

$$|\psi\rangle = e^{i\gamma} \left(\cos\left(\frac{\theta}{2}\right) |0\rangle + e^{i\varphi} \sin\left(\frac{\theta}{2}\right) |1\rangle \right) \quad (1.10)$$

with $\gamma, \theta, \varphi \in \mathbb{R}$. The global phase $e^{i\gamma}$ is irrelevant because it never affects any measurement probabilities. Therefore, without loss of generality, we fix $\gamma := 0$. The two quantities θ and φ can be interpreted as the polar and azimuthal angle of a unit sphere, which is called the Bloch sphere (see figure 1.1). In Cartesian representation,

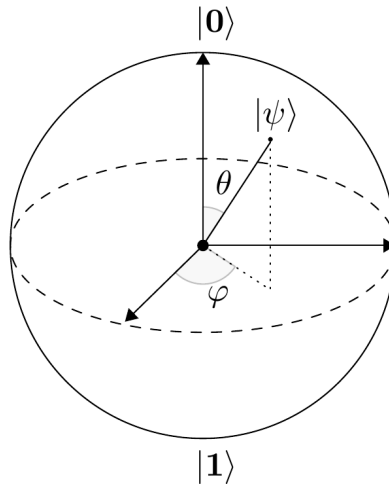


FIGURE 1.1: Illustration of the qubit state $|\psi\rangle$ as a vector on the Bloch sphere. It is fully determined by the polar angles θ and φ .

the quantum state $|\psi\rangle$ is given by the vector

$$|\psi\rangle = \begin{pmatrix} \sin \theta \cos \varphi \\ \sin \theta \sin \varphi \\ \cos \theta \end{pmatrix}. \quad (1.11)$$

In classical computing there are only two possible gates on a single bit: the identity, $0/1 \rightarrow 0/1$, and the negation, $0/1 \rightarrow 1/0$. In quantum computing, this situation changes dramatically. For each initial and each target qubit state $|\psi\rangle$ respectively $|\varphi\rangle$, there exists a rotation of the Bloch sphere \hat{R} which maps $|\psi\rangle$ to $|\varphi\rangle$. As quantum mechanics predicts unitary time-evolution, and rotations are unitary in general, each rotation of the Bloch sphere is a valid *quantum gate*. Therefore, the set of possible quantum gates even for a single qubit is infinite as the set of initial and target states is uncountable.

To build a useful quantum computer, it is not enough to study single-qubit rotations. Analogously to classical computing, we need a *qubit register* out of N qubits and we need the ability to apply *multi-qubit gates* between different qubits. However, it can be shown that it is sufficient to be able to implement a single arbitrary *maximally entangling two-qubit gate* in addition to arbitrary single-qubit gates to build a universal quantum computer [36]. This means, *any* unitary transformation on the multi-qubit register can be realized by this basic set of quantum gates. Which two-qubit entangling gate is used in practice depends on the chosen qubit hardware. The most commonly used ones are the controlled-not-gate (CNOT) and the controlled-phase-gate (CPHASE). Represented in the standard basis $\{|00\rangle, |01\rangle, |10\rangle, |11\rangle\}$, these gates are given by the matrices

$$\text{CNOT} = \begin{pmatrix} 1 & 0 & 0 & 0 \\ 0 & 1 & 0 & 0 \\ 0 & 0 & 0 & 1 \\ 0 & 0 & 1 & 0 \end{pmatrix} \text{ and } \text{CPHASE} = \begin{pmatrix} 1 & 0 & 0 & 0 \\ 0 & 1 & 0 & 0 \\ 0 & 0 & 1 & 0 \\ 0 & 0 & 0 & -1 \end{pmatrix}. \quad (1.12)$$

As we have seen in section 2.1, the Hilbert space of the N -qubit register has dimension 2^N . The exponential growth with the number of qubits causes the simulation of an

all-to-all connected multi-qubit system to be intractable for classical supercomputers even for qubit numbers about $N \approx 50$. In 2019, Google reached *quantum supremacy*: they built the first quantum computer which can not be simulated with the world's largest supercomputers [37, 38]. Although useless for practical applications, this step was a synthetic benchmark in the development of quantum computers.

2.4 Quantum Algorithms

Running *quantum algorithms* is the core motivation to engineer a quantum computer. The most famous quantum algorithms so far are Shor's algorithm for prime factorization of large integers [39] and Grover's algorithm for unsorted database search [40]. The latter is proven to have a quadratical speed-up against any classical algorithm. Shor's algorithm finds the prime factorization in polynomial time in contrast to the best known classical algorithm which needs exponential time. However, there is no proof about speed-up yet, as it is not clear if there is no better classical algorithm for factorization which is not known. Both algorithms are on high importance on cryptoanalysis [11].

However, implementing Shor's and Grover's algorithms on an actual device is still far outside reach in current technology. This is due to the huge required overhead in the number of qubits and quantum gates as a consequence of unavoidable *quantum error correction* [41, 42, 43]. Hence, in the near future, applications will be limited to so-called intermediate scale quantum (NISQ) devices [44]. At this stage of development, these devices are supposed to being used for very specific applications like *quantum simulation* of quantum chemistry, material science or quantum transport [45, 46, 47, 48, 49].

2.5 DiVincenzo Criteria

In the previous sections the basics of quantum information theory like entanglement, qubits and gates have been introduced. However, in order to build a functional quantum computer, it is necessary to translate this abstract logic into physical hardware. In 2000, David DiVincenzo presented five qualitative criteria in order to successfully implement quantum algorithms on an experimental platform [27]. I briefly review these criteria:

1. *A scalable physical system with well characterized qubits*: A qubit is realized by a quantum mechanical two-level system which has to be "well characterized": The states should be well separated by an energy gap and the qubit's parameters should be accurately known to perform single and multi-qubit gates. During the whole run-time of the quantum algorithm, the system should not leak out of the two-level subspace. Furthermore, the qubit system has to be scalable. This means that one has to be able to build a large qubit register and couple these qubits together while not losing the adressability of the single qubits.
2. *The ability to initialize the state of the qubits to a simple fiducial state*: Any computer maps an input to an output. Hence, quantum algorithms always begin with some initial state, which has to be prepared deterministically. A convenient choice is to represent the logical $|0\rangle$ -state by the ground state of the qubit which can be prepared by waiting a multiple of the relaxation time of the qubit. However, this process is too slow if one needs deterministic qubit reset during the run-time of the algorithm. A fast reset can be implemented by projective measurements.

3. *Long relevant coherence times:* The performance of the qubits will always be infected by the interaction with their environment. This interaction induces decoherence transferring the quantum state into a classical one (see section 3). The time this process takes is called *decoherence time* and it limits the gate and measurement times. In most experimental platforms, the decoherence times are rather small which makes active error correction schemes crucial to reduce the computational errors to a reasonable threshold. Unfortunately, these error correction schemes require a significant overhead in the number of qubits and quantum gates.
4. *Universal set of gates:* As mentioned in section 2.3, it is necessary to be able to perform arbitrary single-qubit rotations on the Bloch sphere and to implement one maximally entangling two-qubit gate to run arbitrary quantum algorithms. These operations have to be implemented deterministically with very high fidelities.
5. *Qubit specific measurement capability:* At the end of the quantum algorithm, it is necessary to measure the state of the qubit register with high fidelity to extract the output of the computation and hence, to find an answer to the problem the algorithm is supposed to solve. This qubit readout has to be fast compared to the decoherence rates of the quantum system.

These criteria are of qualitative nature and were established for the gate-based model. A quantitative statement will always depend on the chosen hardware. Moreover, the criteria will slightly change in the regard of alternative models like quantum annealing. However, it is reasonable to treat these criteria as a guideline for quantum hardware development.

3 Open Quantum Systems

In the theory of *open quantum systems*, it is well-known that the coupling between a quantum system and its environment leads to *decoherence*. Decoherence transfers quantum states into classical ones. It destroys quantum superpositions. Therefore, it is crucial to isolate the qubits very well from environmental disturbances according to DiVincenzo's criterion 3. However, the criteria 2, 4 and 5 rely on the coupling between the quantum system and some control electronics respectively its measurement apparatus. These requirements lead to an unavoidable trade-off between coherence and controllability. Therefore, a quantum computer can not be treated as a closed quantum system in practice.

The theory of open quantum systems is a very agile research field on its own since decades. Open quantum systems are hard to simulate on classical computers in general. Equations of motion, which can be solved on classical computers, can usually be derived under strong approximations only. In this section, I review the basic concepts first. In the next step, I assemble a toolbox of different methods (i.e. several quantum master equations and path integral methods) and compare their applicability. For further reading on the theory of open quantum systems, I recommend the textbook written by H.-P. Breuer and F. Petruccione [50].

3.1 Preliminaries

In quantum mechanics of closed systems, the quantum state of a quantum system is described by a vector $|\psi\rangle \in \mathcal{H}$ in a Hilbert space \mathcal{H} and its dynamics is determined

by Schrödinger's equation (see section 2.1). For closed quantum systems, this is a valid description. However, in real-life experiments, the quantum system of interest will unavoidably be coupled to its environment. Therefore, the composite system consisting of quantum system and its environment will follow closed-system dynamics, but not the quantum system on its own. The degrees of freedom of the environment are typically unknown, uncontrolled and their number might be infinite. Hence, the simulation of the full closed-system dynamics of quantum system and its environment is usually intractable. Nevertheless, as we are only interested in the time evolution of the quantum system only rather than the dynamics of the environment, it is possible to derive effective equations of motion for the system. To do so, it is necessary to have some stochastic knowledge of the environment to simulate its influence onto the system. It is convenient to treat the environment as a *heat bath* in thermal equilibrium at temperature T .

In the following, we refer \mathcal{H}_S as the Hilbert space attached to the quantum system and \mathcal{H}_B as the Hilbert space attached to the heat bath. The time-evolution of the state $|\psi\rangle \in \mathcal{H}_S \otimes \mathcal{H}_B$ is given by Schrödinger's equation (1.1). The Hamiltonian \hat{H} can be written as the sum

$$\hat{H} = \hat{H}_S \otimes \hat{\mathbb{I}}_B + \hat{\mathbb{I}}_S \otimes \hat{H}_B + \hat{H}_{\text{int}}. \quad (1.13)$$

Here, the Hamiltonians $\hat{H}_{S/B}$ and the identities $\hat{\mathbb{I}}_{S/B}$ act only on $\mathcal{H}_{S/B}$. To shorten the notation, we will neglect the tensor products in the identities in the following.

The actual quantum state $|\psi(t)\rangle$ of the composite system will not be known in detail, because we assume the microscopic bath degrees of freedom to be unknown. Let $\{|\psi_i(t)\rangle \in \mathcal{H} = \mathcal{H}_S \otimes \mathcal{H}_B\}$ be a (not necessarily orthogonal) set of possible states with corresponding classical probabilities p_i . We define the Hermitian operator

$$\hat{\rho}(t) = \sum_i p_i |\psi_i(t)\rangle \langle \psi_i(t)|. \quad (1.14)$$

If we differentiate equation (1.14) with respect to time and make use of the fact that each of the $|\psi_i(t)\rangle$ follows Schrödinger's equation (1.1), we find the equation of motion

$$\dot{\hat{\rho}}(t) = -\frac{i}{\hbar} [\hat{H}(t), \hat{\rho}(t)]. \quad (1.15)$$

Here, we defined the commutator of two operators $[\hat{A}, \hat{B}] := \hat{A}\hat{B} - \hat{B}\hat{A}$. Equation (1.15) is called the *Liouville-Von Neumann equation*. It is the quantum mechanical analogue to the Liouville equation in classical mechanics with the operator $\hat{\rho}$ taking the role of the classical probability density function. Therefore, the operator $\hat{\rho}$ is called the *density operator* or *density matrix*. If $\hat{\rho}$ is diagonal, it is equivalent to a classical probability distribution.

3.2 Density Matrices and Partial Trace

The Liouville-Von Neumann equation (1.15) gives the exact quantum dynamics for the density matrix (1.14). We rediscover Schrödinger's equation (1.1) in the special case $\hat{\rho} = |\psi\rangle \langle \psi|$ for some $|\psi\rangle \in \mathcal{H}$. Hence, the Liouville-Von Neumann equation is the generalization of Schrödinger's equation to *statistical ensembles* of quantum states, described by a density matrix $\hat{\rho}$. If the ensemble includes only a single quantum state $\hat{\rho} = |\psi\rangle \langle \psi|$, then we refer $\hat{\rho}$ to be a *pure state* and a *mixed state*, otherwise. Obviously, its representation (1.14) is not unique. We postulate the three properties

1. $\hat{\rho} = \hat{\rho}^\dagger$ ($\hat{\rho}$ is Hermitian)
2. $\forall |\psi\rangle \in \mathcal{H} : \langle \psi | \hat{\rho} | \psi \rangle \geq 0$ ($\hat{\rho}$ is positive semi-definite)
3. $\text{Tr}(\hat{\rho}) = 1$ (trace is normalized).

These properties guarantee that the eigenvalues of $\hat{\rho}$ are

1. real,
2. positive,
3. and they add up to 1.

Hence, the eigenvalues of $\hat{\rho}$ can be treated as probabilities. Obviously, any operator written in the form (1.14) satisfies these postulates. Conversely, each operator which satisfies the postulates can be written in the form (1.14) by choosing a specific basis. Hence, both ways to define a density matrix are equivalent.

Let \hat{O} be an arbitrary observable and $\{|\psi_i\rangle \in \mathcal{H}\}$ a complete set of possible states with corresponding probabilities p_i . The expectation value of \hat{O} then reads

$$\langle \hat{O} \rangle = \sum_i p_i \langle \psi_i | \hat{O} | \psi_i \rangle = \sum_i p_i \text{Tr}(|\psi_i\rangle \langle \psi_i | \hat{O}) = \text{Tr}(\overbrace{\sum_i p_i |\psi_i\rangle \langle \psi_i|}^{=\hat{\rho}} \hat{O}). \quad (1.16)$$

Hence, we can compute the expectation value of any observable \hat{O} via $\langle \hat{O} \rangle = \text{Tr}(\hat{\rho} \hat{O})$ if the density matrix $\hat{\rho}$ is known. This property justifies to identify the density matrix with the quantum state of the ensemble.

Now, let $\hat{\rho}_{AB}$ denote the density matrix of a composite quantum system consisting of subsystems A and B. For example, A could be the quantum system of interest and B its environment. In this case, it is obvious that we need a mathematical operation that maps the density matrix $\hat{\rho}_{AB}$ of the composite system uniquely to the *reduced density matrix* $\hat{\rho}_A$ of the system of interest. Crucially, this map has to preserve the postulates of density matrices. The map which satisfies these conditions is the *partial trace*. Let \hat{O}_{AB} be an operator acting on the composite system which can be written as a product $\hat{O}_{AB} = \hat{O}_A \otimes \hat{O}_B$, then the partial trace over the subsystem B is defined as

$$\text{Tr}_B(\hat{O}_A \otimes \hat{O}_B) := \text{Tr}(\hat{O}_B) \cdot \hat{O}_A. \quad (1.17)$$

For the density matrix $\hat{\rho}_A \otimes \hat{\rho}_B$ this gives

$$\text{Tr}_B(\hat{\rho}_A \otimes \hat{\rho}_B) = \text{Tr}(\hat{\rho}_B) \cdot \hat{\rho}_A = \hat{\rho}_A \quad (1.18)$$

as the trace of the density matrix $\hat{\rho}_B$ equals 1 due to normalization. The physical interpretation of equation (1.18) is the following: If the systems A and B separate, then *tracing out* system B has no impact on system A (and vice versa). Hence, A and B are uncorrelated.

The partial trace is a linear map by definition (1.17). Using this and the fact, that every operator \hat{O}_{AB} has a representation in the form

$$\hat{O}_{AB} = \sum_i \hat{O}_A^{(i)} \otimes \hat{O}_B^{(i)}, \quad (1.19)$$

the partial trace generalizes to

$$\mathrm{Tr}_B(\hat{O}_{AB}) = \mathrm{Tr}_B\left(\sum_i \hat{O}_A^{(i)} \otimes \hat{O}_B^{(i)}\right) := \sum_i \mathrm{Tr}(\hat{O}_B^{(i)}) \cdot \hat{O}_A^{(i)}. \quad (1.20)$$

Applying the partial trace over the heat bath to the Liouville-Von Neumann equation (1.15), one obtains the exact equation of motion for the reduced density matrix $\hat{\rho}_S(t)$

$$\dot{\hat{\rho}}_S(t) = -\frac{i}{\hbar} \mathrm{Tr}_B\left(\left[\hat{H}(t), \hat{\rho}(t)\right]\right). \quad (1.21)$$

In the following, we set $\hbar := 1$.

3.3 Entropy

One of the key concepts in the field of open quantum systems is the *Von-Neumann entropy* S . It is defined as the functional

$$S(\hat{\rho}) := -\mathrm{Tr}(\hat{\rho} \log(\hat{\rho})) \quad (1.22)$$

on the density matrix $\hat{\rho}$. The definition (1.22) generalizes the classical entropy to the quantum case. It somehow measures the amount (or more precisely the absence) of information one has about a quantum system described by the density matrix $\hat{\rho}$. There is a huge research field regarding Von-Neumann entropy. Here, we only review a few crucial properties:

1. The Von-Neumann entropy is *nonnegative*: $S(\hat{\rho}) \geq 0$ for all $\hat{\rho}$ and $S(\hat{\rho}) = 0$ if and only if $\hat{\rho} = |\psi\rangle\langle\psi|$ is a pure state.
2. Let $\mathcal{B}(\mathcal{H})$ denote the operator algebra of bounded operators acting on a Hilbert space \mathcal{H} . If $\dim(\mathcal{H}) = d$, then $S(\hat{\rho}) \leq \log(d)$ for all $\hat{\rho} \in \mathcal{B}(\mathcal{H})$. The maximal value is reached if and only if $\hat{\rho} = \frac{1}{d}\mathbb{1}$.
3. For all $\hat{\rho}_{AB} \in \mathcal{B}(\mathcal{H}_A \otimes \mathcal{H}_B)$, the Von-Neumann entropy is *subadditive*: $S(\hat{\rho}_{AB}) \leq S(\hat{\rho}_A) + S(\hat{\rho}_B)$. Equality holds if and only if $\hat{\rho}_{AB} = \hat{\rho}_A \otimes \hat{\rho}_B$ is a product state.

For further details, see [8].

The Liouville-Von-Neumann equation (1.15) keeps Von-Neumann entropy constant as

$$\begin{aligned} S(\hat{\rho}(t)) &= S\left(\hat{U}(t,0)\hat{\rho}(0)\hat{U}^\dagger(t,0)\right) \\ &= -\mathrm{Tr}\left(\hat{U}(t,0)\hat{\rho}(0)\hat{U}^\dagger(t,0)\hat{U}(t,0)\log(\hat{\rho}(0))\hat{U}^\dagger(t,0)\right) \\ &= -\mathrm{Tr}(\hat{\rho}(0)\log(\hat{\rho}(0))) = S(\hat{\rho}(0)). \end{aligned} \quad (1.23)$$

Hence, the entropy of a system following closed system dynamics stays constant. Therefore, any change of entropy in the system has to result from its interaction with unobserved degrees of freedom of its environment. In other words, *decoherence* of the system can only be induced by environmentally driven dynamics.

3.4 Quantum Channels

A linear map $\mathcal{E} : \mathcal{B}(\mathcal{H}) \rightarrow \mathcal{B}(\mathcal{H})$ is called *positive*, if it maps positive semi-definite operators onto positive semi-definite operators. It is called *completely positive* if for

all $k \geq 1$ the *amplification map*

$$\begin{aligned}\mathcal{E}^{(k)} : \mathcal{M}_k(\mathcal{B}(\mathcal{H})) &\longrightarrow \mathcal{M}_k(\mathcal{B}(\mathcal{H})) \\ \mathcal{E}^{(k)} &:= \hat{\mathbb{I}}_k \otimes \mathcal{E}\end{aligned}\quad (1.24)$$

is positive. Here, $\mathcal{M}_k(\mathcal{B}(\mathcal{H}))$ denotes the k^2 -dimensional matrix algebra with matrix entries in $\mathcal{B}(\mathcal{H})$.

Quantum channels are linear, completely positive and trace-preserving maps. These properties guarantee that quantum channels map density matrices to density matrices and hence, physical states to physical states. They are important to study the dynamics of open quantum systems. Here, we briefly review the basic terms and concepts. For the mathematical details including rigorous definitions, theorems and their proofs, I recommend the review [51].

Let $\dim(\mathcal{H}) = N$, $N \in \mathbb{N}$, and let $\mathcal{E} : \mathcal{B}(\mathcal{H}) \longrightarrow \mathcal{B}(\mathcal{H})$ be a linear, completely positive map. Then \mathcal{E} can be represented as

$$\mathcal{E}(\hat{\rho}) = \sum_{i=1}^{N^2} \hat{A}_i \hat{\rho} \hat{A}_i^\dagger \quad \forall \hat{\rho} \in \mathcal{B}(\mathcal{H}). \quad (1.25)$$

This representation is called *Kraus decomposition* and the operators $\hat{A}_i \in \mathcal{B}(\mathcal{H})$ are called *Kraus operators*. If and only if \mathcal{E} is a quantum channel (it preserves additionally the trace), then the \hat{A}_i satisfy the completeness condition

$$\sum_{i=1}^{N^2} \hat{A}_i^\dagger \hat{A}_i = \hat{\mathbb{I}}. \quad (1.26)$$

The choice of the operators \hat{A}_i is not unique and their number can be smaller than N^2 . For $\dim(\mathcal{H}) = 2$, any quantum channel \mathcal{E} can be represented using the Pauli spin matrices $\hat{\mathbb{I}}, \hat{\sigma}_x, \hat{\sigma}_y$ and $\hat{\sigma}_z$ as Kraus operators. For example, the *depolarizing channel* is given by

$$\hat{\rho} \rightarrow \hat{\rho}' = (1-p)\hat{\rho} + \frac{p}{3}(\hat{\sigma}_x \hat{\rho} \hat{\sigma}_x + \hat{\sigma}_y \hat{\rho} \hat{\sigma}_y + \hat{\sigma}_z \hat{\rho} \hat{\sigma}_z) \quad (1.27)$$

with $p \in [0, 1]$. It describes a simple error model: With probability p one of three equally likely errors occurs and changes the qubit state. With probability $1-p$, no error occurs.

3.5 Quantum Dynamical Maps

If we assume that for time $t = 0$, the initial density matrix of the total system is given by a product state

$$\hat{\rho}(0) = \hat{\rho}_S(0) \otimes \hat{\rho}_B(0), \quad (1.28)$$

where $\hat{\rho}_{S/B}(t) := \text{Tr}_{S/B}(\hat{\rho}(t))$, then the state evolution of the reduced density matrix $\hat{\rho}_S(0)$ can be expressed with the help of a *quantum dynamical map* $\mathcal{V}_t : \mathcal{B}(\mathcal{H}_S) \longrightarrow \mathcal{B}(\mathcal{H}_S)$ such that

$$\hat{\rho}_S(0) \mapsto \hat{\rho}_S(t) = \mathcal{V}_t \hat{\rho}_S(0) \quad \forall t \geq 0. \quad (1.29)$$

$$\begin{array}{ccc}
\hat{\rho}(0) = \hat{\rho}_S(0) \otimes \hat{\rho}_B(0) & \xrightarrow{\text{coh. evolution}} & \hat{\rho}(t) = \hat{U}(t) (\hat{\rho}_S(0) \otimes \hat{\rho}_B(0)) \hat{U}^\dagger(t) \\
\text{Tr}_B \downarrow & & \downarrow \text{Tr}_B \\
\hat{\rho}_S(0) & \xrightarrow{\text{quantum dynamical map}} & \hat{\rho}_S(t) = \mathcal{V}_t \hat{\rho}_S(0)
\end{array}$$

FIGURE 1.2: Commutative diagram to illustrate the definition of the quantum dynamical map \mathcal{V}_t .

Its definition is illustrated in the commutative diagram 1.2. The map \mathcal{V}_t is a one-parameter family of completely positive and trace preserving maps. Hence, \mathcal{V}_t can be written in Kraus decomposition (1.25) for all $t > 0$ and $\dim(\mathcal{H}_S) = d$ using time-dependent Kraus operators

$$\hat{\rho}_S(t) = \mathcal{V}_t \hat{\rho}_S(0) = \sum_{i=1}^{d^2} \hat{A}_i(t) \hat{\rho}_S(0) \hat{A}_i^\dagger(t). \quad (1.30)$$

In many cases, correlations between environmental degrees of freedom decay fast compared to the characteristic time-scales of the system, such that it is valid to neglect memory effects in the reduced system dynamics. This *Markovian* approximation can be formulated by the semigroup property

$$\mathcal{V}_{t_1+t_2} = \mathcal{V}_{t_1} \mathcal{V}_{t_2} \quad \forall t_1, t_2 \geq 0. \quad (1.31)$$

If this semigroup property (1.31) holds, then there is a generator \mathcal{L} of the semigroup such that

$$\mathcal{V}_t = \exp(\mathcal{L}t). \quad (1.32)$$

For further details regarding quantum dynamical semigroups I refer the reader to the textbook [26].

3.6 The Lindblad Master Equation

In the following, we derive the most general form of a completely positive and trace-preserving master equation called the *Lindblad master equation* named after G. Lindblad [52]. For simplicity, we consider a finite dimensional Hilbert space \mathcal{H}_S with $\dim(\mathcal{H}_S) = d$.

Using the semigroup property (1.31) and expressing the quantum dynamical map $\mathcal{V}(\Delta t)$ via equation (1.32), the reduced density matrix $\hat{\rho}_S(t + \Delta t)$ equals

$$\hat{\rho}_S(t + \Delta t) = \mathcal{V}_{\Delta t} \hat{\rho}_S(t) = \exp(\mathcal{L}\Delta t) \hat{\rho}_S(t). \quad (1.33)$$

Expanding the exponential in equation (1.33) up to first order gives

$$\hat{\rho}_S(t + \Delta t) - \hat{\rho}_S(t) = \Delta t \mathcal{L} \hat{\rho}_S(t) + \mathcal{O}(\Delta t^2). \quad (1.34)$$

In the limit $\Delta t \rightarrow 0$, equation (1.34) leads to the Markovian master equation

$$\frac{d}{dt} \hat{\rho}_S(t) = \mathcal{L} \hat{\rho}_S(t). \quad (1.35)$$

Now we derive the general form of the generator \mathcal{L} . Let $\{\hat{E}_j | 1 \leq j \leq d^2\}$ be an orthonormal basis of the d^2 -dimensional algebra $\mathcal{B}(\mathcal{H}_S)$ of the operators acting on the d -dimensional Hilbert space \mathcal{H}_S satisfying¹

$$\text{Tr} \left(\hat{E}_i^\dagger \hat{E}_j \right) = \delta_{ij}. \quad (1.36)$$

Without loss of generality, we choose $\hat{E}_{d^2} = \frac{1}{\sqrt{d}} \hat{\mathbb{I}}$. This choice forces all the other operators to be traceless. As any operator in $\mathcal{B}(\mathcal{H}_S)$ can be expressed in terms of the operators \hat{E}_j , so can the Kraus operators in equation (1.30). We hence find

$$\mathcal{V}_{\Delta t} \hat{\rho}_S(t) = \sum_{i,j=1}^{d^2} c_{ij}(\Delta t) \hat{E}_i \hat{\rho}_S(t) \hat{E}_j^\dagger \quad (1.37)$$

with coefficient functions $c_{ij}(\Delta t)$. Equation (1.37) will now be used to find an expression for the generator. After some algebra we find

$$\begin{aligned} \mathcal{L} \hat{\rho}_S(t) &= \lim_{\Delta t \rightarrow 0} \frac{\mathcal{V}_{\Delta t} \hat{\rho}_S(t) - \hat{\rho}_S(t)}{\Delta t} \\ &= c(0) \hat{\rho}_S(t) + \hat{O} \hat{\rho}_S(t) + \hat{\rho}_S(t) \hat{O}^\dagger + \sum_{i,j=1}^{d^2-1} \alpha_{ij} \hat{E}_i \hat{\rho}_S(t) \hat{E}_j^\dagger \\ &= -i \left[\hat{H}, \hat{\rho}_S(t) \right] + \left\{ \hat{G}, \hat{\rho}_S(t) \right\} + \sum_{i,j=1}^{d^2-1} \alpha_{ij} \hat{E}_i \hat{\rho}_S(t) \hat{E}_j^\dagger, \end{aligned} \quad (1.38)$$

where

$$c(0) := \lim_{\Delta t \rightarrow 0} \frac{\frac{1}{d} c_{d^2 d^2}(\Delta t) - 1}{\Delta t}, \quad (1.39)$$

$$\alpha_{ij} := \lim_{\Delta t \rightarrow 0} \frac{c_{ij}(\Delta t)}{\Delta t}, \quad (1.40)$$

$$\hat{O} := \sum_{j=1}^{d^2-1} \frac{1}{\sqrt{d}} \alpha_{d^2 j} \hat{E}_j^\dagger, \quad (1.41)$$

$$\hat{G} := \frac{1}{2} \left(\hat{O} + \hat{O}^\dagger + c(0) \hat{\mathbb{I}} \right), \quad (1.42)$$

$$\hat{H} := -\frac{i}{2} \left(\hat{O} - \hat{O}^\dagger \right). \quad (1.43)$$

The operator $\mathcal{L} \hat{\rho}_S(t)$ is traceless, because

$$0 = \frac{d}{dt} 1 = \frac{d}{dt} \text{Tr} \left(\hat{\rho}_S(t) \right) = \text{Tr} \left(\frac{d}{dt} \hat{\rho}_S(t) \right) = \text{Tr} \left(\mathcal{L} \hat{\rho}_S(t) \right). \quad (1.44)$$

If we take the trace over equation (1.38) and we find by equation (1.44) that

$$\hat{G} = -\frac{1}{2} \sum_{i,j=1}^{d^2-1} \alpha_{ij} \hat{E}_j^\dagger \hat{E}_i, \quad (1.45)$$

¹For operators $\hat{O}_1, \hat{O}_2 \in \mathcal{B}(\mathcal{H}_S)$, the map $\text{Tr} \left(\hat{O}_2^\dagger \hat{O}_1 \right)$ defines the scalar product on $\mathcal{B}(\mathcal{H}_S)$.

and hence

$$\mathcal{L}\hat{\rho}_S(t) = -i \left[\hat{H}, \hat{\rho}_S(t) \right] + \sum_{i,j=1}^{d^2-1} \alpha_{ij} \left(\hat{E}_i \hat{\rho}_S(t) \hat{E}_j^\dagger - \frac{1}{2} \left\{ \hat{E}_j^\dagger \hat{E}_i, \hat{\rho}_S(t) \right\} \right). \quad (1.46)$$

Equation (1.46) is called the *first standard form* of the generator \mathcal{L} . The coefficient matrix $(\alpha_{ij})_{i,j=1}^{d^2-1}$ is positive semidefinite and can be diagonalized with the help of a unitary transformation \hat{u} satisfying

$$\hat{u} (\alpha_{ij})_{i,j=1}^{d^2-1} \hat{u}^\dagger = \text{diag} (\gamma_1, \dots, \gamma_{d^2-1}). \quad (1.47)$$

If we define the *Lindblad operators* \hat{L}_k as

$$\hat{L}_k := \sum_{j=1}^{d^2-1} \hat{E}_j \hat{u}_{jk}^\dagger, \quad (1.48)$$

we find the *second standard form* or *Lindblad form* of the generator

$$\mathcal{L}\hat{\rho}_S(t) = -i \left[\hat{H}, \hat{\rho}_S(t) \right] + \sum_{k=1}^{d^2-1} \gamma_k \left(\hat{L}_k \hat{\rho}_S(t) \hat{L}_k^\dagger - \frac{1}{2} \left\{ \hat{L}_k^\dagger \hat{L}_k, \hat{\rho}_S(t) \right\} \right). \quad (1.49)$$

If we insert equation (1.49) into the master equation (1.35) we reach the *Lindblad master equation*

$$\frac{d}{dt} \hat{\rho}_S(t) = -i \left[\hat{H}, \hat{\rho}_S(t) \right] + \sum_{k=1}^{d^2-1} \gamma_k \left(\hat{L}_k \hat{\rho}_S(t) \hat{L}_k^\dagger - \frac{1}{2} \left\{ \hat{L}_k^\dagger \hat{L}_k, \hat{\rho}_S(t) \right\} \right). \quad (1.50)$$

The Lindblad master equation (1.50) is the most general form of a completely positive and trace-preserving master equation. In other words, any master equation which guarantees to map density matrices to density matrices¹ can be written in Lindblad form. The generator \mathcal{L} is fully determined by a unitary part, generated by the Hermitian operator \hat{H} , and a dissipative part given by $d^2 - 1$ Lindblad operators \hat{L}_k . Their choice is not unique, because the Lindblad master equation (1.50) is invariant under two kinds of transformations:

- $\hat{L}_k \rightarrow \sum_j \hat{V}_{kl} \hat{L}_j$ with a unitary matrix \hat{V} .
- $\hat{L}_k \rightarrow \hat{L}_k + l_k \hat{\mathbb{1}}$ and $\hat{H} \rightarrow \hat{H} + \frac{1}{2i} \sum_j \gamma_j \left(l_j^* \hat{L}_j - l_j \hat{L}_j^\dagger \right) + m$ where $l_k \in \mathbb{C}$ and $m \in \mathbb{R}$.

Therefore, the Hermitian operator $\hat{H}(t)$ is not necessarily the system Hamiltonian. But it will be in typical cases of interest. Further, we rediscover the Liouville-Von Neumann equation (1.15) as a special case of equation (1.50) with vanishing Lindblad operators. Hence, the Liouville-Von Neumann equation is a completely positive and trace-preserving master equation too. However, the Lindblad master equation does not keep entropy constant and does not conserve energy in general. The second part of equation (1.50) is suitably called the *dissipator* $\mathcal{D}(\hat{\rho}_S(t))$.

¹And hence physically meaningful states to physically meaningful states!

3.7 The Redfield Master Equation

In section 3.6, we have shown that any completely positive and trace-preserving master equation can be written in Lindblad form (1.50). However, it is not clear how to derive the concrete master equation of an open quantum system based on a microscopic model at this stage. In other words, given a concrete open quantum system, how do we find the corresponding Lindblad operators \hat{L}_k ? In this section, we review the standard steps and approximations that lead to the *Redfield master equation*¹. Its derivation is an intermediate step to reach Lindblad form and hence, it is not completely positive and trace-preserving in general. Nevertheless, the Redfield master equation is a useful tool to simulate open quantum system dynamics as long as the positivity of the density matrix is preserved. If applicable, the Redfield master equation is more accurate than the Lindblad equation as it needs one questionable approximation less. A complete description can be found in [26].

We start the derivation with the system-bath Hamiltonian (1.13)

$$\hat{H} = \hat{H}_S + \hat{H}_B + \hat{H}_{\text{int}}, \quad (1.51)$$

where the interaction Hamiltonian \hat{H}_{int} can always be written as

$$\hat{H}_{\text{int}} = \sum_j \hat{S}_j \otimes \hat{B}_j \quad (1.52)$$

using proper Hermitian operators \hat{S}_j and \hat{B}_j only acting on the system respectively the bath. The time evolution of the total density matrix follows the Liouville-Von-Neumann equation (1.15). It is convenient to transform it to the interaction picture with respect to $\hat{H}_0 := \hat{H}_S + \hat{H}_B$ ². We find

$$\dot{\hat{\rho}}_{\text{int}}(t) = -i \left[\hat{H}_{\text{int}}(t), \hat{\rho}_{\text{int}}(t) \right]. \quad (1.53)$$

To shorten the notation, we drop the index $\hat{\rho}_{\text{int}}(t) \rightarrow \hat{\rho}(t)$ in the following. The integral form of equation (1.53) reads

$$\hat{\rho}(t) = \hat{\rho}(0) - i \int_0^t \left[\hat{H}_{\text{int}}(s), \hat{\rho}(s) \right] ds. \quad (1.54)$$

Inserting equation (1.54) into equation (1.53) and taking the partial trace over the bath we get the integro-differential equation

$$\dot{\hat{\rho}}_S(t) = -i \text{Tr}_B \left[\hat{H}_{\text{int}}(t), \hat{\rho}(0) \right] - \int_0^t \text{Tr}_B \left[\hat{H}_{\text{int}}(t), \left[\hat{H}_{\text{int}}(s), \hat{\rho}(s) \right] \right] ds. \quad (1.55)$$

This exact equation is equivalent to equation (1.21). In the thermodynamic equilibrium, we can assume that the expectation value of the bath operators $\langle \hat{B}_j(t) \rangle = \text{Tr}_B \left[\hat{B}_j(t) \hat{\rho}(0) \right] = 0$ vanishes for all j without loss of generality. In consequence, the inhomogeneous term in equation (1.55) vanishes.

Equation (1.55) is at least very hard or even impossible to solve as it contains the knowledge of the full density matrix $\hat{\rho}(s)$ at all times $0 \leq s \leq t$. In order to eliminate $\hat{\rho}(s)$ inside the integral, we first perform an approximation called the

¹For qubits, the Redfield master equation is typically called the *Bloch-Redfield master equation*.

²Indeed, the transformation to the interaction picture is crucial to perform the Markov approximation later on.

Born approximation. This approximation relies on the assumption that the coupling between the system and the heat bath is weak. Hence, the influence of the system on the heat bath is negligibly small such that the density matrix $\hat{\rho}_B := \hat{\rho}_B(0)$ is stationary for all times $0 \leq s \leq t$ and the total density matrix can be approximated by a product state

$$\hat{\rho}(s) \approx \hat{\rho}_S(s) \otimes \hat{\rho}_B. \quad (1.56)$$

Thus, equation (1.55) can be approximated by

$$\dot{\hat{\rho}}_S(t) = - \int_0^t \text{Tr}_B \left[\hat{H}_{\text{int}}(t), \left[\hat{H}_{\text{int}}(s), \hat{\rho}_S(s) \otimes \hat{\rho}_B \right] \right] ds. \quad (1.57)$$

Equation (1.57) is still hard to solve as it contains a time-convolution. In order to get rid of this, we perform the *Markov approximation*. Here, we assume that environmental excitations decay very fast against all system dynamics such that, on a coarse-grained time scale, we can replace $\hat{\rho}_S(s)$ inside the integral by the instantaneous value $\hat{\rho}_S(t)$. In other words, the Markov approximation neglects memory effects. It yields

$$\dot{\hat{\rho}}_S(t) = - \int_0^t \text{Tr}_B \left[\hat{H}_{\text{int}}(t), \left[\hat{H}_{\text{int}}(s), \hat{\rho}_S(t) \otimes \hat{\rho}_B \right] \right] ds. \quad (1.58)$$

Equation (1.58) is the Redfield master equation [53]. It is local in time but not completely Markovian, because the time evolution of the reduced density matrix depends on the initial preparation at time $t = 0$. Nevertheless, it is possible to make it Markovian by applying a further approximation. Be τ_B the time scale over which the bath correlation functions decay (see section 3.8 for further information). If we substitute s in equation (1.58) by $t - s$ and let the upper limit of the integral go to infinity, we achieve the Markovian master equation

$$\dot{\hat{\rho}}_S(t) = - \int_0^\infty \text{Tr}_B \left[\hat{H}_{\text{int}}(t), \left[\hat{H}_{\text{int}}(t - s), \hat{\rho}_S(t) \otimes \hat{\rho}_B \right] \right] ds. \quad (1.59)$$

This approximation is valid if the integrand vanishes sufficiently fast for $s > \tau_B$. In other words, equation (1.59) describes the time evolution of the reduced density matrix on a coarse-grained time scale.

Equation (1.59) can not be written in Lindblad form (1.50) and hence, it does not guarantee to preserve the properties of density matrices at all times. Particularly, it does not preserve positivity in general. Nevertheless, it is possible to derive a master equation in Lindblad form by applying a further approximation to equation (1.59) called the *secular approximation*. However, a further approximation means further inaccuracy of the resulting master equation and hence, the Redfield equation is more precise than the corresponding Lindblad equation if it preserves positivity.

3.8 Bath Correlation Functions

As mentioned in section 3.2, every operator of a composite system has a representation given by equation (1.19). Hence, we can decompose the operator $\hat{H}_{\text{int}}(t)$ in the integrand of equation (1.59) as

$$\hat{H}_{\text{int}}(t) = \sum_k g_k \hat{S}_k(t) \otimes \hat{B}_k(t) \quad (1.60)$$

with coupling strengths g_k and appropriate Hermitian operators $\hat{S}_k(t)$ and $\hat{B}_k(t)$ with unit operator norm acting only on the system or the bath respectively. For simplicity, we assume $g_k = g$ for all k . If we insert equation (1.60) into equation (1.59), we get

$$\begin{aligned} \dot{\hat{\rho}}_S(t) = & -g^2 \sum_{k,k'} \int_0^\infty \left(\text{Tr}_B \left[\hat{S}_k(t) \hat{S}_{k'}(t-s) \hat{\rho}_S(t) \otimes \hat{B}_k(t) \hat{B}_{k'}(t-s) \hat{\rho}_B \right] \right. \\ & - \text{Tr}_B \left[\hat{S}_k(t) \hat{\rho}_S(t) \hat{S}_{k'}(t-s) \otimes \hat{B}_k(t) \hat{\rho}_B \hat{B}_{k'}(t-s) \right] \\ & + \text{Tr}_B \left[\hat{\rho}_S(t) \hat{S}_{k'}(t-s) \hat{S}_k(t) \otimes \hat{\rho}_B \hat{B}_{k'}(t-s) \hat{B}_k(t) \right] \\ & \left. - \text{Tr}_B \left[\hat{S}_{k'}(t-s) \hat{\rho}_S(t) \hat{S}_k(t) \otimes \hat{B}_{k'}(t-s) \hat{\rho}_B \hat{B}_k(t) \right] \right) ds. \quad (1.61) \end{aligned}$$

Using the definition of the partial trace (1.20) as well as the cyclic property of the trace we find

$$\begin{aligned} \dot{\hat{\rho}}_S(t) = & -g^2 \sum_{k,k'} \int_0^\infty \left(\text{Tr} \left[\hat{\rho}_B \hat{B}_k(t) \hat{B}_{k'}(t-s) \right] \hat{S}_k(t) \hat{S}_{k'}(t-s) \hat{\rho}_S(t) \right. \\ & - \text{Tr} \left[\hat{\rho}_B \hat{B}_{k'}(t-s) \hat{B}_k(t) \right] \hat{S}_k(t) \hat{\rho}_S(t) \hat{S}_{k'}(t-s) \\ & + \text{Tr} \left[\hat{\rho}_B \hat{B}_{k'}(t-s) \hat{B}_k(t) \right] \hat{\rho}_S(t) \hat{S}_{k'}(t-s) \hat{S}_k(t) \\ & \left. - \text{Tr} \left[\hat{\rho}_B \hat{B}_k(t) \hat{B}_{k'}(t-s) \right] \hat{S}_{k'}(t-s) \hat{\rho}_S(t) \hat{S}_k(t) \right) ds. \quad (1.62) \end{aligned}$$

Regarding equation (1.62), we make the following observation: The influence of the bath on the system appears only through the *bath correlation functions*

$$\mathcal{B}_{kk'}(t, t-s) := \left\langle \hat{B}_k(t) \hat{B}_{k'}(t-s) \right\rangle = \text{Tr} \left[\hat{\rho}_B \hat{B}_k(t) \hat{B}_{k'}(t-s) \right]. \quad (1.63)$$

As we assumed the density matrix of the heat bath $\hat{\rho}_B$ to be stationary, the correlation function

$$\mathcal{B}_{kk'}(t, t-s) = \left\langle \hat{B}_k(t) \hat{B}_{k'}(t-s) \right\rangle = \left\langle \hat{B}_k(s) \hat{B}_{k'}(0) \right\rangle = \mathcal{B}_{kk'}(s, 0) \quad (1.64)$$

only depends on the time difference s and hence, we can drop the second argument $\mathcal{B}_{kk'}(s) := \mathcal{B}_{kk'}(s, 0)$. Then, equation (1.62) can be written in the form

$$\dot{\hat{\rho}}_S(t) = g^2 \sum_{k,k'} \int_0^\infty \mathcal{B}_{kk'}(s) \left(\hat{S}_{k'}(t-s) \hat{\rho}_S(t) \hat{S}_k(t) - \hat{S}_k(t) \hat{S}_{k'}(t-s) \hat{\rho}_S(t) \right) ds + \text{H.c.} \quad (1.65)$$

where H.c. denotes the Hermitian conjugate of the first term. As mentioned in section 3.7, equation (1.59), and consequently equation (1.65), can not be written in Lindblad form.

3.9 Quantum Adiabatic Markovian Master Equations

In many cases, the quantum system of interest undergoes an external drive which causes its Hamiltonian $\hat{H}_S = \hat{H}_S(t)$ to be time-dependent. There are different options to tackle such problems like the time-dependent Redfield master equation or path integral methods (see sections 3.7 and 3.13). Here, I review a very useful master equation

approach proposed by T. Albash et al. which relies on an *adiabatic approximation* [54].

We assume the Hamiltonian $\hat{H}(t)$ of the total system formed by the time-dependent quantum system of interest and its time-independent environment to be of the form

$$\hat{H}(t) = \hat{H}_S(t) + \hat{H}_B + \hat{H}_{\text{int}} \quad (1.66)$$

with

$$\hat{H}_{\text{int}} = g \sum_k \hat{S}_k \otimes \hat{B}_k. \quad (1.67)$$

The first steps of the derivation are similar to the derivation of the Redfield master equation (1.58): We transform the Liouville-Von-Neumann equation (1.15) to interaction picture using the unitary

$$\hat{U}_0(t, t') := \hat{U}_S(t, t') \otimes \hat{U}_B(t, t') = \hat{\mathcal{T}} e^{-i \int_{t'}^t \hat{H}_S(s) ds} \otimes e^{-i \hat{H}_B t} \quad (1.68)$$

and follow the same strategy as in section (3.7), we find equation (1.57)

$$\dot{\rho}_S^{\text{I}}(t) = - \int_0^t \text{Tr}_B \left[\hat{H}_{\text{int}}^{\text{I}}(t), \left[\hat{H}_{\text{int}}^{\text{I}}(t-s), \hat{\rho}_S(t-s) \otimes \hat{\rho}_B \right] \right] ds. \quad (1.69)$$

Here, the index I indicates the interaction picture¹ and we substituted the variable s by $t-s$. Inserting equation (1.67) into equation (1.69) we find after some algebra

$$\begin{aligned} \dot{\rho}_S^{\text{I}}(t) = g^2 \sum_{k, k'} \int_0^t & \left(\left(\hat{S}_{k'}^{\text{I}}(t-s) \hat{\rho}_S^{\text{I}}(t-s) \hat{S}_k^{\text{I}}(t) - \hat{S}_k^{\text{I}}(t) \hat{S}_{k'}^{\text{I}}(t-s) \hat{\rho}_S^{\text{I}}(t-s) \right) \mathcal{B}_{kk'}(s) \right. \\ & \left. + \left(\hat{S}_k^{\text{I}}(t) \hat{\rho}_S^{\text{I}}(t-s) \hat{S}_{k'}^{\text{I}}(t-s) - \hat{\rho}_S^{\text{I}}(t-s) \hat{S}_{k'}^{\text{I}}(t-s) \hat{S}_k^{\text{I}}(t) \right) \mathcal{B}_{k'k}(s) \right) ds, \end{aligned} \quad (1.70)$$

where $\mathcal{B}_{kk'}(s)$ denotes the bath correlation function defined in equation (1.63). Equation (1.70) looks similar to equation (1.65), but it is not as there was no Markovian approximation made yet.

Now, we shall replace the operator $\hat{S}_{k'}^{\text{I}}(t-s) = \hat{U}_S^\dagger(t-s, 0) \hat{S}_{k'} \hat{U}_S(t-s, 0)$ by an appropriate *adiabatic approximation* to take it in front of the integral. To do so, we have to talk about the *adiabatic limit* first.

3.9.1 Adiabatic Limit

Let $\{|\epsilon_a(t)\rangle\}$ be the instantaneous eigenbasis of $\hat{H}_S(t)$ with the corresponding eigenvalues $\hat{H}_S(t)|\epsilon_a(t)\rangle = \epsilon_a(t)|\epsilon_a(t)\rangle$ and Bohr frequencies $\omega_{ba}(t) = \epsilon_b(t) - \epsilon_a(t)$. The unitary $\hat{U}_S(t, t')$ follows the Schrödinger equation

$$\begin{aligned} i \frac{\partial}{\partial t} \hat{U}_S(t, t') &= \hat{H}_S(t) \hat{U}_S(t, t') \\ &= \sum_a \epsilon_a(t) |\epsilon_a(t)\rangle \langle \epsilon_a(t)| \hat{U}_S(t, t'). \end{aligned} \quad (1.71)$$

¹We keep the index I this time to avoid confusion in the end.

It can be written as the ideal *adiabatic propagator* $\hat{U}_S^{\text{ad}}(t, t')$ plus an error term

$$\hat{U}_S(t, t') = \hat{U}_S^{\text{ad}}(t, t') + \mathcal{O}\left(\frac{h}{\Delta^2 t_f}\right), \quad (1.72)$$

where we introduced the definitions

$$\hat{U}_S^{\text{ad}}(t, t') := \sum_a |\epsilon_a(t)\rangle \langle \epsilon_a(t)| e^{-i\mu_a(t, t')}, \quad (1.73)$$

$$\Delta := \min_{t \in [0, t_f]} \epsilon_1(t) - \epsilon_0(t) \quad (1.74)$$

$$\mu_a(t, t') := \int_{t'}^t \epsilon_a(\tau) - \phi_a(\tau) d\tau \quad (1.75)$$

$$\phi_a(t) := i \langle \epsilon_a(t) | \dot{\epsilon}_a(t) \rangle \quad (1.76)$$

$$h := \max_{\substack{\tau \in [0, 1] \\ a, b}} \left| \left\langle \epsilon_a(\tau) \left| \frac{\partial}{\partial \tau} \hat{H}_S(\tau) \right| \epsilon_b(\tau) \right\rangle \right|. \quad (1.77)$$

Here, $\epsilon_0(t)$ and $\epsilon_1(t)$ denote the energies of the instantaneous ground and first excited state of $\hat{H}_S(t)$ respectively. Additionally, we set the dimensionless time $\tau := t/t_f$, where t_f denotes the final time of the adiabatic time evolution¹. In the following, we derive equation (1.72). First, we define the *adiabatic intertwiner* $\hat{W}(t, t')$ by

$$\hat{W}(t, t') := \sum_a |\epsilon_a(t)\rangle \langle \epsilon_a(t)| = \hat{\mathcal{T}} \exp \left[-i \int_{t'}^t \hat{K}(s) ds \right] \quad (1.78)$$

and the *adiabatic Hamiltonian*

$$\hat{K}(t) := i \left[\frac{\partial}{\partial t} \hat{W}(t, t') \right] \hat{W}^\dagger(t, t') = i \sum_a |\dot{\epsilon}_a(t)\rangle \langle \epsilon_a(t)|. \quad (1.79)$$

To extract the geometric phase we define further

$$\hat{H}_G(t) := \sum_a \phi_a(t) |\epsilon_a(t)\rangle \langle \epsilon_a(t)| \quad (1.80)$$

and

$$\hat{H}'_S(t) := \hat{H}_S(t) - \hat{H}_G(t) \quad (1.81)$$

as well as the operator $\hat{V}(t, t')$ via the transform to the *adiabatic interaction picture*

$$\hat{V}(t, t') = \hat{W}^\dagger(t, t') \hat{U}_S(t, t'). \quad (1.82)$$

¹In quantum annealing literature, and particularly in Ref. [54] where this derivation was taken, the usual term for the dimensionless time is s . We used τ instead to avoid confusion with the s as the integration variable in equations like (1.70).

We find the transformation rules

$$\hat{\hat{H}}_S(t, t') = \hat{W}^\dagger(t, t') \hat{H}_S(t) \hat{W}(t, t') = \sum_a \epsilon_a(t) |\epsilon_a(t')\rangle \langle \epsilon_a(t')|, \quad (1.83)$$

$$\hat{\hat{H}}_G(t, t') = \hat{W}^\dagger(t, t') \hat{H}_G(t) \hat{W}(t, t') = \sum_a \phi_a(t) |\epsilon_a(t')\rangle \langle \epsilon_a(t')|, \quad (1.84)$$

$$\hat{\hat{H}}'_S(t, t') = \hat{\hat{H}}_S(t) - \hat{\hat{H}}_G(t), \quad (1.85)$$

$$\hat{\hat{K}}(t, t') = \hat{W}^\dagger(t, t') \hat{K}(t) \hat{W}(t, t') = i \hat{W}^\dagger(t, t') \frac{\partial}{\partial t} \hat{W}(t, t'). \quad (1.86)$$

Note that the time dependence of the operators $\hat{\hat{H}}_S(t, t')$ and $\hat{\hat{H}}'_S(t, t')$ is completely determined by the time dependence of their corresponding eigenvalues. Hence, $\hat{V}(t, t')$ follows the equation

$$i \frac{\partial}{\partial t} \hat{V}(t, t') = \hat{\hat{H}}_S^{\text{ad}}(t, t') \hat{V}(t, t') \quad (1.87)$$

where

$$\hat{\hat{H}}_S^{\text{ad}}(t, t') := \hat{\hat{H}}_S(t, t') - \hat{\hat{K}}(t, t'). \quad (1.88)$$

If the time evolution is nearly adiabatic, then $\hat{\hat{H}}_S^{\text{ad}}(t, t')$ can only represent a weak disturbance. Therefore, we can use the ansatz

$$\hat{V}(t, t') = \hat{V}_0(t, t') \left(\hat{\mathbb{I}} + \hat{V}_1(t, t') + \dots \right). \quad (1.89)$$

Here, the first term represents the pure adiabatic time evolution including the geometric phase

$$\hat{V}_0(t, t') := \hat{\mathcal{T}} \exp \left[-i \int_{t'}^t \hat{\hat{H}}'_S(s, t') ds \right] \quad (1.90)$$

and hence

$$\hat{\hat{U}}_S^{\text{ad}}(t, t') := \hat{W}(t, t') \hat{V}_0(t, t') = \sum_a |\epsilon_a(t)\rangle \langle \epsilon_a(t')| e^{-i \int_{t'}^t \epsilon_a(s) - \phi_a(s) ds}. \quad (1.91)$$

If we derive equation (1.91) with respect to t we find the differential equation

$$\begin{aligned} \dot{\hat{\hat{U}}}_S^{\text{ad}}(t, t') &= \dot{\hat{W}}(t, t') \hat{V}_0(t, t') + \hat{W}(t, t') \dot{\hat{V}}_0(t, t') \\ &= -i \hat{\hat{K}}(t) \hat{W}(t, t') \hat{V}_0(t, t') - i \hat{W}(t, t') \hat{\hat{H}}'_S(t, t') \hat{V}_0(t, t') \\ &= -i \left[\hat{\hat{H}}_S^{\text{ad}}(t) - \hat{\hat{H}}_G(t) \right] \hat{\hat{U}}_S^{\text{ad}}(t, t'), \end{aligned} \quad (1.92)$$

where

$$\hat{\hat{H}}_S^{\text{ad}}(t) := \hat{\hat{K}}(t) + \hat{\hat{H}}_S(t). \quad (1.93)$$

Inserting (1.89) into equation (1.87) leads after some algebra using the identities (1.85) and (1.88)

$$\begin{aligned}
i\dot{\hat{V}}_1(t, t') \left(\hat{\mathbb{I}} + \hat{V}_2(t, t') + \dots \right) &= \hat{V}_0^\dagger(t, t') \hat{H}_S^{\text{ad}}(t, t') \hat{V}_0(t, t') \left(\hat{\mathbb{I}} + \hat{V}_1(t, t') + \dots \right) \\
&\quad - \hat{V}_0^\dagger(t, t') \hat{H}'_S(t, t') \hat{V}_0(t, t') \left(\hat{\mathbb{I}} + \hat{V}_1(t, t') + \dots \right) \\
&= -\hat{V}_0^\dagger(t, t') \left[\hat{K}(t, t') - \hat{H}_G(t, t') \right] \hat{V}_0(t, t') \\
&\quad - \hat{V}_0^\dagger(t, t') \left[\hat{K}(t, t') - \hat{H}_G(t, t') \right] \hat{V}_0(t, t') \hat{V}_1(t, t') + \dots
\end{aligned} \tag{1.94}$$

The expansion (1.89) is an expansion in the parameter $1/t_f$. Up to first order in $1/t_f$, equation (1.94) becomes

$$\begin{aligned}
i\dot{\hat{V}}_1(t, t') &= -\hat{V}_0^\dagger(t, t') \left[\hat{K}(t, t') - \hat{H}_G(t, t') \right] \hat{V}_0(t, t') \\
&= -i\hat{U}_S^{\text{ad}\dagger}(t, t') \hat{W}(t, t') \hat{V}_0(t, t') + \hat{U}_S^{\text{ad}\dagger}(t, t') \hat{H}_G(t) \hat{U}_S^{\text{ad}}(t, t').
\end{aligned} \tag{1.95}$$

Equation (1.95) can be integrated:

$$\begin{aligned}
\hat{V}_1(t, t') &= -\int_{t'}^t \left[\hat{U}_S^{\text{ad}\dagger}(s, t') \frac{\partial}{\partial s} \hat{W}(s, t') \hat{V}_0(s, t') - \sum_a \phi_a(s) |\epsilon_a(t')\rangle \langle \epsilon_a(t')| \right] ds \\
&= -\sum_{a \neq b} \int_{t'}^t e^{-i\mu_{ba}(s, t')} |\epsilon_a(t')\rangle \langle \epsilon_b(t')| \langle \epsilon_a(s) | \dot{\epsilon}_b(s) \rangle ds,
\end{aligned} \tag{1.96}$$

because

$$\hat{U}_S^{\text{ad}\dagger}(t, t') \hat{H}_G(t) \hat{U}_S^{\text{ad}}(t, t') = \sum_a \phi_a(t') |\epsilon_a(t')\rangle \langle \epsilon_a(t')| \tag{1.97}$$

holds. Here, we defined

$$\mu_{ba}(t, t') := \int_{t'}^t ([\epsilon_b(s) - \phi_b(s)] - [\epsilon_a(s) - \phi_a(s)]) ds. \tag{1.98}$$

Now, we can write the system propagator $\hat{U}_S(t, t')$ as

$$\hat{U}_S(t, t') = \hat{U}_S^{\text{ad}}(t, t') + Q(t, t') \hat{U}_S^{\text{ad}}(t, t') + \mathcal{O} \left(\left(\frac{1}{t_f} \right)^2 \right), \tag{1.99}$$

with

$$\begin{aligned}
\hat{Q}(t, t') &:= \hat{U}_S^{\text{ad}}(t, t') \hat{V}_1(t, t') \hat{U}_S^{\text{ad}\dagger}(t, t') \\
&= \sum_{a \neq b} e^{-i\mu_{ba}(t, t')} \left(-\int_{t'}^t \langle \epsilon_a(s) | \dot{\epsilon}_b(s) \rangle ds \right) |\epsilon_a(t)\rangle \langle \epsilon_b(t')|.
\end{aligned} \tag{1.100}$$

Equation (1.99) shows, that the first order correction to the pure adiabatic time evolution is given by the operator $\hat{Q}(t, t')$ in equation (1.100). Therefore, we can find the adiabatic time scale by forcing its matrix elements to be small. In the following, we show that a sufficient condition is given by the condition $\frac{\hbar}{\Delta^2 t_f} \ll 1$.

Regarding the matrix elements of $\hat{Q}(t, t')$, we find using (1.100)

$$\hat{Q}_{ab}(t, t') = e^{-i\mu_{ba}(t, t')} \left(- \int_{t'}^t e^{i\mu_{ba}(s, t')} \langle \epsilon_a(s) | \partial_s | \epsilon_b(s) \rangle ds \right). \quad (1.101)$$

If we substitute $\tau := t/t_f$ and use the definition

$$\tilde{\mu}_{ba}(\tau, t'/t_f) := \int_{t'/t_f}^{\tau} \omega_{ba}(\tau') d\tau' = \frac{1}{t_f} \mu_{ba}(t, t'), \quad (1.102)$$

we find

$$\int_{t'}^t e^{i\mu_{ba}(s, t')} \langle \epsilon_a(s) | \partial_s | \epsilon_b(s) \rangle ds = \int_{t'/t_f}^{\tau} e^{it_f \tilde{\mu}_{ba}(\tau', t'/t_f)} \langle \epsilon_a(\tau') | \partial_{\tau'} | \epsilon_b(\tau') \rangle d\tau'. \quad (1.103)$$

Using

$$e^{it_f \tilde{\mu}_{ba}(\tau', t'/t_f)} = \frac{i}{t_f \omega_{ab}(\tau')} \frac{d}{d\tau'} e^{it_f \tilde{\mu}_{ba}(\tau', t'/t_f)} \quad (1.104)$$

we can integrate the right hand side of equation (1.103) by parts leading to

$$\begin{aligned} \int_{t'/t_f}^{\tau} e^{it_f \tilde{\mu}_{ba}(\tau', t'/t_f)} \langle \epsilon_a(\tau') | \partial_{\tau'} | \epsilon_b(\tau') \rangle d\tau' &= \frac{i}{t_f \omega_{ab}(\tau')} e^{it_f \tilde{\mu}_{ba}(\tau', t'/t_f)} \langle \epsilon_a(\tau') | \partial_{\tau'} | \epsilon_b(\tau') \rangle \Big|_{t'/t_f}^{\tau} \\ &\quad - \frac{i}{t_f} \int_{t'/t_f}^{\tau} \frac{e^{it_f \tilde{\mu}_{ba}(\tau', t'/t_f)}}{\omega_{ab}(\tau')} \frac{d}{d\tau'} \langle \epsilon_a(\tau') | \partial_{\tau'} | \epsilon_b(\tau') \rangle d\tau'. \end{aligned} \quad (1.105)$$

If $|\epsilon_a(t)\rangle$ and $|\epsilon_b(t)\rangle$ are not degenerate, then

$$\langle \epsilon_b(t) | \dot{\epsilon}_a(t) \rangle = \frac{\langle \epsilon_b(t) | \dot{\hat{H}}_S(t) | \epsilon_a(t) \rangle}{\omega_{ab}(t)}, \quad (1.106)$$

because

$$\begin{aligned} &\hat{H}_S(t) | \epsilon_a(t) \rangle = \epsilon_a(t) | \epsilon_a(t) \rangle \\ \Rightarrow &\dot{\hat{H}}_S(t) | \epsilon_a(t) \rangle + \hat{H}_S(t) | \dot{\epsilon}_a(t) \rangle = \dot{\epsilon}_a(t) | \epsilon_a(t) \rangle + \epsilon_a(t) | \dot{\epsilon}_a(t) \rangle \\ \Rightarrow &\langle \epsilon_b(t) | \dot{\hat{H}}_S(t) | \epsilon_a(t) \rangle + \epsilon_b(t) \langle \epsilon_b(t) | \dot{\epsilon}_a(t) \rangle = \dot{\epsilon}_a(t) \delta_{ab} + \epsilon_a(t) \langle \epsilon_b(t) | \dot{\epsilon}_a(t) \rangle \\ \Rightarrow &\langle \epsilon_b(t) | \dot{\epsilon}_a(t) \rangle = \frac{\langle \epsilon_b(t) | \dot{\hat{H}}_S(t) | \epsilon_a(t) \rangle}{\epsilon_b(t) - \epsilon_a(t)}. \end{aligned}$$

Now, we have all the ingredients to bound the matrix elements (1.101):

$$\begin{aligned}
\left| \hat{Q}_{ab}(t, t') \right| &\stackrel{(1.105)}{\leq} \left| \frac{\langle \epsilon_a(\tau') | \partial_{\tau'} | \epsilon_b(\tau') \rangle}{t_f \omega_{ab}(\tau')} \right| \Big|_{\frac{t'}{t_f}}^{\tau} + \left| \int_{\frac{t'}{t_f}}^{\tau} \frac{e^{it_f \bar{\mu}_{ba}(\tau', t'/t_f)}}{t_f \omega_{ab}(\tau')} \frac{d}{d\tau'} \langle \epsilon_a(\tau') | \partial_{\tau'} | \epsilon_b(\tau') \rangle \right| \\
&\stackrel{(1.106)}{=} \underbrace{\left| \frac{\langle \epsilon_a(\tau') | \partial_{\tau'} \hat{H}_S(\tau') | \epsilon_b(\tau') \rangle}{t_f \omega_{ab}^2(\tau')} \right|}_{=:\xi} \Big|_{\frac{t'}{t_f}}^{\frac{t'}{t_f}} \\
&\quad + \left| \int_{\frac{t'}{t_f}}^{\frac{t'}{t_f}} \frac{e^{it_f \bar{\mu}_{ba}(\tau', t'/t_f)}}{t_f \omega_{ab}^2(\tau')} \frac{d}{d\tau'} \langle \epsilon_a(\tau') | \partial_{\tau'} \hat{H}_S(\tau') | \epsilon_b(\tau') \rangle \right|. \quad (1.107)
\end{aligned}$$

Iterative integration by parts of the second term in equation (1.107) always leads to increasing powers of the dimensionless number ξ . Therefore, the matrix element $\left| \hat{Q}_{ab}(t, t') \right|$ is small for all a and b , if the sufficient condition

$$\max_{\substack{\tau' \in [0,1] \\ a,b}} |\langle \epsilon_a(\tau') | \partial_{\tau'} \hat{H}_S(\tau') | \epsilon_b(\tau') \rangle| \Big/ \min_{\substack{\tau' \in [0,1] \\ a,b}} t_f \omega_{ab}^2(\tau') \ll 1 \quad (1.108)$$

is satisfied. If we assume that the minimal Bohr frequency equals the gap between ground state and first excited state Δ , then (1.108) means

$$\frac{\hbar}{\Delta^2 t_f} \ll 1, \quad (1.109)$$

with which we have derived equation (1.72).

3.9.2 Derivation of the Master Equation

In the adiabatic limit, which is defined by the inequalities (1.108) respectively (1.109), we can now go ahead to derive the desired quantum master equation. To do so, we shall express the integrals in equation (1.70) by the one-sided Fourier transform¹

$$\Gamma_{kk'}(\omega) := \int_0^{\infty} e^{i\omega s} \mathcal{B}_{kk'}(s) ds. \quad (1.110)$$

It can be written as a sum of Hermitian matrices with the use of the *spectral function*

$$\gamma_{kk'}(\omega) := \int_{-\infty}^{\infty} e^{i\omega s} \mathcal{B}_{kk'}(s) ds = \gamma_{k'k}^*(\omega) \quad (1.111)$$

and

$$S_{kk'}(\omega) := \frac{1}{2\pi} \int_{-\infty}^{\infty} \gamma_{kk'}(\omega') \mathcal{P} \left(\frac{1}{\omega - \omega'} \right) d\omega' = S_{k'k}^*(\omega) \quad (1.112)$$

¹The one-sided Fourier transform $\Gamma_{kk'}(\omega)$ is called *spectral density matrix* or *spectral function* depending on author and context. Here, we follow the terminology of Ref. [54], where »spectral density matrix« refers to $\Gamma_{kk'}(\omega)$ and »spectral function« to $\gamma_{kk'}(\omega)$.

as

$$\begin{aligned}
\Gamma_{kk'}(\omega) &= \int_0^\infty e^{i\omega s} \left(\frac{1}{2\pi} \int_{-\infty}^\infty \gamma_{kk'}(\omega') e^{-i\omega' s} d\omega' \right) ds \\
&= \int_{-\infty}^\infty \frac{\gamma_{kk'}(\omega')}{2\pi} \left(\int_0^\infty e^{i(\omega-\omega')s} ds \right) d\omega' \\
&\stackrel{(*)}{=} \frac{1}{2} \gamma_{kk'}(\omega) + iS_{kk'}(\omega).
\end{aligned} \tag{1.113}$$

In (*), we used the well-known relation

$$\int_0^\infty e^{i(\omega-\omega')s} ds = \pi\delta(\omega-\omega') + i\mathcal{P} \left(\frac{1}{\omega-\omega'} \right) \tag{1.114}$$

with the Dirac δ -function and the Cauchy principle value $\mathcal{P}(\cdot)$.

As mentioned before, the strategy is to replace the operator $\hat{S}_{k'}^I(t-s) = \hat{U}_S^\dagger(t-s, 0) \hat{S}_{k'} \hat{U}_S(t-s, 0)$ by an appropriate adiabatic approximation to take it in front of the integral. To do this, we decompose the system propagator

$$\hat{U}_S(t-s, 0) = \hat{U}_S(t-s, t) \hat{U}_S(t, 0) = \hat{U}_S^\dagger(t, t-s) \hat{U}_S(t, 0), \tag{1.115}$$

and we replace $\hat{U}_S(t, 0)$ by

$$\hat{U}_S(t, 0) \rightarrow \hat{U}_S^{\text{ad}}(t, 0), \tag{1.116}$$

where $\hat{U}_S^{\text{ad}}(t, 0)$ is the ideal *adiabatic propagator* defined in equation (1.73) and the order of the error caused by this approximation is given by equation (1.72). Additionally, we replace $\hat{U}_S^\dagger(t, t-s)$ by

$$\hat{U}_S^\dagger(t, t-s) \rightarrow e^{is\hat{H}_S(t)}. \tag{1.117}$$

This approximation is called *adiabatic Markovian approximation*. Here, s sets a time scale of the interaction between system and heat bath over which the system Hamiltonian $\hat{H}_S(t)$ can be treated as a constant. Hence, it can be evaluated at any time, conveniently at the instantaneous time t . The error caused by this approximation is bounded by

$$\left\| \hat{\Theta}(t, s) \right\|_\infty \leq \min \left\{ 2, \frac{h}{\Delta^2 t_f} + \frac{hs^2}{t_f} \right\}, \tag{1.118}$$

where

$$\hat{\Theta}(t, s) := \hat{U}_S(t-s, 0) - e^{is\hat{H}_S(t)} \hat{U}_S^{\text{ad}}(t, 0). \tag{1.119}$$

Finally, we apply a Markovian approximation for each of the four summands in equation (1.70): If the time scale τ_B , over which the bath correlation functions decay, satisfies $\tau_B \ll \frac{1}{g}$, then we can replace $\hat{\rho}_S^I(t-s)$ by

$$\hat{\rho}_S^I(t-s) \rightarrow \hat{\rho}_S^I(t) \tag{1.120}$$

up to an error of $\mathcal{O}(\tau_{\text{B}}^3 g^2)$. Applying these approximations to the first integral of equation (1.70) we find

$$\begin{aligned} & \int_0^\infty \hat{S}_{k'}^{\text{I}}(t-s) \hat{\rho}_{\text{S}}^{\text{I}}(t-s) \hat{S}_k^{\text{I}}(t) \mathcal{B}_{kk'}(s) ds \\ &= \int_0^\infty \hat{U}_{\text{S}}^\dagger(t-s, 0) \hat{S}_{k'} \hat{U}_{\text{S}}(t-s, 0) \hat{\rho}_{\text{S}}^{\text{I}}(t) \hat{S}_k^{\text{I}}(t) \mathcal{B}_{kk'}(s) ds + \mathcal{O}(\tau_{\text{B}}^3 g^2) \\ &\approx \int_0^\infty \hat{U}_{\text{S}}^{\text{ad}\dagger}(t, 0) e^{-is\hat{H}_{\text{S}}(t)} \hat{S}_{k'} e^{is\hat{H}_{\text{S}}(t)} \hat{U}_{\text{S}}^{\text{ad}}(t, 0) \hat{\rho}_{\text{S}}^{\text{I}}(t) \hat{S}_k^{\text{I}}(t) \mathcal{B}_{kk'}(s) ds. \end{aligned} \quad (1.121)$$

Now, we replace the operator $\hat{U}_{\text{S}}^{\text{ad}}(t, 0)$ according to its definition (1.73) and make use of the equation $\hat{H}_{\text{S}}(t)|\epsilon_a(t)\rangle = \epsilon_a(t)|\epsilon_a(t)\rangle$. We find

$$\begin{aligned} & \int_0^\infty \hat{S}_{k'}^{\text{I}}(t-s) \hat{\rho}_{\text{S}}^{\text{I}}(t-s) \hat{S}_k^{\text{I}}(t) \mathcal{B}_{kk'}(s) ds \\ &\approx \sum_{a,b} e^{-i\mu_{ba}(t,0)} |\epsilon_a(0)\rangle \langle \epsilon_a(t) | \hat{S}_{k'} | \epsilon_b(t) \rangle \langle \epsilon_b(0) | \hat{\rho}_{\text{S}}^{\text{I}}(t) \hat{S}_k^{\text{I}}(t) \int_0^\infty e^{is(\epsilon_b(t) - \epsilon_a(t))} ds \\ &= \sum_{a,b} e^{-i\mu_{ba}(t,0)} S_{k'ab}(t) \hat{\Pi}_{ab}(0) \hat{\rho}_{\text{S}}^{\text{I}}(t) \hat{S}_k^{\text{I}}(t) \Gamma_{kk'}(\omega_{ba}(t)), \end{aligned} \quad (1.122)$$

where

$$S_{k'ab}(t) := \langle \epsilon_a(t) | \hat{S}_{k'} | \epsilon_b(t) \rangle = S_{k'ba}^*(t) \quad (1.123)$$

$$\hat{\Pi}_{ab}(t) := |\epsilon_a(t)\rangle \langle \epsilon_b(t)|. \quad (1.124)$$

A similar derivation can be made for the second integral in equation (1.70). The result is

$$\begin{aligned} & \int_0^\infty \hat{S}_k^{\text{I}}(t) \hat{S}_{k'}^{\text{I}}(t-s) \hat{\rho}_{\text{S}}^{\text{I}}(t-s) \mathcal{B}_{kk'}(s) \\ &\approx \sum_{a,b} e^{-i\mu_{ba}(t,0)} S_{k'ab}(t) \hat{S}_k^{\text{I}}(t) \hat{\Pi}_{ab}(0) \hat{\rho}_{\text{S}}^{\text{I}}(t) \Gamma_{kk'}(\omega_{ba}(t)). \end{aligned} \quad (1.125)$$

The third and the fourth integral in (1.70) are the Hermitian conjugates of the first two. Now, we insert the approximations of the four integrals into equation (1.70). After some algebra, we derived the one-sided adiabatic master equation in the interaction picture

$$\begin{aligned} \dot{\hat{\rho}}_{\text{S}}^{\text{I}}(t) &= g^2 \left(\sum_{a,b} e^{-i\mu_{ba}(t,0)} \sum_{k,k'} \Gamma_{kk'}(\omega_{ba}(t)) S_{k'ab}(t) \left[\hat{\Pi}_{ab}(0) \hat{\rho}_{\text{S}}^{\text{I}}(t), \hat{S}_k^{\text{I}}(t) \right] \right. \\ &\quad \left. + \sum_{a,b} e^{i\mu_{ba}(t,0)} \sum_{k,k'} \Gamma_{kk'}^*(\omega_{ba}(t)) S_{k'ab}^*(t) \left[\hat{S}_k^{\text{I}}(t), \hat{\rho}_{\text{S}}^{\text{I}}(t) \hat{\Pi}_{ba}(0) \right] \right). \end{aligned} \quad (1.126)$$

The same approximations which have been applied to $\hat{S}_{k'}^{\text{I}}(t-s)$ can also be applied to $\hat{S}_k^{\text{I}}(t)$. Doing so in equation (1.126), and transforming this equation back to Schrödinger picture, it is straightforward to derive the desired quantum adiabatic

Markovian master equation

$$\begin{aligned} \dot{\hat{\rho}}_S(t) = & -i \left[\hat{H}_S(t), \hat{\rho}_S(t) \right] + g^2 \left(\sum_{a,b} \sum_{k,k'} \Gamma_{kk'}(\omega_{ba}(t)) \left[\hat{L}_{ab,k'}(t) \hat{\rho}_S(t), \hat{S}_k \right] \right. \\ & \left. + \sum_{a,b} \sum_{k,k'} \Gamma_{kk'}^*(\omega_{ba}(t)) \left[\hat{S}_k, \hat{\rho}_S(t) \hat{L}_{ab,k'}^\dagger(t) \right] \right) \end{aligned} \quad (1.127)$$

with the definition

$$\hat{L}_{ab,k}(t) := S_{kab}(t) |\epsilon_a(t)\rangle \langle \epsilon_b(t)| = \hat{L}_{ba,k}^\dagger(t). \quad (1.128)$$

For more details we refer again to Ref. [54]. The final master equation (1.127) is not in Lindblad form. To achieve this, we further have to apply the secular approximation to it, like it has been the case for the Bloch-Redfield equation (1.58).

3.10 The Secular Approximation

The secular approximation is needed to achieve Lindblad form as well for the Redfield master equation as for the adiabatic master equation. It discards fast oscillating terms which average out on the time scale of interest. Hence, the idea is similar to the well-known *rotating-wave approximation (RWA)* [55]. However, the secular approximation is carried out on the level of the quantum master equation rather than on the level on the interaction Hamiltonian as this can cause problems which are discussed in Ref. [56]. To apply the secular approximation, we again follow Ref. [54] for the adiabatic master equation. The derivation for the Redfield master equation can be found in Ref. [26] and is similar to the version which will be reviewed briefly here.

Suppose we follow the arguments leading to equation (1.121) but without the limit $t \rightarrow \infty$. This yields

$$\begin{aligned} & \int_0^t \hat{S}_{k'}^I(t-s) \hat{\rho}_S^I(t-s) \hat{S}_k^I(t) \mathcal{B}_{kk'}(s) ds \\ & \approx \int_0^t \sum_{abcd} e^{-i(\mu_{ba}(t,0) + \mu_{cd}(t,0))} |\epsilon_a(0)\rangle \langle \epsilon_a(t)| \hat{S}_{k'}^I | \epsilon_b(t)\rangle \langle \epsilon_b(0)| \hat{\rho}_S^I(t) | \epsilon_c(0)\rangle \times \\ & \quad \times \langle \epsilon_c(t)| \hat{S}_k^I | \epsilon_d(t)\rangle \langle \epsilon_d(0)| e^{i\omega_{ba}(t)s} \mathcal{B}_{kk'}(s) ds. \end{aligned} \quad (1.129)$$

One can now make the argument that when the $t \rightarrow \infty$ limit is taken, terms for which the integrand vanishes will dominate, thus enforcing the "energy conservation" condition $\omega_{ba} = -\omega_{dc}$. This is a similar rotating wave approximation as made in the standard time-independent treatment, although here, the approximation of phase cancellation is made along the entire time evolution of the instantaneous energy eigenstates¹. In the $t \rightarrow \infty$ limit, we find

$$\begin{aligned} & \int_0^t \hat{S}_{k'}^I(t-s) \hat{\rho}_S^I(t-s) \hat{S}_k^I(t) \mathcal{B}_{kk'}(s) ds \\ & \approx \sum_{\omega(t)} S_{\omega(t),k'} S_{\omega(t),k} \hat{\Pi}_{\omega(t)}(0) \hat{\rho}_S^I(t) \hat{\Pi}_{\omega(t)}(0) \Gamma_{kk'}(\omega(t)) \end{aligned} \quad (1.130)$$

¹This is a questionable approximation. For instance, the harmonic oscillator fails to meet this condition dramatically. However, for qubit systems, the approximation typically holds if they do not experience effects like frequency crowding during the complete time-evolution.

where we defined

$$S_{\omega(t),k} := \sum_{a,b} \sum_{\epsilon_b(t) - \epsilon_a(t) = \omega(t)} \langle \epsilon_a(t) | \hat{S}_k | \epsilon_b(t) \rangle \quad (1.131)$$

$$\hat{\Pi}_{\omega(t)}(0) := \sum_{a,b} \sum_{\epsilon_b(t) - \epsilon_a(t) = \omega(t)} |\epsilon_a(0)\rangle \langle \epsilon_b(0)|. \quad (1.132)$$

An analogue calculation as in section 3.9.2 leads to the quantum adiabatic Markovian master equation in Lindblad form

$$\begin{aligned} \dot{\hat{\rho}}_S(t) = & -i \left[\hat{H}_S(t) + \hat{H}_{LS}(t), \hat{\rho}_S(t) \right] \\ & + \sum_{\omega(t)} \sum_{k,k'} \gamma_{kk'}(\omega(t)) \left(\hat{L}_{\omega(t),k'}(t) \hat{\rho}_S(t) \hat{L}_{\omega(t),k}^\dagger(t) + \frac{1}{2} \left\{ \hat{L}_{\omega(t),k}^\dagger(t) \hat{L}_{\omega(t),k'}(t), \hat{\rho}_S(t) \right\} \right), \end{aligned} \quad (1.133)$$

where

$$\hat{H}_{LS}(t) := \sum_{\omega(t)} \sum_{k,k'} \hat{L}_{\omega(t),k}^\dagger(t) \hat{L}_{\omega(t),k'}(t) S_{kk'}(\omega(t)) \quad (1.134)$$

denotes the Lamb shift and we have defined

$$\hat{L}_{\omega(t),k}(t) := \sum_{a,b} \sum_{\epsilon_b(t) - \epsilon_a(t) = \omega(t)} \hat{L}_{ab,k}(t). \quad (1.135)$$

Equation (1.133) is transformed back to Schrödinger picture already. It is in Lindblad form and hence preserves the positivity of the density matrix. The secular approximation has been shown here in a very dense fashion. We recommend Ref. [54] for more details.

3.11 Comparison of Master Equations

In section 3.6, I have reviewed the proof of the Lindblad theorem that states that any master equation, which guarantees to preserve the properties of density matrices, can be written in Lindblad form. Therefore, the Lindblad master equation (1.50) is the tool of choice for simulating open quantum system dynamics if its conditions are fulfilled. However, the Born approximation, the Markov approximation and the secular approximation need to be made to derive a quantum master equation in Lindblad form for the reduced system starting from a microscopic model: As it is typically not possible to solve the complete Liouville-Von Neumann equation (1.15) for system and bath, we have to apply the Born and the Markov approximation to trace out the heat bath resulting in the Redfield master equation (1.65). This procedure causes two kinds of drawbacks: First, the conditions of these approximations have to be satisfied to get the correct time evolution of the state, and second, we lost the desired Lindblad form¹. Hence, the outcome of the Redfield master equation might be not a valid density matrix and hence, it does not represent a valid physical state. This drawback can be overcome by a further approximation, namely the secular approximation discussed

¹It is possible to achieve Lindblad form by a different but less popular approach pursued in Ref. [57]. Here, the authors perform the Born and Markov approximations in a different way such that the resulting master equation preserves positivity.

in section 3.10. Obviously, this causes an additional approximation error and hence, this procedure is questionable¹.

The adiabatic master equation of Ref. [54], which I have reviewed in section 3.9, is a useful tool for simulating time-dependent open quantum systems in the adiabatic limit. Nevertheless, it relies on a bunch of uncontrolled approximations too and hence, its use is only reliably justified if its conditions are satisfied. Particularly, the secular approximation is even more questionable compared to the time-independent case.

To conclude, all the presented master equations have their own benefits and drawbacks. Therefore, the answer to the question "Which one is the best?" will strongly depend on the system of interest and it might happen, that none of these are reliably applicable. However, it is legitimate to use them anyways, if there is no other tool available². In this case, their predictions need to be judged by experiments.

3.12 Harmonic Baths

To solve any of the equations (1.65), (1.127) or (1.133), an expression for the bath correlation function $\mathcal{B}_{kk'}(s)$ is needed. Hence, it is crucial to find a model for the heat bath. A widely applicable model is to write down the bath Hamiltonian \hat{H}_B as a sum of non-interacting harmonical oscillators

$$\hat{H}_B := \sum_j \omega_j \hat{b}_j^\dagger \hat{b}_j. \quad (1.136)$$

Here, \hat{b}_j and \hat{b}_j^\dagger denote the annihilation and the creation operator of the j -th oscillator mode at frequency ω_j . Even though this model looks quite artificial and specific, it applies as long as the heat bath can be treated within linear response theory, meaning that it is essentially infinite, has a regular spectrum, and is in thermal equilibrium [58, 59]. In this setting, the central limit theorem applies. Hence, all the bath fluctuations are Gaussian distributed and therefore, can be modeled by harmonical oscillators. We derive the general form of the correlation function $\mathcal{B}_{kk'}(s)$ for harmonic baths in the following.

We insert equations (1.136) and (1.52) into equation (1.51) and obtain

$$\hat{H} = \hat{H}_S + \sum_j \omega_j \hat{b}_j^\dagger \hat{b}_j + \sum_i \hat{S}_i \hat{B}_i, \quad (1.137)$$

with appropriate system and bath operators \hat{S}_i and \hat{B}_i whose sum describes a bilinear interaction between system and bath. Note that the system Hamiltonian \hat{H}_S may depend on time i.e. if a laser drive is applied. For simplicity, we restrict ourselves to the case with only a single coupling term. The derivation generalizes trivially to more terms. For a suitable choice operators \hat{b}_k , the bath operator \hat{B} equals

$$\hat{B} = \sum_k \lambda_k \left(\hat{b}_k + \hat{b}_k^\dagger \right). \quad (1.138)$$

This assumption can always be satisfied³. We can choose λ_k real as it is just a global phase (corresponding to the choice of zero of time and energy).

¹The secular approximation is typically performed off the cuff by neglecting "fast oscillating terms" and hence, the approximation error is typically uncontrolled.

²In some cases, path integral methods can do the job.

³For Gaussian noise, it needs to be a quadrature $\lambda_k \hat{b}_k + \text{H.c.}$

First, we transform the Hamiltonian \hat{H} to the interaction picture with respect to $\hat{H}_0 := \hat{H}_S + \hat{H}_B$. The time evolution is then given by

$$\hat{H}_{\text{int}}(t) = \underbrace{\hat{U}_S^\dagger(t, 0) \hat{S} \hat{U}_S(t, 0)}_{=: \hat{S}(t)} \cdot \underbrace{e^{i\hat{H}_B t} \hat{B} e^{-i\hat{H}_B t}}_{=: \hat{B}(t)}, \quad (1.139)$$

where $\hat{U}_S(t, 0)$ denotes the propagator of the quantum system only. We calculate

$$\begin{aligned} \hat{B}(t) &= e^{i\sum_j \omega_j \hat{b}_j^\dagger \hat{b}_j t} \left(\sum_k \lambda_k (\hat{b}_k + \hat{b}_k^\dagger) \right) e^{-i\sum_j \omega_j \hat{b}_j^\dagger \hat{b}_j t} \\ &= \sum_k \lambda_k \prod_j e^{i\omega_j \hat{b}_j^\dagger \hat{b}_j t} (\hat{b}_k + \hat{b}_k^\dagger) \prod_j e^{-i\omega_j \hat{b}_j^\dagger \hat{b}_j t} \\ &= \sum_k \lambda_k \prod_j e^{i\omega_j \hat{b}_j^\dagger \hat{b}_j t} \underbrace{\left(\prod_{j \neq k} e^{-i\omega_j \hat{b}_j^\dagger \hat{b}_j t} \right)}_{=: e^{i\omega_k \hat{b}_k^\dagger \hat{b}_k t}} (\hat{b}_k + \hat{b}_k^\dagger) e^{-i\omega_k \hat{b}_k^\dagger \hat{b}_k t} \\ &= \sum_k \lambda_k e^{i\omega_k \hat{b}_k^\dagger \hat{b}_k t} (\hat{b}_k + \hat{b}_k^\dagger) e^{-i\omega_k \hat{b}_k^\dagger \hat{b}_k t}. \end{aligned} \quad (1.140)$$

For linear operators \hat{X} , \hat{Y} and $m \in \mathbb{N}$ we define recursively

$$[\hat{X}, \hat{Y}]_m := \left[\hat{X}, [\hat{X}, \hat{Y}]_{m-1} \right] \quad \text{with} \quad [\hat{X}, \hat{Y}]_0 = \hat{Y}. \quad (1.141)$$

Using this notation, we can write down the genral Baker-Campbell-Hausdorff formula in the form¹

$$e^{\hat{X}} \hat{Y} e^{-\hat{X}} = \sum_{m=0}^{\infty} \frac{1}{m!} [\hat{X}, \hat{Y}]_m \quad (1.142)$$

Inserting $[\hat{X}, \hat{Y}]_m = [i\omega_k t \hat{b}_k^\dagger \hat{b}_k, \hat{b}_k + \hat{b}_k^\dagger]_m = (i\omega_k t)^m \left((-1)^m \hat{b}_k + \hat{b}_k^\dagger \right)$ into equation (1.142) gives

$$\begin{aligned} e^{i\omega_k \hat{b}_k^\dagger \hat{b}_k t} (\hat{b}_k + \hat{b}_k^\dagger) e^{-i\omega_k \hat{b}_k^\dagger \hat{b}_k t} &= \sum_{m=0}^{\infty} \frac{1}{m!} [i\omega_k t \hat{b}_k^\dagger \hat{b}_k, \hat{b}_k + \hat{b}_k^\dagger]_m \\ &= (\hat{b}_k + \hat{b}_k^\dagger) \cos(\omega_k t) + i \left(-\hat{b}_k + \hat{b}_k^\dagger \right) \sin(\omega_k t) \\ &= \hat{b}_k e^{-i\omega_k t} + \hat{b}_k^\dagger e^{i\omega_k t} \end{aligned} \quad (1.143)$$

and hence

$$\hat{B}(t) = \sum_k \lambda_k \left(\hat{b}_k e^{-i\omega_k t} + \hat{b}_k^\dagger e^{i\omega_k t} \right). \quad (1.144)$$

¹We do not discuss mathematical details like convergence here. See [60] for further information.

Using equation (1.144), it is now possible to calculate the correlation function for harmonic baths $\mathcal{B}(s)$ as

$$\begin{aligned}
\mathcal{B}(s) &= \langle \hat{B}(s) \hat{B}(0) \rangle \\
&= \sum_{j,k} \lambda_j \lambda_k \langle (\hat{b}_j(s) + \hat{b}_j^\dagger(s)) (\hat{b}_k(0) + \hat{b}_k^\dagger(0)) \rangle \\
&\stackrel{(*)}{=} \sum_k \lambda_k^2 \left(\langle \hat{b}_k(s) \hat{b}_k^\dagger(0) \rangle + \langle \hat{b}_k^\dagger(s) \hat{b}_k(0) \rangle \right) \\
&= \sum_k \lambda_k^2 \left((\bar{n}_k + 1) e^{-i\omega_k s} + \bar{n}_k e^{i\omega_k s} \right), \tag{1.145}
\end{aligned}$$

where $\bar{n}_k := \langle \hat{b}_k^\dagger(0) \hat{b}_k(0) \rangle$ denotes the average number of excitations of the k -th bath mode with frequency ω_k . In step (*) we used that $\langle \hat{b}_j(s) \hat{b}_k(0) \rangle = \langle \hat{b}_j^\dagger(s) \hat{b}_k^\dagger(0) \rangle = 0$ and $\langle \hat{b}_j(s) \hat{b}_k^\dagger(0) \rangle \propto \delta_{jk}$ which are due to the thermodynamic equilibrium. Harmonic baths in thermodynamic equilibrium obey Bose-Einstein statistics, which means that \bar{n}_k equals the Bose function

$$\bar{n}_k = \bar{n}(\omega_k) = \frac{1}{e^{\hbar\beta\omega_k} - 1}, \tag{1.146}$$

where $\beta = \frac{1}{k_B T}$ denotes inverse temperature and k_B is the well-known Boltzmann constant. We define the *spectral density function*

$$J(\omega) := \sum_k \lambda_k^2 \delta(\omega - \omega_k). \tag{1.147}$$

Inserting equation (1.147) into equation (1.145) yields

$$\mathcal{B}(s) = \int_0^\infty J(\omega) \left((\bar{n}(\omega) + 1) e^{-i\omega s} + \bar{n}(\omega) e^{i\omega s} \right) d\omega. \tag{1.148}$$

All the information about the structure of a specific harmonic bath is encoded in the spectral density function $J(\omega)$. Typically, it can be treated as a continuous function.

Equation (1.148) can be simplified using

$$\bar{n}(-\omega) = \frac{1}{e^{-\hbar\beta\omega} - 1} = -\frac{e^{\hbar\beta\omega}}{e^{\hbar\beta\omega} - 1} = -\left(\frac{1}{e^{\hbar\beta\omega} - 1} + 1 \right) = -(\bar{n}(\omega) + 1). \tag{1.149}$$

Hence

$$\begin{aligned}
\mathcal{B}(s) &= \int_0^\infty J(\omega) (\bar{n}(\omega) + 1) e^{-i\omega s} d\omega + \int_0^\infty J(\omega) \bar{n}(\omega) e^{i\omega s} d\omega \\
&= \int_0^\infty J(\omega) (\bar{n}(\omega) + 1) e^{-i\omega s} d\omega + \int_{-\infty}^0 J(|\omega|) \bar{n}(-\omega) e^{-i\omega s} d\omega \\
&= \int_0^\infty J(\omega) (\bar{n}(\omega) + 1) e^{-i\omega s} d\omega - \int_{-\infty}^0 J(|\omega|) (\bar{n}(\omega) + 1) e^{-i\omega s} d\omega \\
&= \int_{-\infty}^\infty \text{sgn}(\omega) J(|\omega|) (\bar{n}(\omega) + 1) e^{-i\omega s} d\omega, \tag{1.150}
\end{aligned}$$

where $\text{sgn}(\cdot)$ denotes the signum function. Now, we define the *spectral function* $S(\omega)$ as the inverse Fourier transform of the bath correlation function

$$S(\omega) := \int_{-\infty}^{\infty} e^{i\omega s} \mathcal{B}(s) ds. \quad (1.151)$$

Finally, we get

$$S(\omega) = \text{sgn}(\omega) J(|\omega|) (\bar{n}(\omega) + 1). \quad (1.152)$$

As mentioned before, all the information on the structure of a specific harmonic bath is encoded in the spectral density function $J(\omega)$. Equation (1.152) shows, that it is also possible to use the spectral function $S(\omega)$ instead. For harmonic baths, it is usually just a matter of taste which of these functions is more practical to use. However, the spectral function $S(\omega)$ can be defined even if the bath is not harmonic whereas the spectral density function $J(\omega)$ is only well-defined for harmonic baths.

3.13 The Quasi-Adiabatic Propagator Path Integral Method

Quantum mechanics can be completely reformulated in terms of *path integrals* which are also named *Feynman integrals* after Nobel laureate Richard P. Feynman [61]. This equivalent approach to standard quantum mechanics can be beneficial depending on the context. Particularly, diverse path integral based methods can be used to simulate open quantum system dynamics with their own benefits and drawbacks compared to master equation approaches discussed above. The most prominent path integral techniques are *quantum Monte Carlo* (QMC) methods [62, 63, 64]. In many cases, QMC algorithms are the only tools available for studying large quantum many body systems. Therefore, QMC algorithms are used in a variety of fields [65, 66, 67, 68, 69].

However, the applicability of QMC techniques suffers from the so-called *sign problem*: QMC techniques evaluate thermal averages of physical observables by the sampling of quantum configuration space. To achieve this goal, it is crucial to decompose the partition function of the model of interest into a sum of easily computable non-negative weights that are subsequently interpreted as probabilities in a Markovian sampling process [70]. Whenever terms appear with a negative sign, QMC methods tend to converge exponentially slowly and become impractical. Due to this sign problem, QMC methods will not play any role in this work and hence, we do not pay heed to them anymore in the following.

Here, we follow another approach: the *quasi-adiabatic propagator path integral method* (QUAPI) invented by N. Makri in 1992 avoids the sign problem accepting the trade-off to scale exponentially in computing memory. It is thus limited to small-sized quantum systems [71, 72, 73]. For simplicity, we review its derivation following Ref. [74] for time-independent Hamiltonians. However, the method can also be applied to time-dependent Hamiltonians with minor changes in the derivation.

Let \hat{H} be the Hamiltonian of the total system consisting of the quantum system S of interest and its environment B. The density matrix $\hat{\rho}(t)$ follows the Liouville-Von Neumann equation (1.15) with the solution

$$\hat{\rho}(t) = e^{-i\hat{H}t} \hat{\rho}(0) e^{i\hat{H}t}. \quad (1.153)$$

Our goal is to compute the reduced density matrix $\hat{\rho}_S$. To this end, we calculate the probability amplitude

$$\rho_S(s'', s'; t) := \left\langle s'' \left| \text{Tr}_B \left[e^{-i\hat{H}t} \hat{\rho}(0) e^{i\hat{H}t} \right] \right| s' \right\rangle, \quad (1.154)$$

where $|s'\rangle, |s''\rangle$ denote eigenstates of the system Hamiltonian¹ \hat{H}_S . Obviously, if we would be able to solve equation (1.154) for all $|s'\rangle, |s''\rangle$, then we would obtain the time evolution of the full density matrix.

First, we decompose the Hamiltonian \hat{H} into the form as discussed in section 3

$$\hat{H} = \hat{H}_S + \hat{H}_B + \hat{H}_{\text{int}} =: \hat{H}_0 + \hat{H}_1 \quad (1.155)$$

with $\hat{H}_0 := \hat{H}_S + \hat{H}_B$ and $\hat{H}_1 := \hat{H}_{\text{int}}$. We assume the Hamiltonian H_0 can be diagonalized analytically. Next, we decompose the propagator into a product of N exponentials

$$e^{i\hat{H}t} = \left(e^{i\hat{H}\delta t} \right)^N, \quad \delta t := \frac{t}{N}, \quad (1.156)$$

and define the discrete-time evolution operator $\hat{\mathcal{G}} := e^{i\hat{H}\delta t} = e^{i(\hat{H}_0 + \hat{H}_1)\delta t}$. The next step is to apply a suitable Trotter decomposition to the operator $\hat{\mathcal{G}}$. To do this, we have many options and it depends on the context which one is most appropriate. Different examples can be found in [75]. Here, we take

$$\hat{\mathcal{G}} = e^{i\hat{H}_1 \frac{\delta t}{2}} e^{i\hat{H}_0 \delta t} e^{i\hat{H}_1 \frac{\delta t}{2}} + \mathcal{O}(\delta t^3). \quad (1.157)$$

We note that this approximation can be made arbitrarily accurate by increasing the number of time steps N . Hence, this approximation only causes a numerical error. After inserting equation (1.157) into equation (1.154) we obtain

$$\begin{aligned} \rho_S(s'', s'; t) &= \left\langle s'' \left| \text{Tr}_B \left[\hat{\mathcal{G}}^{\dagger N} \hat{\rho}(0) \mathcal{G}^N \right] \right| s' \right\rangle + \mathcal{O}(\delta t^3) \\ &= \left\langle s'' \left| \text{Tr}_B \left[\left(\hat{\mathcal{G}}^\dagger \hat{\mathbb{I}} \right)^N \hat{\rho}(0) \left(\hat{\mathbb{I}} \mathcal{G} \right)^N \right] \right| s' \right\rangle + \mathcal{O}(\delta t^3). \end{aligned} \quad (1.158)$$

The identities in the second step of equation (1.158) allow us to rewrite the matrix element $\rho_S(s'', s'; t)$ in the path integral formulation

$$\rho_S(s'', s'; t) \approx \int ds_0^+ \int ds_1^+ \cdots \int ds_{N-1}^+ \int ds_0^- \int ds_1^- \cdots \int ds_{N-1}^- I(s_0^\pm, \dots, s_N^\pm), \quad (1.159)$$

where s_k^+, s_k^- for $\{0 \leq k \leq N-1\}$ index the eigenstates of the system, representing the discrete path on the forward (+) and backward (-) contours. Furthermore, we

¹In the time-dependent case, $|s'\rangle, |s''\rangle$ correspond to the instantaneous eigenbasis of the Hamiltonian $\hat{H}(t)$.

defined the *influence functional*¹

$$I(s_0^\pm, \dots, s_N^\pm) := \text{Tr}_B \left[\left\langle s_N^+ \left| \hat{\mathcal{G}}^\dagger \right| s_{N-1}^+ \right\rangle \left\langle s_{N-1}^+ \left| \hat{\mathcal{G}}^\dagger \right| s_{N-2}^+ \right\rangle \cdots \left\langle s_0^+ \left| \hat{\rho}(0) \right| s_0^- \right\rangle \cdots \right. \\ \left. \left\langle s_{N-2}^- \left| \hat{\mathcal{G}}^\dagger \right| s_{N-1}^- \right\rangle \left\langle s_{N-1}^- \left| \hat{\mathcal{G}}^\dagger \right| s_N^- \right\rangle \right], \quad (1.160)$$

with $s_N^+ := s''$ and $s_N^- := s'$. In general, computing $I(s_0^\pm, \dots, s_{N-1}^\pm)$ is a non-easy or even impossible task. However, if the heat bath is harmonic, it the influence functional can be determined analytically. It then reads [74]

$$I_H(s_0^\pm, \dots, s_N^\pm) = \exp \left(- \sum_{k=0}^N \sum_{k'=0}^k (s_k^+ - s_k^-) (\eta_{k,k'} s_{k'}^+ - \eta_{k,k'}^* s_{k'}^-) \right) \times \\ \times \left\langle s_N^+ \left| e^{-i\hat{H}_0\delta t} \right| s_{N-1}^+ \right\rangle \cdots \left\langle s_0^+ \left| \hat{\rho}_S(0) \right| s_0^- \right\rangle \cdots \left\langle s_{N-1}^- \left| e^{i\hat{H}_0\delta t} \right| s_N^- \right\rangle. \quad (1.161)$$

Here, the coefficients $\eta_{k,k'}$ depend on the bath spectral density function $J(\omega)$ and temperature T . Their precise form can be found in Ref. [73].

So far, the derivation shown here is rather general with a well-controlled numerical error caused by the Trotter decomposition, which can be made arbitrarily small by increasing the number of time steps N , in contrast to master equation approaches that rely on uncontrolled approximations as shown in sections (3.6) to (3.11). However, the drawback here is the terrible scaling in computing resources and hence, brute force direct numerical simulations can only simulate very short time scales, even when the form of the influence functional is analytically known as in equation (1.161). This case arises typically for very small bath temperatures as the bath correlation time diverges for $T \rightarrow 0$ thereby demanding shorter time-steps and hence longer simulation times. Furthermore, the method is of iterative nature: To compute $\hat{\rho}_S(t + \delta t)$, all the intermediate states from $\hat{\rho}_S(0)$ to $\hat{\rho}_S(t)$ enter the calculation. The size of the influence functional $I(s_0^\pm, \dots, s_N^\pm)$, interpreted as a huge tensor, therefore increases exponentially with the number of time-steps N . Hence, the primary memory cost (PMC) is proportional to

$$\text{PMC} \propto M^{2(N+1)}, \quad (1.162)$$

where $M = \dim(\mathcal{H}_S)$ denotes the Hilbert space dimension of the quantum system S . For more detailed discussions we refer to Refs. [73] and [74].

It is possible to reduce the computational overhead by a controlled approximation: If there is only a single heat bath at temperature T , its memory time τ_B is of finite length enabling us to truncate the influence functional after this time in a controlled way. In other words, in order to compute $\hat{\rho}_S(t + \delta t)$, it is sufficient to take into account the last Δk time-steps satisfying

$$\delta t = \frac{\tau_B}{\Delta k}. \quad (1.163)$$

Obviously, the practical limitation of the number Δk limits the reachable precision as we have to satisfy the convergence condition (1.163) and the error scales with

¹The original but less general definition of the influence functional goes back to Feynman and Vernon [76].

δt^3 . Following this argument, the influence functional can be written as a cumulant expansion resulting in

$$I(s_0^\pm, \dots, s_N^\pm) \approx I_{\Delta k}(s_0^\pm, \dots, s_{\Delta k}^\pm) I_{\Delta k}(s_1^\pm, \dots, s_{\Delta k+1}^\pm) \cdots I_{\Delta k}(s_{N-\Delta k}^\pm, \dots, s_N^\pm) \quad (1.164)$$

with

$$I_{\Delta k}(s_k^\pm, \dots, s_{k+\Delta k}^\pm) := \frac{I(s_k^\pm, \dots, s_{k+\Delta k}^\pm)}{I(s_k^\pm, \dots, s_{k+\Delta k-1}^\pm)}. \quad (1.165)$$

The details of this approximation can be found in Ref. [77]. We observe that we can compute the influence functional iteratively. This avoids the sign problem in contrast to QMC. Due to the truncation after the bath memory time τ_B , the primary memory cost scales as

$$\text{PMC} \propto M^{2(\Delta k+1)} \ll M^{2(N+1)}. \quad (1.166)$$

However, the memory scaling is still exponential and hence, the method is limited to small system sizes. Additionally, the temperature T should not be too small as, for limited Δk , the numerical error caused by the minimal step size δt might become too large.

To conclude, QUAPI is a mighty tool if the Hilbert space dimension of the system of interest is small and the temperature is large enough to ensure a sufficiently small error. However, these assumptions are quite restrictive. We note that there is an open source code implementing QUAPI available [73].

4 Summary

In this chapter, I have provided a review on quantum computing and open quantum systems, which establishes the foundation for the rest of the thesis. In section 1, I have given an historical overview on the development of modern computers, from early implementations till the current development of quantum computers. In the next step, I have discussed the paradigms of quantum information theory in section 2. As a functional quantum computer is fundamentally described by the theory of open quantum systems, I have derived the standard tools for simulating open quantum system dynamics in section 3, comparing their respective advantages and disadvantages and the resulting fields of application.

Chapter II

Quantum Simulations of Quantum Stochastic Walks

Quantum walks have been shown to have a wide range of applications, from artificial intelligence, to photosynthesis, and quantum transport. Quantum stochastic walks (QSWs) generalize this concept to additional non-unitary evolution. This allows for incoherent movement of the walker, and therefore, directionality. In this chapter, we propose two trajectory-based quantum simulation protocols to effectively implement two kinds of QSWs in a quantum device. First, we show how to simulate a family of continuous-time QSWs. In the second case, we demonstrate how to simulate a family of discrete-time QSWs on a coherent quantum computer. In both cases, the desired decoherence is implemented via a suitable measurement and feed-forward scheme.

This chapter is based on Refs. [47] and [78]. It is organized as follows. In section 4, we review the basics on quantum stochastic walks and we briefly discuss the issues to implement the latter directly in a quantum device. In section 5, we present our results on continuous-time QSWs and in section 6, we give a description of our results on discrete-time QSWs. In particular, we show how to simulate a restricted set of continuous-time quantum stochastic walks by suitable discrete-time quantum stochastic walks.

Preface

This chapter is based on joint work of four authors including me. Initially, the goal has been to find a direct way to implement QSWs in a quantum device. After a few months, we realized that, in general, this constitutes a very hard or even impossible task. Afterwards, the project developed into various directions: Bruno G. Taketani focussed on the direct realizability, Luke C. G. Govia developed the protocol for continuous-time QSWs and I found the protocol for discrete-time QSWs. However, we collaborated very closely, particularly through fruitful discussions. In this sense it is true joint work which justifies to use both protocols as parts of my thesis.

4 Introduction to Quantum Stochastic Walks (QSWs)

In 1993, Y. Aharonov, L. Davidovich and N. Zagury invented the concept of *quantum random walks* (*quantum walks*) as the quantum mechanical analogue to the ubiquitous classical random walk [13]: a "walker" can "jump" between the vertices on a graph $\mathcal{G} = (V(\mathcal{G}), E(\mathcal{G}))$ along the edges. However, this jump follows the laws of quantum physics resulting in a unitary evolution. This property distinguishes the quantum walk fundamentally from its classical counterpart: While the classical walker jumps between graph vertices according to some probability distribution defined by the structure of the underlying graph, the quantum walker takes all the possible paths at the same time resulting in constructive and destructive interference along the edges. Here, the probabilities are replaced by probability amplitudes. In other words, the classical walk is completely incoherent whereas the quantum walk is fully coherent. For an introductory overview on quantum walks, we refer to Ref. [79].

Quantum walks can be either continuous-time [14], or discrete-time [15, 16], and both types have been shown to be universal for quantum computation [17, 18]. As a result, they can have computational advantages over classical algorithms, and quantum walks have been proposed for application in a variety of fields. Promising examples include machine learning [80, 81], search algorithms [82], and photosynthetic excitation transfer [83, 84].

Extending on the idea of the quantum walk is the *quantum stochastic walk* (QSW), which combines the unitary evolution of a quantum walk with non-unitary stochastic evolution [85]. This breaks time-reversal symmetry of the walker's evolution, and allows for the possibility of directed walks¹. During the last years, it has been shown that when compared to their coherent counterparts, QSWs can have beneficial properties, such as speeding-up learning algorithms [87, 88], or enhancing excitation transport [83, 89]. Again, QSWs can either be continuous-time or discrete-time². Both versions will be discussed in the following.

4.1 Continuous-Time Quantum Stochastic Walks

The continuous-time quantum stochastic walk of Ref. [85] is given by a Lindblad master equation of the form

$$\dot{\hat{\rho}} = (\omega - 1)i \left[\hat{H}_{\mathcal{G}}, \hat{\rho} \right] + \omega \sum_k \gamma_k \left(\hat{L}_k \hat{\rho} \hat{L}_k^\dagger - \frac{1}{2} \{ \hat{L}_k^\dagger \hat{L}_k, \hat{\rho} \} \right), \quad (2.1)$$

where $\hat{\rho}$ is the density operator of the system, \hat{L}_k are the Lindblad operators with γ_k their associated incoherent transition rates, $\hat{H}_{\mathcal{G}}$ is the Hamiltonian of the underlying graph \mathcal{G} and $\omega \in [0, 1]$. For $\omega = 0$, we obtain the completely coherent quantum walk and for $\omega = 1$, pure environmentally driven dynamics like the classical random walk. Hence, for $\omega \in (0, 1)$, equation (2.1) leads to dynamics we could not obtain in a purely coherent or incoherent framework³. In Ref. [47], we were guided by proposals for QSWs solving various computational problems [87, 88] in which the walker is restricted to the single excitation subspace of the graph. Therefore, each node can be described by a qubit, with the excited state indicating the presence of the walker. For such a

¹Time-reversal symmetry can also be broken in chiral quantum walks [86]; however, these are completely coherent and therefore not QSWs.

²In literature, the term "quantum stochastic walk" often refers to the continuous-time version only.

³The notations used here slightly differ from the notations in the papers to be consistent throughout the thesis.

situation, the QSW can be described by the Lindblad master equation

$$\dot{\rho} = -i [\hat{H}, \rho] + \sum_{nm} \gamma_{nm} \left(\hat{\sigma}_m^+ \hat{\sigma}_n^- \hat{\rho} \hat{\sigma}_n^+ \hat{\sigma}_m^- - \frac{1}{2} \{ \hat{\sigma}_n^+ \hat{\sigma}_m^- \hat{\sigma}_m^+ \hat{\sigma}_n^-, \hat{\rho} \} \right), \quad (2.2)$$

where $\hat{\sigma}_n^{+/-}$ is the raising/lowering operator for node n , and in general $\gamma_{nm} \neq \gamma_{mn}$. Additionally, we have absorbed the prefactors in equation (2.1) into \hat{H} and γ_{nm} to shorten the notation. Crucially, the incoherent evolution of equation (2.2) also conserves the total excitation number in the graph, and as such the walker cannot be lost. It is important to point out that the QSWs considered here have only a positional degree of freedom, and are distinct from the open quantum walks of Refs. [90, 91], which contain both positional and internal (coin) degrees of freedom.

The QSW of equation (2.2) is a non-standard open system evolution, as incoherent excitation exchange occurs between the nodes, without local decay from the nodes into their environment, and possibly without local dephasing. As it has been shown in Ref. [92], using standard two-body system-bath interactions and assuming an unstructured bath in the weak coupling limit, it is not possible to microscopically build a Lindblad equation of the form of equation (2.2). Heuristically, this can be understood to result from the fact that any incoherent evolution must arise from unitary coupling of the system to an environment, and that such coupling must take the form of local decay to the environment or local dephasing due to it. Therefore, one cannot avoid both of these local incoherent process and still have incoherent excitation exchange between nodes.

The restrictions found in Ref. [92] can be circumvented with knowledge of the eigenspectrum of the graph Hamiltonian, and/or elaborate reservoir engineering. However, for QSWs of practical interest, the graph Hamiltonian will be sufficiently complicated that obtaining its eigenspectrum will be computational impractical on a classical computer. Also, while reservoir engineering can be useful in many circumstances [93, 94, 95, 96, 97, 98], it requires an understanding and control of the environment that makes it impractical for implementing general, large-scale QSWs.

In Ref. [47], we proposed another way to circumvent the restrictions of Ref. [92], by simulating the desired QSW on a fully coherent quantum computer. In doing so, we use the QSW only as a quantum algorithm, and not a physical implementation. We will introduce the concept of *quantum trajectories on a quantum computer (QTQC)* in section 5, which is a way of simulating general Lindblad open system evolution on a coherent quantum simulator.

4.2 Discrete-Time Quantum Stochastic Walks

Discrete-time quantum stochastic walks are by far less popular than their continuous-time counterparts. First, they were mentioned in Ref. [85] but in a side note only. In Ref. [78], we defined them as follows.

Let $\mathcal{G} = (V(\mathcal{G}), E(\mathcal{G}))$ be an arbitrarily connected (and possibly directed) graph with vertices $V(\mathcal{G})$ and edges $E(\mathcal{G})$, and $\{|n\rangle, 1 \leq n \leq |V(\mathcal{G})|\}$ a set of pairwise orthonormal quantum states which enumerate the location of a “walker” on the graph vertices. We will restrict our system to the single excitation subspace, so that $|n\rangle$ denotes a quantum state with a single excitation in vertex n and all other vertices empty.

For any connected graph \mathcal{G} , we consider a quantum stochastic map \mathcal{B} representing a single time-step of a QSW, which can be written in Kraus form as

$$\mathcal{B}[\rho] := \alpha \hat{U}_{\mathcal{G}}(\Delta t) \rho(t) \hat{U}_{\mathcal{G}}^{\dagger}(\Delta t) + \sum_{(m,n) \in E(\mathcal{G})} \kappa_{nm} |m\rangle \langle n| \rho |n\rangle \langle m|. \quad (2.3)$$

Here, $\hat{U}_{\mathcal{G}}(\Delta t) := e^{-i\hat{H}_{\mathcal{G}}\Delta t}$ is the propagator of the graph coherent evolution for a time-step of length Δt , generated by the Hamiltonian $\hat{H}_{\mathcal{G}}$ of the graph \mathcal{G} . The coefficients $\alpha, \kappa_{nm} \in [0, 1]$ represent the weights for coherent or incoherent processes to happen and satisfy $\sum_m \kappa_{nm} = 1 - \alpha$ for all $n \in V(\mathcal{G})$ due to trace-preservation.

We define a discrete-time quantum stochastic walk by the repeated application of the single time-step quantum stochastic map \mathcal{B} to the initial state ρ_0

$$\rho_n = \mathcal{B}^n[\rho_0] := \underbrace{\mathcal{B}[\mathcal{B}[\dots \mathcal{B}[\rho_0] \dots]]}_{n \text{ times}}. \quad (2.4)$$

We are not aware of any publication which applies discrete-time QSWs to any problem of interest. However, we are optimistic that, when further developed, discrete-time QSWs will have their own applications in the future, because, in contrast to their continuous-time counterparts, there are no fundamental restrictions to simulate them on a coherent quantum simulator. The way this is done will be shown in section 6. Further, it is possible to simulate a restricted set of continuous-time QSWs by discrete-time QSWs. This will be shown in section 6.3.

5 Quantum Simulation of a Continuous-Time QSW

As we have discussed in section 4.1, direct physical implementation of a system that evolves under the master equation of equation (2.2) poses a significant challenge. To circumvent this restriction, we propose simulation of equation (2.2) on a quantum computer using a quantum trajectories [99] style approach.

To begin, we consider the stochastic master equation unraveling of equation (2.43), which is given by

$$\begin{aligned} d|\psi(t)\rangle = \sum_k \left[dN_k(t) \left(\frac{\hat{L}_k}{\sqrt{\langle \hat{L}_k^{\dagger} \hat{L}_k \rangle(t)}} - 1 \right) \right. \\ \left. + dt \left(\frac{\gamma_k \langle \hat{L}_k^{\dagger} \hat{L}_k \rangle(t)}{2} - \frac{\gamma_k \hat{L}_k^{\dagger} \hat{L}_k}{2} - i\hat{H} \right) \right] |\psi(t)\rangle, \end{aligned} \quad (2.5)$$

where $dN_k(t)$ is the stochastic increment for each Lindblad operator, for which the mean value is $E[dN_k(t)] = \langle \psi(t) | \hat{L}_k^{\dagger} \hat{L}_k | \psi(t) \rangle$. We will first briefly review the quantum trajectories procedure used to simulate this equation on a *classical* computer and to find the density matrix of equation (2.43). A full description of this technique can be found in Refs. [99, 100].

*Section 5 was published in "Luke C. G. Govia, Bruno G. Taketani, Peter K. Schuhmacher and Frank K. Wilhelm, *Quantum Science and Technology* (2017)". Copyright (2017) by IOP Publishing. The majority of the text was written by Luke C. G. Govia.

5.1 Quantum Trajectories on a Classical Computer

The approach to simulate quantum trajectories on a classical computer (QTCC) relies on a discretization of time and a separation between coherent and incoherent evolution. It consists of the following steps.

(1) *Coherent Evolution*: Starting at $t = 0$, the system evolves under the unnormalized, non-Hermitian evolution

$$\frac{d}{dt} |\psi(t)\rangle = -i(\hat{H} - i\hat{K}) |\psi(t)\rangle, \quad (2.6)$$

until a time t_1 such that $\langle \psi(t_1) | \psi(t_1) \rangle = R_1$, where R_1 is a random number from the closed unit interval $[0, 1]$. Here $K = \sum_k \gamma_k \hat{L}_k^\dagger \hat{L}_k / 2$, and the random number R_1 is used to determine when an incoherent process (a quantum jump) occurs.

(2) *Incoherent Evolution or Quantum Jump*: The normalized expectation values

$$E_k(t_1) = \frac{\gamma_k \langle \psi(t_1) | \hat{L}_k^\dagger \hat{L}_k | \psi(t_1) \rangle}{\sum_k \gamma_k \langle \psi(t_1) | \hat{L}_k^\dagger \hat{L}_k | \psi(t_1) \rangle}, \quad (2.7)$$

are calculated, and used as weights to determine, via a second random number, which incoherent process \hat{L}_k occurs at time t_1 . Assuming that \hat{L}_n is selected, then the state is updated via the rule

$$|\psi'(t_1)\rangle = \frac{\hat{L}_n |\psi(t_1)\rangle}{\langle \psi(t_1) | \hat{L}_n^\dagger \hat{L}_n | \psi(t_1) \rangle}, \quad (2.8)$$

which both applies the relevant jump operator, and renormalizes the state. The state $|\psi'(t_1)\rangle$ is then used as the new initial state.

Steps (1) and (2) are repeated, with new random numbers generated for each iteration, until the total simulation time T is reached, producing an output state $|\psi(T)\rangle$ which corresponds to a single trajectory of the system evolution. An ensemble average of all possible trajectories gives the correct density matrix for a system evolving under the master equation of equation (2.43), i.e.

$$\rho(T) = \mathbb{E} [|\psi(T)\rangle \langle \psi(T)|]. \quad (2.9)$$

Note that if $t_n > T$ no final incoherent jump is performed.

Quantum trajectory simulations on a classical computer of a system of Hilbert space dimension D require S trajectories to converge to an answer for the density matrix at time T . The runtime required is $O(SD^2)$, compared to the $O(D^4)$ runtime required for a numerical master equation solver [99]. For $S < D^2$, QTCC is the more efficient technique [99]. It can also be beneficial if the density matrix is too large to store on a classical computer, but the state vector is not. Nevertheless, quantum trajectories is still an inefficient algorithm on a classical computer, as the Hilbert space dimension increases exponentially with the number of qubits.

5.2 Quantum Trajectories on a Quantum Computer

Practical implementations of the above protocol are inefficient on a classical computer, and hence would be limited to small graphs. To overcome this, one could envision implementation on a quantum computer. For this, the protocol requires the following modifications:

(1) *Coherent Evolution*: The evolution described by equation (2.6) is in general nonphysical, and therefore is impossible to implement on a quantum computer with Hamiltonian evolution only. For time independent \hat{H} and \hat{K} , the solution to equation (2.6) is

$$|\psi(t)\rangle = e^{-i(\hat{H}-i\hat{K})t} |\psi(0)\rangle. \quad (2.10)$$

If \hat{H} and \hat{K} commute, then this can be written as

$$|\psi(t)\rangle = e^{-i\hat{H}t} e^{-\hat{K}t} |\psi(0)\rangle, \quad (2.11)$$

and furthermore, if $|\psi(0)\rangle$ is an eigenvector of \hat{K} with eigenvalue λ , then the solution for $|\psi(t)\rangle$ becomes

$$|\psi(t)\rangle = e^{-\lambda t} e^{-i\hat{H}t} |\psi(0)\rangle. \quad (2.12)$$

As can clearly be seen, equation (2.12) is equivalent to the solution for evolution under the physical Hamiltonian \hat{H} alone, up to a normalization factor $e^{-\lambda t}$. To render this nontrivial while obeying the condition that K and H commute, the eigenvalues of K need to be degenerate. In section 5.3 we will discuss the implications of this restriction in a specific example.

Therefore, we see that we can implement the coherent evolution step of the quantum trajectories algorithm on a quantum computer provided the following three conditions hold:

1. $[\hat{H}, \hat{K}] = 0$,
2. The initial state, $|\psi(0)\rangle$, and the states at the start of each further coherent evolution step, $|\psi'(t_i)\rangle$, are all eigenstates of \hat{K} .
3. $|\psi'(t_i)\rangle$ is known at the end of each iteration, so that $e^{-\lambda_i t}$ can be calculated and used to determine the coherent evolution time t_{i+1} for the next iteration, using $\langle \psi(t_{i+1}) | \psi(t_{i+1}) \rangle = e^{-2\lambda_i t_{i+1}} = R_{i+1}$, with R_{i+1} a random number from the unit interval.

Note that the second restriction can be lifted by simulating $e^{-\hat{K}t} |\psi(0)\rangle$ using a large ancilla system (see A.b), and if this is the case, the formula to calculate the norm in restriction (iii) changes. Moreover, for large enough incoherent rates, under certain circumstances the first condition may be relaxed as the small average coherent time steps t_i will justify a Suzuki-Trotter decomposition. See A.a for further details.

(2) *Incoherent Evolution*: On a classical computer, the complete state $|\psi(t)\rangle$ after the previous coherent evolution is known, and so calculation of expectation values is simple. However, on a quantum computer the state is not known, and at each time t_i either full state tomography must be performed to determine $|\psi(t_i)\rangle$, or each observable from equation (2.7) must be measured sufficient times to obtain the relevant expectation values. Therefore, the first immediate problem with implementation of the incoherent step of the quantum trajectories algorithm on a quantum computer is efficient calculation of the expectation values $E_k(t)$ of equation (2.7).

As a result, each iteration step in a single trajectory must be run many times. The first $N - 1$ times to generate sufficient measurement statistics so as to be able to determine the next incoherent quantum jump, and the N 'th time to actually implement the next quantum jump, and continue on with the trajectory. This introduces considerable overhead to the protocol. If S trajectories are required for convergence,

a total of $O(N_{\text{jumps}}NS)$ runs will be needed, where N_{jumps} is the average number of jumps per trajectory.

However, for certain classes of quantum jumps this overhead can be avoided. We will discuss one such case in the next section, where we consider a ‘‘quantum trajectories on a quantum computer’’ (QTQC) implementation of the class of quantum stochastic walks described by equation (2.2).

5.3 QTQC of a Quantum Stochastic Walk

For the quantum stochastic walk of equation (2.2) we have

$$\hat{K} = \sum_{nm} \frac{\gamma_{nm}}{2} \sigma_n^+ \sigma_m^- \sigma_m^+ \sigma_n^- = \frac{1}{2} \sum_{n \neq m} \gamma_{nm} P_n^{(1)} \otimes P_m^{(0)} + \frac{1}{2} \sum_n \gamma_{nn} P_n^{(1)} \quad (2.13)$$

where $P_n^{(1)}$ is the projector onto the excited state of the qubit at node n and $P_m^{(0)}$ the projector onto the ground state of the qubit at node m .

As we have a single walker on the graph, we can restrict our system to the single excitation subspace, and we use the notation $|\phi_k\rangle$ to indicate that the walker is in the k 'th node of the graph. In the single excitation subspace the \hat{K} matrix is diagonal and given by

$$\hat{K}_{\text{SE}} = \frac{1}{2} \sum_k \lambda_k |\phi_k\rangle \langle \phi_k|, \quad (2.14)$$

where $\lambda_k = \sum_n \gamma_{kn}$ is the total rate at which an excitation incoherently decays from node k (into the other nodes). We consider a general Hamiltonian for a graph consisting of qubits coupled resonantly via the Jaynes-Cummings interaction, which in the single excitation subspace takes the form

$$\hat{H}_{\text{SE}} = \sum_{ij} g_{ij} |\phi_i\rangle \langle \phi_j|, \quad (2.15)$$

where the coupling strengths satisfy $|g_{ij}| = |g_{ji}|$ due to the symmetry of the Hamiltonian.

5.3.1 Coherent Evolution

To simulate this stochastic quantum walk with a QTQC approach, we still require that $[\hat{H}_{\text{SE}}, \hat{K}_{\text{SE}}] = 0$. A simple calculation (see A.a) shows that this is equivalent to the condition

$$g_{nm} (\lambda_n - \lambda_m) = 0 \quad (2.16)$$

for all nodes n and m . What this means is that any two nodes with non-zero coherent coupling must have the same total incoherent decay rate λ . This is not in general true, and only a restricted set of graphs will satisfy this condition. An example of such a graph is shown in figure 2.1. Extending this condition to a coherently connected subgraph, one sees that all nodes of this subgraph must have the same total decay rate. The subgraph need not be completely connected, a single coherent connection between a new node and an existing subgraph is enough to enforce that the new node must have the same total decay rate as the nodes of the subgraph, see for example node 2 in the right panel of figure 2.1. In addition, the only way to connect subgraphs

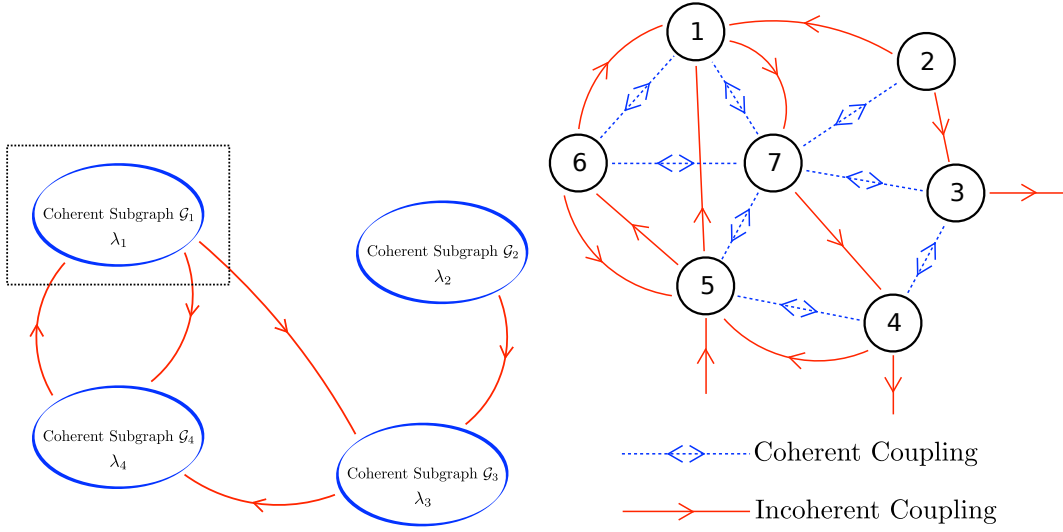


FIGURE 2.1: *Left Panel:* A sample graph, showing four coherently connected subgraphs linked by incoherent connections. *Right Panel:* Zoom in of the dashed square in the left panel, an example of a single coherently connected subgraph with complicated network connectivity. The only restriction on the incoherent rates for this subgraph is that $\gamma_{17} + \gamma_{11} = \gamma_{21} + \gamma_{23} + \gamma_{22} = \gamma_{3*} + \gamma_{33} = \gamma_{4*} + \gamma_{45} + \gamma_{44} = \gamma_{56} + \gamma_{51} + \gamma_{55} = \gamma_{65} + \gamma_{61} + \gamma_{66} = \gamma_{74} + \gamma_{77} = \lambda_1$. Here γ_{3*} and γ_{4*} indicate the incoherent connections from nodes 3 and 4 that leave the subgraph. Notice that γ_{*5} , the incoherent connection entering the subgraph at node 5, plays no role in the definition of λ_1 .

with different λ 's is through a purely incoherent connection, as shown in the left panel of figure 2.1.

In summary, the condition $[\hat{H}_{\text{SE}}, \hat{K}_{\text{SE}}] = 0$ enforces that the total decay rate λ must be the same for nodes that are coherently connected. We emphasize that this does not mean all γ_{nm} must be the same *within* a coherently connected graph, only $\sum_k \gamma_{nk} = \lambda_n = \lambda$ must be constant for each node in the graph. Moreover, while all nodes have equal loss rates, the gain rates need not be equal, one can, for example, easily design a graph where an excitation can incoherently decay from, but never into, some given nodes. This implies that graphs with both source and sink nodes can be implemented.

Furthermore, the coherent couplings between elements are unrestricted. As such, complicated connectivity networks are still possible, as demonstrated by the connectivity of the subgraph shown in the right panel of figure 2.1. In addition, QSWs that satisfy the required criteria for QTQC simulation have already been shown to be advantageous in learning processes using neural networks [80].

In light of the previous discussion, we see that \hat{K}_{SE} takes the form

$$\hat{K}_{\text{SE}} = \frac{1}{2} \sum_i \sum_{k \in \mathcal{G}_i} \lambda_i |\phi_k\rangle \langle \phi_k|, \quad (2.17)$$

where \mathcal{G}_i are the incoherently connected subgraphs of the graph \mathcal{G} , and λ_i is the total decay rate of each node belonging to subgraph \mathcal{G}_i (the left panel of figure 2.1 is an example of such a complete graph). To perform a QTQC simulation we also require that the initial state $|\psi(0)\rangle$ is an eigenstate of \hat{K}_{SE} . From equation (2.17) we see that

this is satisfied provided $|\psi(0)\rangle$ is a superposition of nodes contained within a single subgraph \mathcal{G}_i (assuming all λ_i are distinct). In addition, we require that after each quantum jump the state $|\psi'(t_i)\rangle$ is an eigenstate of \hat{K}_{SE} . Luckily, the form of the Lindblad operator, $\hat{L}_{nm} = \sigma_n^- \sigma_m^+$, ensures this is the case, as it localizes the excitation at node m of the graph.

5.3.2 Incoherent Evolution

The fact that all Lindblad operators \hat{L}_{nm} localize the walker to a single node is also beneficial for implementing the incoherent quantum jumps. This comes from the realization that the normalized expectation values

$$\begin{aligned}
 E_{nm}(t) &= \frac{\gamma_{nm} \langle \psi(t) | P_n^{(1)} \otimes P_m^{(0)} | \psi(t) \rangle}{\sum_{nm} \gamma_{nm} \langle \psi(t) | P_n^{(1)} \otimes P_m^{(0)} | \psi(t) \rangle} \\
 &= \frac{\gamma_{nm} |\langle \psi(t) | \phi_n \rangle|^2}{2 \langle \psi(t) | \hat{K}_{\text{SE}} | \psi(t) \rangle} \\
 &= \frac{\gamma_{nm} |\langle \psi(t) | \phi_n \rangle|^2}{\lambda_n} \\
 &= \frac{\gamma_{nm} |\langle \psi(t) | \phi_n \rangle|^2}{\sum_k \gamma_{nk}} \tag{2.18}
 \end{aligned}$$

are equivalent to the probability that the excitation is in node n , given by $|\langle \psi(t) | \phi_n \rangle|^2$, multiplied by the probability the excitation decays into node m from node n , given by $\gamma_{nm} / \sum_k \gamma_{nk}$.

If we measure the entire graph, we localize the excitation at a specific node n , which occurs with probability $|\langle \psi(t) | \phi_n \rangle|^2$. Next, using a random number and the weighted distribution $\gamma_{nm} / \sum_k \gamma_{nk}$ (which we know from designing the graph) we can determine into which node m the excitation decays, and implement this transition. The net effect of this two-step process is that the probability of the transition from mode n to mode m is given by

$$P_{nm} = \frac{\gamma_{nm} |\langle \psi(t) | \phi_n \rangle|^2}{\sum_k \gamma_{nk}} = E_{nm}(t). \tag{2.19}$$

The choice of node n is random due to the nature of quantum measurement, while the choice of node m is random as we use a classical random number to choose m . Therefore, this hybrid quantum-classical probabilistic process samples randomly from the weighted distribution given by the expectation values $\{E_{nm}(t)\}$. In doing so, it correctly mimics the statistics of the QTQC simulation outlined in section 5.2, which allows the quantum jump to be implemented in a single shot with the correct statistics, without the large number of identical pre-runs normally required for a QTQC simulation.

It is important to point out that the simple form of the denominator of equation (2.18) is due to the fact that all coherently coupled nodes must have the same total decay rate λ . Therefore, since $|\psi(0)\rangle$ is an eigenstate of \hat{K}_{SE} , then $|\psi(t)\rangle$ will also be an eigenstate of \hat{K}_{SE} as coherent evolution can only lead to a superposition of nodes which all have the same total decay rate.

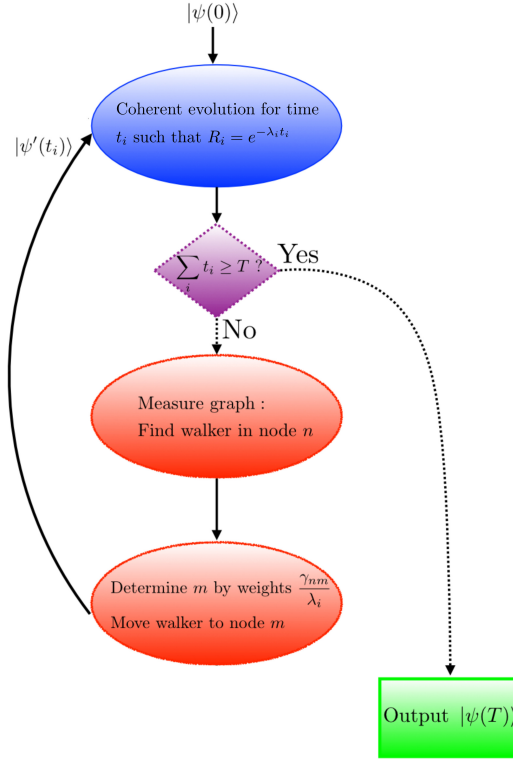


FIGURE 2.2: Algorithm to simulate a quantum stochastic walk via quantum trajectories on a quantum computer.

5.3.3 QTQC Protocol

Putting everything together, the full procedure for simulating a quantum stochastic walk using a QTQC protocol is as follows (also shown in figure 2.2).

1. The system starts in a state $|\psi(0)\rangle$ for which $\hat{K}_{\text{SE}}|\psi(0)\rangle = \frac{\lambda}{2}|\psi(0)\rangle$. The system evolves coherently under \hat{H}_{SE} until a time t_1 , such that $e^{-\lambda t_1} = R_1$, where R_1 is a random number from the unit interval.
2. The local population of the complete graph is measured (this measurement does *not* need to be quantum non-demolition). The walker is found in node n with probability $|\langle\psi(t_1)|\phi_n\rangle|^2$, where $|\phi_n\rangle$ is the single excitation subspace state with the walker in node n .
3. A second random number is selected from the weighted distribution $\gamma_{nm}/\sum_k \gamma_{nk}$ to determine the destination node m , and the walker is re-initialized in node m . The graph is now in the state $|\phi_m\rangle$.
4. The above process is repeated, replacing $|\psi(0)\rangle$ with the localized state $|\psi'(t_1)\rangle = |\phi_m\rangle$, until the total evolution time T is reached, with new random numbers being generated for each iteration. Due to the fact that the state at the beginning of each iteration is localized, it is guaranteed that $\hat{K}_{\text{SE}}|\psi'(t_i)\rangle = \frac{\lambda_i}{2}|\psi'(t_i)\rangle$ for each iteration. However, λ_i may change between iterations, as the walker moves between subgraphs.

Following this procedure, the quantum stochastic walk along any graph that satisfies equation (2.16) can be simulated. The density matrix for the walker can be obtained using sufficient trajectories and state tomography.

5.3.4 Resource Analysis and Scalability

In this section we consider the resources required for a physical implementation of the QTQC simulation of a quantum stochastic walk. The number of trajectories required to accurately calculate the expectation value of an observable depends on the nature of the graph connectivity and on the observable, so general statements are difficult to make. However, the number of trajectories required for accurate results in a QTQC simulation will be the same as in QTCC, as the statistical procedure is effectively the same.

As described before, a QTCC has a run time that scales as $O(SD^2)$, where S is the number of trajectories required for converging results, and D is the Hilbert space dimension of the system, while a numerical solution of the master equation has a runtime that scales as $O(D^4)$. Therefore, a trajectories simulation is more efficient for $S < D^2$ [99]. In the situation considered here, D is the number of nodes of the graph, as we have restricted ourselves to the single excitation subspace. In a QTQC simulation the coherent part of the evolution is run on an actual quantum computer. Therefore, for a useful QSW, QTQC will have a computational speed-up over the best classical algorithm for the given problem. It is important to note that the best classical algorithm may not be QTCC, but nevertheless, for a useful QSW the QTQC simulation will be at least polynomially faster (in terms of the Hilbert space dimension D) than the best classical algorithm.

The main resource requirements present in a QTQC simulation that do not have clear analogues in QTCC are steps (2) and (3) of the protocol. These are full measurements of the graph to locate the walker, and moving the walker from one node to another, respectively. As a walker move only ever occurs after a graph measurement, we will only discuss the average number of measurements in a given trajectory.

Sampling uniformly over the unit interval gives an expected R_1 of $\langle R_1 \rangle = 1/2$. Therefore, the average coherent evolution time before a quantum jump (and therefore a full graph measurement) satisfies

$$e^{-\lambda t_{\text{avg}}} = \langle R_1 \rangle = \frac{1}{2}, \quad (2.20)$$

which implies that

$$t_{\text{avg}} = \frac{\log(2)}{\lambda}, \quad (2.21)$$

where λ is the eigenvalue of \hat{K}_{SE} for the graph initial state. If λ does not change after each measurement, then the average number of measurements per trajectory is simply given by

$$\langle N_{\text{meas}} \rangle = \frac{T}{t_{\text{avg}}}, \quad (2.22)$$

where T is the total time of the trajectory. When λ does change this formula is no longer accurate, but by choosing the smallest t_{avg} (corresponding to the largest eigenvalue) one can calculate the ‘‘worst case’’ average number of measurements per trajectory.

However, it is not the number of required measurements that is most limiting to the size and complexity of the graph on which a QTQC simulation can be run. It is the required coherence time of the graph that is most limiting, as keeping large, strongly coupled networks of qubits coherent is a challenging experimental task. However,

the coherence time is not given by the total length T of a trajectory as one might naïvely expect, but instead by the average time between quantum jumps t_{avg} , as after each quantum jump the graph is “reset” into a definite (classically localized) state with no coherence. This potentially significant reduction in required coherence time increases the size of graphs on which a QTQC simulation could be run. In addition, the required coherence time actually decreases with the average number of measurements performed per trajectory, as the more measurements that are required, the stronger the incoherent process in the simulated quantum stochastic walk are in comparison to the coherent evolution.

It is also possible to use QTQC to simulate walks on graphs with more nodes than are experimentally feasible. Since the connections between coherent subgraphs are purely incoherent, they occur as quantum jumps, and the state of the walker is always confined to a single coherent subgraph. When a quantum jump between coherent subgraphs occurs, the experimental set-up needs only to be “rewired” so that it expresses the connectivity of the new coherent subgraph (and the excitation placed in the appropriate node). Therefore, the total number of physical nodes need only be as large as the largest coherently connected subgraph, provided the coherent coupling between physical nodes is tunable. One can imagine creating very large graphs built up of smaller coherent subgraphs in this way. Another approach one can envision would be to have different physical set-ups for each subgraph. As jumps effectively erase the memory of system, the statistical behaviour of each subgraph can be investigated independently and the final (complete) trajectories determined by connecting corresponding subgraph trajectories. This approach would require no rewiring of the set-up.

5.4 Conclusion

In this work we have introduced the concept of “quantum trajectories on a quantum computer” (QTQC), which is a quantum trajectories simulation of open system dynamics run on a quantum computer instead of a classical computer. As we have shown, QTQC cannot be used to simulate all Lindblad master equations, but when it can, it is more efficient than the classical simulation, owing to its quantum nature.

We have applied QTQC to simulating quantum stochastic walks (QSWs), a class of quantum algorithms that have many applications, including machine learning [80, 87], and quantum transport [83, 89]. We have found that using QTQC, one can simulate a restricted class of QSWs that still exhibit a flexible and rich graph topology. Examples of interesting QSWs that can be simulated with QTQC already exist [80]. Additionally, for some graphs the restrictions can be lifted using ancillary systems and/or approximately lifted using a Suzuki-Trotter decomposition of the coherent evolution.

The coherence time of a QTQC simulator for a QSW need only be longer than the average time between quantum jumps, which can be many times shorter than the total simulation time. In addition, the QTQC simulator must only contain as many nodes as the largest coherently connected subgraph of the QSW, as QTQC trajectories can be pieced together. With these points in mind, QTQC simulation of a complex QSW on a large graph is likely achievable in the near future.

6 Quantum Simulation of a Discrete-Time QSW

In this section we propose an algorithm to simulate discrete-time QSWs. The central concept behind our protocol is that if one performs randomly chosen unitary dynamics from a carefully designed set, this can implement a specific non-unitary evolution in the ensemble average [101]. Our protocol is based on ancilla systems and a feed-forward scheme to implement the required evolution. The simplicity of the implementation of a single edge leads to straight-forward scaling to more complex graphs, and is a key feature of the protocol.

6.1 Quantum Simulation of a Kraus Map

The algorithm proposed here will be formulated on the Kraus decomposition of the desired QSW. Any completely-positive and trace preserving quantum operation [8], can be written in Kraus operator form as

$$\mathcal{B}[\rho] = \sum_j \hat{K}_j \rho \hat{K}_j^\dagger, \quad (2.23)$$

where $\{\hat{K}_j\}$ are the Kraus operators, which must satisfy $\sum_j \hat{K}_j^\dagger \hat{K}_j = \hat{\mathbb{I}}$ to preserve the trace of the quantum state. This condition implies that

$$\text{Tr} \left[\sum_j \hat{K}_j^\dagger \hat{K}_j \rho \right] = 1 \Rightarrow \sum_j \text{Tr} \left[\hat{K}_j^\dagger \hat{K}_j \rho \right] = \sum_j \tilde{P}_j = 1, \quad (2.24)$$

where we have defined the probabilities $\tilde{P}_j = \text{Tr}[\hat{K}_j^\dagger \hat{K}_j \rho]$, which are guaranteed to be non-negative as $\hat{K}_j^\dagger \hat{K}_j$ is Hermitian. We can then rewrite our original quantum operation as

$$\mathcal{B}[\rho] = \sum_j \tilde{P}_j \tilde{K}_j \rho \tilde{K}_j^\dagger, \quad (2.25)$$

where $\tilde{K}_j = \hat{K}_j / \sqrt{\tilde{P}_j}$. This definition will easily allow us to define our protocol through the ensemble average of quantum trajectories.

We now suppose that we have a protocol (which in our case uses ancilla systems and quantum measurement), labeled $\tilde{\mathcal{B}}$, that implements one of the \tilde{K}_j sampled from the set $\{\tilde{K}_j\}$ with the correct probability \tilde{P}_j . Then, if we implement this protocol many times on identical copies of the same initial state ρ , we have that

$$\mathbb{E} \left(\tilde{\mathcal{B}}[\rho] \right) = \sum_j \tilde{P}_j \tilde{K}_j \rho \tilde{K}_j^\dagger = \mathcal{B}[\rho], \quad (2.26)$$

where $\mathbb{E}(\cdot)$ is the ensemble average. We will use the above description as a single time-step of the discrete-time QSW.

Let us now consider repeated action of $\tilde{\mathcal{B}}$, and in analogy to the ‘‘quantum trajectories on a quantum computer’’ scheme developed in Ref. [47] (see section 5) we shall refer to each instance of such repeated action as a *trajectory*. By linearity of the

*Section 6 is available as an outdated preprint ‘‘P. K. Schuhmacher, L. C. G. Govia, B. G. Taketani and Frank K. Wilhelm’’, [arXiv:2004.06151](https://arxiv.org/abs/2004.06151) (2020). It has recently been accepted for publication in Europhysics Letters. The majority of the text was written by P. K. Schuhmacher.

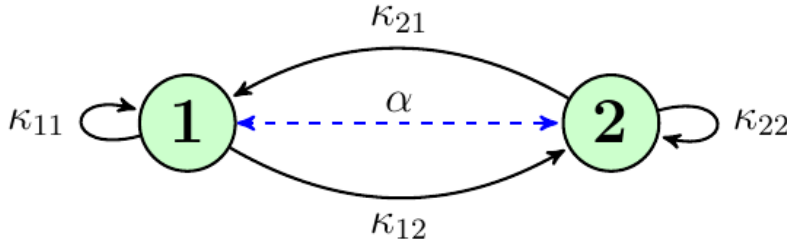


FIGURE 2.3: The most general 2-vertex-graph as the key building-block for arbitrary graphs. The vertices are coherently coupled (blue dashed arrow) as well as incoherently coupled (black arrows). The probabilities satisfy $\kappa_{11} + \kappa_{12} = \kappa_{21} + \kappa_{22} = 1 - \alpha$ due to trace-preservation of the density matrix.

quantum operations, we see that

$$\mathbb{E} \left(\tilde{\mathcal{B}} \left[\tilde{\mathcal{B}}[\rho] \right] \right) = \mathbb{E} \left(\tilde{\mathcal{B}} \left[\mathbb{E} \left(\tilde{\mathcal{B}}[\rho] \right) \right] \right) = \mathcal{B}[\rho], \quad (2.27)$$

which can be trivially extended to any number of actions of $\tilde{\mathcal{B}}$. Thus, by averaging over the final outcome of many trajectories we can simulate the action of an arbitrary number of repetitions of the Kraus map \mathcal{B} . In the rest of this manuscript, we detail how to implement a map of the form of $\tilde{\mathcal{B}}$ for the case of a discrete-time QSW.

6.2 Protocol

In the following, we show how to construct the quantum stochastic map $\tilde{\mathcal{B}}$ that, as described previously, can be used to simulate \mathcal{B} via the ensemble average. To do this for any connected graph \mathcal{G} , we use its key building-block: the 2-vertex graph \mathcal{G}_2 with a single (possibly directed) edge. Notice that Eq. (2.3) is of the form of the single time-step quantum operation, see Eq. (2.25). We thus need to define how to implement each of its Kraus operators.

6.2.1 A general 2-vertex graph

Let us consider the most general 2-vertex graph \mathcal{G}_2 with coherent edge coupling and all possible directed¹ edges, see figure 2.3. As we will argue, the procedure outlined below easily generalizes to larger graphs. For such 2-vertex graphs, Eq. (2.3) becomes

$$\mathcal{B}[\rho] := \alpha \hat{U}_{\mathcal{G}_2}(\Delta t) \rho(t) \hat{U}_{\mathcal{G}_2}^\dagger(\Delta t) + \sum_{m,n=1}^2 \kappa_{nm} |m\rangle \langle n| \rho |n\rangle \langle m|, \quad (2.28)$$

where trace-preservation implies that $\kappa_{11} + \kappa_{12} = \kappa_{21} + \kappa_{22} = 1 - \alpha$. The full system will be comprised of the original graph vertices, represented by the basis states $|n\rangle$, and one ancillary quantum state coupled to each graph vertex. We shall refer to the graph vertices simply as the *system*, and the ancillary states as the *ancillae*. The ancillae will be used to implement the stochastic processes. A single time-step of the QSW, given by Eq. (2.28), will be divided into three parts (see figure 2.4):

¹We call an edge directed if any of the $\kappa_{nm} > 0$, since that is the defining difference between a QSW and a coherent QW.

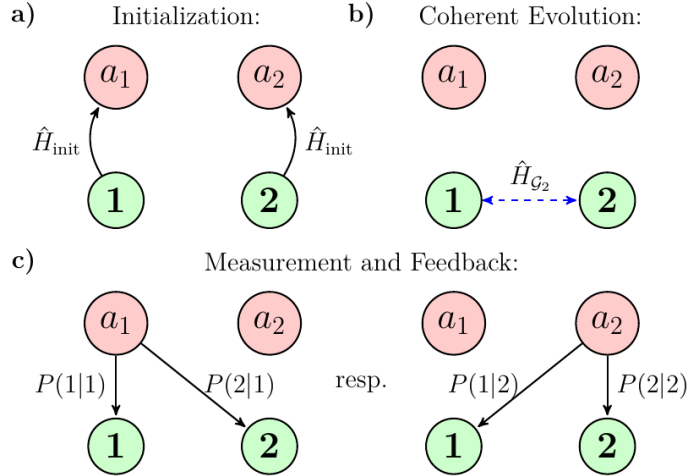


FIGURE 2.4: Protocol to simulate a discrete-time quantum stochastic walk on the most general 2-vertex graph \mathcal{G}_2 . **a)** The vertex-states are coherently coupled to their corresponding ancillae via \hat{H}_{init} for time Δt_{init} such that $g\Delta t_{\text{init}} = \arccos(\sqrt{\alpha})$. **b)** The vertex-states are coupled according to the coherent part of the graph \mathcal{G}_2 . **c)** The population of the ancillae is measured. If one of them is found to be occupied, the excitation is transitioned to one of the vertices according to the corresponding rates. If the ancillae are both found to be empty, no further feed-forward step is needed. This completes a single time-step of the discrete-time quantum stochastic walk.

(1) *Initialization*: At the start of each time-step, the system and ancillae are uncoupled with no excitations in the ancillae. The density matrix can then be written as

$$\rho_0 = \begin{pmatrix} \rho_{11} & \rho_{12} & \rho_{1a_1} & \rho_{1a_2} \\ \rho_{21} & \rho_{22} & \rho_{2a_1} & \rho_{2a_2} \\ \rho_{a_1 1} & \rho_{a_1 2} & \rho_{a_1 a_1} & \rho_{a_1 a_2} \\ \rho_{a_2 1} & \rho_{a_2 2} & \rho_{a_2 a_1} & \rho_{a_2 a_2} \end{pmatrix} = \begin{pmatrix} \rho_{11} & \rho_{12} & 0 & 0 \\ \rho_{21} & \rho_{22} & 0 & 0 \\ 0 & 0 & 0 & 0 \\ 0 & 0 & 0 & 0 \end{pmatrix}, \quad (2.29)$$

where the subscript 1 (2) denotes vertex 1 (2), and subscripts a_1 , a_2 denote the corresponding ancillae. All vertices are then coupled to their corresponding ancillae via the interaction Hamiltonian

$$\hat{H}_{\text{init}} := g(|1\rangle\langle a_1| + |a_1\rangle\langle 1| + |2\rangle\langle a_2| + |a_2\rangle\langle 2|), \quad (2.30)$$

for time Δt_{init} . All couplings are equal and Δt_{init} is chosen such that

$$g\Delta t_{\text{init}} = \arccos(\sqrt{\alpha}). \quad (2.31)$$

This choice is crucial, as will become clear in the second step discussed below. It results in a density matrix ρ_{init} right after the initialization step that is given by

$$\rho_{\text{init}} = \hat{U}_{\text{init}}\rho_0\hat{U}_{\text{init}}^\dagger = \begin{pmatrix} \alpha\rho_{11} & \alpha\rho_{12} & \Upsilon_1 \\ \alpha\rho_{21} & \alpha\rho_{22} & \\ \Upsilon_1^\dagger & & \Upsilon_0 \end{pmatrix}, \quad (2.32)$$

where $\hat{U}_{\text{init}} = e^{-i\hat{H}_{\text{init}}\Delta t_{\text{init}}}$ and the Υ symbols represent generic 2×2 matrices whose precise form is not relevant at this stage.

(2) *Coherent Evolution*: We now decouple the ancillae from the system and implement the desired coherent evolution between the graph vertices within the system

$$\hat{H}_{\mathcal{G}_2} := g_{\text{coh}} (|1\rangle\langle 2| + |2\rangle\langle 1|) \quad (2.33)$$

for the desired length of the time-step Δt . Note that $\hat{H}_{\mathcal{G}_2}$ is the Hamiltonian of the graph \mathcal{G}_2 , which has one free element $g_{\text{coh}} \geq 0$. The density matrix ρ_{coh} after the coherent evolution is

$$\rho_{\text{coh}} = \hat{U}_{\mathcal{G}_2}(\Delta t)\rho_{\text{init}}\hat{U}_{\mathcal{G}_2}^\dagger(\Delta t), \quad (2.34)$$

where $\hat{U}_{\mathcal{G}_2} = e^{-i\hat{H}_{\mathcal{G}_2}\Delta t}$ is the propagator of the graph Hamiltonian. Explicitly, at the end of the coherent evolution step we obtain

$$\rho_{\text{coh}} = \left(\alpha \hat{U}_{\mathcal{G}_2}(\Delta t) \begin{pmatrix} \rho_{11} & \rho_{12} \\ \rho_{21} & \rho_{22} \end{pmatrix} \hat{U}_{\mathcal{G}_2}^\dagger(\Delta t) \quad \Upsilon \\ \Upsilon \quad \Upsilon \right). \quad (2.35)$$

which is an implementation of the first term (coherent evolution) on the right-hand side of Eq. (2.28) in the subspace of the vertices.

(3) *Measurement and Feed-Forward*: The final part of the protocol uses quantum measurement to randomly determine which term from Eq. (2.28) is implemented for each time-step in a given trajectory. The coherence between vertices and ancillae is also removed, guaranteeing that once each time-step is concluded the system state is of the form of Eq. (2.29). To do this, we decouple the system vertices and measure all ancillae simultaneously. As the system is restricted to the single-excitation subspace, there are three possible results:

1. the excitation is measured in ancilla a_1 ,
2. the excitation is measured in ancilla a_2 ,
3. all ancillae are found empty.

For an n -vertex graph there are $n + 1$ possible measurement outcomes. The last outcome guarantees that the walker is in one of the system vertices, and the second step implements the coherent evolution part of Eq. (2.28) in this case. No further action is required, and we can proceed to the next time-step in the trajectory.

The other measurement results are interpreted as one of the incoherent processes having taken place. To determine which, we use the incoherent rates κ_{ij} of the intended QSW as follows. If the excitation is found in ancilla a_i this fixes the index i in κ_{ij} , i.e. the starting vertex of the incoherent process. To determine the index j and implement the incoherent evolution, we randomly choose j from a probability distribution given by the conditional probabilities $P(j|i)$, and then move the excitation to system vertex j . These conditional probabilities are given by

$$P(j|i) = \frac{\kappa_{ij}}{\sum_j \kappa_{ij}}. \quad (2.36)$$

In this feed-forward operation, the outcome of the quantum measurement combined with the outcome of the classical random choice determines which of the incoherent terms in Eq. (2.28) is implemented in this time-step of the trajectory.

The complete set of operators which describe the measurement and feed-forward step for a two-vertex graph is given by $\{\hat{M}_0, \hat{M}_1^{a_1}, \hat{M}_2^{a_1}, \hat{M}_1^{a_2}, \hat{M}_2^{a_2}\}$. Their precise forms are given in appendix A.c. \hat{M}_0 describes the measurement outcome where both ancillae are found to be empty, and we write

$$\hat{M}_{1/2}^{a_1} = \hat{F}_{1/2}^{a_1} \hat{M}_{a_1} \text{ and } \hat{M}_{1/2}^{a_2} = \hat{F}_{1/2}^{a_2} \hat{M}_{a_2}, \quad (2.37)$$

where \hat{M}_{a_1/a_2} describes the measurement where the excitation is found in ancilla a_1/a_2 , and $\hat{F}_{1/2}^{a_1/a_2}$ describes the conditional feed-forward according to the measurement result and classical random choice.

The three step procedure outlined above implements a single step of a single trajectory of the discrete-time QSW. Averaging over many trajectories we obtain the density matrix

$$\begin{aligned} \rho_{\Delta t} &:= \hat{M}_0 \rho_{\text{coh}} \hat{M}_0^\dagger + \sum_{y \in \{1,2\}} \sum_{x \in \{a_1, a_2\}} \hat{M}_y^x \rho_{\text{coh}} \hat{M}_y^{x\dagger} \\ &= \begin{pmatrix} \mathcal{B} \left[\begin{pmatrix} \rho_{11} & \rho_{12} \\ \rho_{21} & \rho_{22} \end{pmatrix} \right] & 0 & 0 \\ & 0 & 0 \\ & 0 & 0 & 0 & 0 \end{pmatrix}. \end{aligned} \quad (2.38) \quad (2.39)$$

A k -step trajectory is performed by k successive implementations of the above protocol, with its ensemble average having the desired statistics to simulate the QSW.

6.2.2 Arbitrary Graphs

The protocol proposed in section 6.2.1 generalizes trivially to any larger graph \mathcal{G} , with each system vertex requiring an ancilla. As before, a single time-step is split into three parts:

- (1) *Initialization*: System states are coupled to their corresponding ancillae via

$$\hat{H}_{\text{init}} := \sum_{m \in V(\mathcal{G})} g (|m\rangle \langle a_m| + |a_m\rangle \langle m|), \quad (2.40)$$

for a time Δt_{init} . Here, the summation covers all the graph vertices $m \in V(\mathcal{G})$ and the state $|a_m\rangle$ denotes the ancilla state which corresponds to vertex m . Again, Δt_{init} is chosen such that

$$g \Delta t_{\text{init}} = \arccos(\sqrt{\alpha}). \quad (2.41)$$

During this step, there is no coupling between the vertices at all. Hence, the scalability of this step to larger graphs is trivial, since each vertex-ancilla pair is independent of the others.

- (2) *Coherent Evolution*: The ancillae are now decoupled from the system and the system evolves coherently with

$$\hat{H}_{\mathcal{G}} := \sum_{(n,m) \in E(\mathcal{G})} g_{nm} (|m\rangle \langle n| + |n\rangle \langle m|), \quad (2.42)$$

for a time Δt . Note that Eq. (2.42) is the full Hamiltonian of the graph as the summation covers all the edges of the graph.

(3) *Measurement and Feed-Forward*: Finally, the ancillae are measured. As before, if the ancilla are all found to be empty the time-step is complete. If the excitation is found in an ancilla, then the excitation will be incoherently moved to a randomly chosen system vertex that is connected to the system vertex corresponding to the excited ancilla. This process is identical to that described previously for a two-vertex graph, but with the choice of final vertex expanded to include all vertices connected incoherently ($\kappa_{ij} > 0$) to the initial vertex.

Parts (1)-(3) implement a single time-step of Eq. (2.28). Again, the complete walk will be given by iterating this procedure. We note that the projective measurement resets all the ancillae at each logical time-step. Therefore, all the correlations between the ancilla states one could imagine due to the repetition of the whole protocol will be erased at every single logical time-step. Hence, there is no disturbing indirect coupling between ancillae induced dependent on the graph topology.

We remark that the protocol presented here is distinct from the one introduced in appendix A.b, to simulate non-unitary dynamics. The discrete time of the model presented here allows for the design of system-ancilla interactions and a measurement scheme such that all possible measurement outcomes are interpreted as part of a given trajectory. This overcomes an important drawback of the more broad protocol of appendix A.b, where post-selection is in general required.

6.3 Simulating a Continuous-Time QSW by a Discrete-Time QSW

In the previous sections we showed how to simulate discrete-time quantum stochastic walks as defined by Eq. (2.3) and Eq. (2.4), using a trajectory approach. However, currently the majority of applications of QSWs use the continuous-time version, as is widely documented in literature [80, 83, 87, 89, 102, 103, 104, 105]. Therefore, we now show how to implement a restricted set of continuous-time QSW by a discrete-time QSW, such that our method for simulating discrete-time QSWs is also applicable.

As mentioned in section 4, the continuous-time quantum stochastic walk of Ref. [85] is given by a Lindblad master equation of the form

$$\dot{\rho} = (\omega - 1)i [\hat{H}_{\mathcal{G}}, \rho] + \omega \sum_k \gamma_k \left(\hat{L}_k \rho \hat{L}_k^\dagger - \frac{1}{2} \{ \hat{L}_k^\dagger \hat{L}_k, \rho \} \right), \quad (2.43)$$

where ρ is the density operator of the system, \hat{L}_k are the Lindblad operators with γ_k their associated incoherent transition rates, $\hat{H}_{\mathcal{G}}$ is the Hamiltonian of the underlying graph \mathcal{G} and $\omega \in [0, 1]$. We write the Liouvillian \mathcal{L}_ω of equation (2.43) as

$$\mathcal{L}_\omega \rho = (1 - \omega) \mathcal{H} \rho + \omega \Lambda \rho, \quad (2.44)$$

where $\mathcal{H} \rho = -i [\hat{H}_{\mathcal{G}}, \rho]$ and

$$\Lambda \rho = \sum_k \gamma_k \left(\hat{L}_k \rho \hat{L}_k^\dagger - \frac{1}{2} \{ \hat{L}_k^\dagger \hat{L}_k, \rho \} \right). \quad (2.45)$$

The Liouvillian (2.44) is the generator of a quantum dynamical semigroup [26]. Therefore, we can write

$$\rho(t + \Delta t) = \exp(\mathcal{L}_\omega \Delta t) \rho(t) = \left(\sum_{l=0}^{\infty} \frac{1}{l!} \mathcal{L}_\omega^l \Delta t^l \right) \rho(t). \quad (2.46)$$

Inserting Eq. (2.44) into Eq. (2.46) yields, up to first order in Δt ,

$$\begin{aligned}\rho(t + \Delta t) &= \left(1 + \Delta t ((1 - \omega)\mathcal{H}_{\mathcal{G}} + \omega\Lambda) + \mathcal{O}(\Delta t^2)\right)\rho(t) \\ &= \left((1 - \omega)(1 + \Delta t\mathcal{H}_{\mathcal{G}}) + \omega(1 + \Delta t\Lambda) + \mathcal{O}(\Delta t^2)\right)\rho(t).\end{aligned}\quad (2.47)$$

Prima facie, this short-time Taylor expansion violates completely positive and trace preserving (CPTP) conditions on the dynamics in general. However, we will soon derive the necessary and sufficient condition to ensure that the simulated dynamics are CPTP.

The first term on the right-hand side of Eq. (2.47) can be interpreted as pure coherent evolution that occurs with probability $(1 - \omega)$. Analogously, we interpret the second term as describing incoherent evolution occurring with probability ω .

We now consider continuous-time QSWs where the incoherent evolution describes incoherent excitation transfer between system vertices [87], such that $\hat{L}_k = |m\rangle\langle n|$. In this case, the incoherent evolution of Eq. (2.47) becomes

$$\begin{aligned}\omega(1 + \Delta t\Lambda)\rho &= \omega\rho \\ &+ \sum_{(m,n) \in E(\mathcal{G})} \omega\Delta t\gamma_{nm} \left(|m\rangle\langle n|\rho|n\rangle\langle m| - \frac{1}{2}\{|n\rangle\langle n|, \rho\}\right).\end{aligned}\quad (2.48)$$

Here, the k -th Lindblad operator $\hat{L}_k = |m\rangle\langle n|$ generates an incoherent jump from vertex n to vertex m , and γ_{nm} describes the transition rate for this process, with $E(\mathcal{G})$ the set of connected edges of the graph.

To first order in Δt , we see that $p_{nm} = \Delta t\gamma_{nm}$ can be treated as the conditional probability to transition to vertex m if the excitation is in vertex n during time-step Δt , if the Lindblad rates satisfy

$$\sum_{m \in V(\mathcal{G})} p_{nm} = \sum_{m \in V(\mathcal{G})} \Delta t\gamma_{nm} = 1, \quad (2.49)$$

to ensure conservation of probability. In other words, satisfying Eq. (2.49) guarantees that the simulated dynamics are CPTP. This condition must be satisfied simultaneously for all n , which is possible if and only if

$$\sum_{m \in V(\mathcal{G})} \gamma_{nm} = \gamma \quad \forall n \in V(\mathcal{G}), \quad (2.50)$$

such that $\Delta t = \gamma^{-1}$ can be chosen uniquely to simultaneously guarantee Eq. (2.49) for all n . We note that this is the same restriction on the Lindblad rates as was necessary for protocols to simulate continuous time QSWs using quantum trajectories on a quantum computer [47].

Under this restriction, we can write the incoherent evolution as

$$\begin{aligned}
& \omega\rho + \omega \sum_{(m,n) \in E(\mathcal{G})} p_{nm} \left(|m\rangle\langle n|\rho|n\rangle\langle m| - \frac{1}{2}\{|n\rangle\langle n|, \rho\} \right) \\
&= \omega\rho + \omega \sum_{(m,n) \in E(\mathcal{G})} p_{nm} |m\rangle\langle n|\rho|n\rangle\langle m| \\
&\quad - \frac{\omega}{2} \underbrace{\sum_{n \in V(\mathcal{G})} \{|n\rangle\langle n|, \rho\}}_{=2\rho} \underbrace{\sum_{m \in V(\mathcal{G})} p_{nm}}_{=1} \\
&= \sum_{(m,n) \in E(\mathcal{G})} \kappa_{nm} |m\rangle\langle n|\rho|n\rangle\langle m|, \tag{2.51}
\end{aligned}$$

where in the last line we have defined $\kappa_{nm} = \omega p_{nm}$. Thus, we see that the short-time incoherent evolution for this restricted class of continuous-time QSWs has the same form of the incoherent part of the discrete-time QSW we have used throughout this manuscript.

Similarly, we replace $(1 + \Delta t \mathcal{H}_{\mathcal{G}})$ with the unitary propagator $\hat{U}_{\mathcal{G}}(\Delta t) = e^{-i\hat{H}_{\mathcal{G}}\Delta t}$ for the coherent evolution. Combining these results, and defining $\alpha = 1 - \omega$, we see that we can write the continuous-time evolution for short Δt as

$$\begin{aligned}
\rho(t + \Delta t) &= \alpha \hat{U}_{\mathcal{G}}(\Delta t) \rho(t) \hat{U}_{\mathcal{G}}^{\dagger}(\Delta t) \\
&\quad + \sum_{(m,n) \in E(\mathcal{G})} \kappa_{nm} |m\rangle\langle n|\rho|n\rangle\langle m| + \mathcal{O}(\Delta t^2). \tag{2.52}
\end{aligned}$$

This has the form of a Kraus map for a discrete-time QSW, and as such, we have shown how to implement the short time evolution of a restricted class of continuous-time QSWs with a discrete-time QSW, broadening the applicability of our simulation method for discrete-time QSWs.

6.4 Conclusion

In this section, we developed a trajectory-based protocol to simulate discrete-time QSWs on a coherent quantum computer. This ancilla-based protocol breaks down each time-step of the QSW into three parts that require only coherent couplings, measurements, and feed-forward operations, and thus are suitable to implementation on quantum hardware. Subsequent applications of this process create a single quantum trajectory with a certain probability, and we show that, as with the standard quantum trajectories approach, ensemble averages over many trajectories mimics the desired QSW dynamics.

The full time-step was carefully detailed for the most general graph of two vertices and we have shown that this serves as a building block to simulate arbitrary graphs. The simple procedure to generalize to complex graphs is one of the key features of our proposal, as no complicated design of system-ancillae interaction is needed. The protocol can also be employed for simulations of continuous-time QSWs satisfying certain conditions, which are also present in previously proposed simulation methods using quantum computers.

We note that as our protocol is designed on the single-excitation subspace, hardware implementations using qubits to represent vertices and ancillae are not resource efficient. Such qubit implementations use a 2^{2N} -dimensional Hilbert space to simulate a graph \mathcal{G} with $|V(\mathcal{G})| = N$, which only requires $2N$ degrees of freedom including

ancillae¹. The system size scales linearly as the walk size increases, and we have demonstrated that the same scaling is possible for the additional ancillae resources. Reducing this further to a constant scaling necessitates an increase in protocol complexity, and requires increased device connectivity and protocol time. For near-term devices, we believe that our simple protocol, even with its linear resource scaling, will be the better option. Particularly, the initialization step becomes very easy independently of the graph topology if we use one ancilla per vertex. This is due to the fact that it is sufficient to turn the coupling on and off between each vertex and its ancilla and hence, no further control is needed.

As it is usual for quantum trajectory based protocols, our proposal will be more suited for simulations for which convergence scales faster than D^2 , where D is the Hilbert space dimension of the system to be simulated. As this heavily depends on the underlying graph \mathcal{G} , no general statement is possible. However, we note that as the system evolution is reset to a specific state after any ancilla is measured to be occupied, the protocol requires coherence times much shorter than the total simulation time and could therefore be useful for near-term quantum hardware implementations.

¹An alternative approach could use qutrits to represent each vertex, with the third energy level representing the ancillae.

Appendices

A.a Graph Restriction due to Commutation of \hat{K}_{SE} and \hat{H}_{SE}

To simulate a quantum stochastic walk using a QTQC protocol, it is required that the operators \hat{K}_{SE} and \hat{H}_{SE} commute. Using the form of these operators given in equations (2.14) and (2.15), we see that

$$\begin{aligned} [\hat{H}_{\text{SE}}, \hat{K}_{\text{SE}}] &= \frac{1}{2} \sum_{ijk} \left(g_{ij} \lambda_k |\phi_i\rangle \langle \phi_j| \phi_k \langle \phi_k| - g_{ij} \lambda_k |\phi_k\rangle \langle \phi_k| \phi_i \langle \phi_j| \right) \\ &= \frac{1}{2} \sum_{ijk} \left(g_{ij} \lambda_k \delta_{jk} |\phi_i\rangle \langle \phi_k| - g_{ij} \lambda_k \delta_{ki} |\phi_k\rangle \langle \phi_j| \right) \\ &= \frac{1}{2} \sum_{ij} g_{ij} (\lambda_j - \lambda_i) |\phi_i\rangle \langle \phi_j|, \end{aligned} \quad (2.53)$$

where δ_{nm} is the usual Kronecker delta, and we have used the fact that the single excitation subspace states $|\phi_n\rangle$ are orthonormal. As the set of operators $\{|\phi_i\rangle \langle \phi_j|\}_{ij}$ are mutually orthogonal, then each term in the sum in equation (2.53) must vanish independently, which leads to the graph restriction of equation (2.16).

The restriction $g_{ij}(\lambda_i - \lambda_j) = 0$ does not need to precisely hold for the QTQC protocol to be applicable. If $(\lambda_i - \lambda_j)/\lambda_i \ll 1$ for all $\{i, j\}$ for which $g_{ij} \neq 0$, then the Suzuki-Trotter decomposition of equation (2.10) can be applied and the protocol can be used as an approximate solution.

A.b Simulating Nonphysical Evolution

In this appendix we describe a protocol to simulate nonphysical evolution. Previous protocols have been developed to simulate specific nonphysical evolutions [106], and here we present a protocol to simulate the evolution $|\psi(t)\rangle = e^{-\hat{K}t} |\psi(0)\rangle$, where K is a normal operator that is *not* skew-Hermitian, such that $e^{-\hat{K}t}$ is not a unitary matrix.

However, as \hat{K} is a normal matrix it is diagonalizable in its eigenbasis, which we shall label by $\{|K_n\rangle\}_{n=1}^D$, where D is the dimension of the Hilbert space of the graph. We begin by expressing the initial state in terms of the eigenbasis of \hat{K}

$$|\psi(0)\rangle = \sum_{n=1}^D c_n |K_n\rangle, \quad (2.54)$$

and it is clear that in this basis the final state is given by

$$|\psi(t)\rangle = \sum_{n=1}^D e^{-k_n t} c_n |K_n\rangle, \quad (2.55)$$

where k_n is the n 'th eigenvalue of \hat{K} .

We introduce an ancillary quantum system of dimension D spanned by the basis $\{|\eta_n\rangle\}_{n=1}^D$, which is initialized in a state $|\Omega\rangle$. Next, we perform the controlled entangling unitary

$$\hat{U} = \sum_{n=1}^D |K_n\rangle \langle K_n| \otimes \hat{U}_n, \quad (2.56)$$

where $\hat{U}_n |\Omega\rangle = |\eta_n\rangle$, such that the state of the joint system becomes

$$|\varphi\rangle = \sum_{n=1}^D c_n |K_n\rangle |\eta_n\rangle. \quad (2.57)$$

Finally, we perform a measurement of the ancilla system in a basis that contains the state

$$|M\rangle = \frac{1}{\sqrt{\mathcal{N}}} \sum_{n=1}^D e^{-knt} |\eta_n\rangle, \quad (2.58)$$

where $\mathcal{N} = \sum_{n=1}^D e^{-2knt}$. When the outcome of the measurement is the state $|M\rangle$ the final state of the joint system is

$$\begin{aligned} |\varphi'\rangle &= \frac{\hat{\mathbb{I}} \otimes |M\rangle \langle M|\varphi\rangle}{\sqrt{\text{Tr} [\hat{\mathbb{I}} \otimes |M\rangle \langle M|\varphi\rangle \langle \varphi|]}} \\ &= \frac{1}{\sqrt{\mathcal{N}}} \sum_{n=1}^D c_n e^{-knt} |K_n\rangle \otimes |M\rangle = \frac{1}{\sqrt{\mathcal{N}}} |\psi(t)\rangle |M\rangle. \end{aligned} \quad (2.59)$$

As can be seen, the graph has been unentangled from the ancilla, and is now in the desired state $|\psi(t)\rangle$ (up to an irrelevant normalization factor).

The protocol is probabilistic, as it succeeds only when the outcome of the ancilla measurement is $|M\rangle$, which happens with a probability given by the normalization factor \mathcal{N} . The longer the desired simulation time t , the smaller this factor, and therefore, the less likely the protocol is to succeed.

In addition, this protocol creates the state $|\psi(t)\rangle$ for a single time t , and cannot simulate continuous time evolution under the nonphysical \hat{K} . For QTQC, one still needs to know the state $|\psi'(t_i)\rangle$ at the beginning of each coherent time step, in order to calculate the norm as a function of time, now given by the formula

$$\langle \psi(t_{i+1}) | \psi(t_{i+1}) \rangle = \langle \psi'(t_i) | e^{-2\hat{K}t} | \psi'(t_i) \rangle = \sum_{n=1}^D |c_n|^2 e^{-2knt}. \quad (2.60)$$

The protocol presented here is one example of a protocol to simulate $e^{-\hat{K}t} |\psi(0)\rangle$, and is neither meant to be optimal in any sense (resources, complexity, etc.), nor simple to implement in a physical system. It is only meant to highlight the fact that simulation of $e^{-\hat{K}t} |\psi(0)\rangle$ is possible in principle, and we anticipate that physical implementation of such a simulation will require extensive further theoretical and experimental work.

One advantage of this approach based on quantum trajectories is that the dimension of the ancillary system scales with D , whereas general environmental representations require ancillary systems with dimension scaling with D^2 [107]. We note that related protocols have recently been proposed in Ref. [108].

A.c Measurement Operators

The measurement operators in Eq. (2.37) for a 2-vertex graph are:

$$\hat{M}_0 = |1000\rangle\langle 1000| + |0100\rangle\langle 0100| \quad (2.61)$$

$$\hat{M}_{a_1} = |0010\rangle\langle 0010| \quad (2.62)$$

$$\hat{M}_{a_2} = |0001\rangle\langle 0001| \quad (2.63)$$

$$\begin{aligned} \hat{F}_1^{a_1} = P(1|1) & (|1000\rangle\langle 0010| + |0100\rangle\langle 0100| \\ & + |0010\rangle\langle 1000| + |0001\rangle\langle 0001|) \end{aligned} \quad (2.64)$$

$$\begin{aligned} \hat{F}_2^{a_1} = P(2|1) & (|1000\rangle\langle 1000| + |0100\rangle\langle 0010| \\ & + |0010\rangle\langle 0100| + |0001\rangle\langle 0001|) \end{aligned} \quad (2.65)$$

$$\begin{aligned} \hat{F}_1^{a_2} = P(1|2) & (|1000\rangle\langle 0001| + |0100\rangle\langle 0100| \\ & + |0010\rangle\langle 0010| + |0001\rangle\langle 1000|) \end{aligned} \quad (2.66)$$

$$\begin{aligned} \hat{F}_2^{a_2} = P(2|2) & (|1000\rangle\langle 1000| + |0100\rangle\langle 0001| \\ & + |0010\rangle\langle 0010| + |0001\rangle\langle 0100|). \end{aligned} \quad (2.67)$$

Chapter III

Hybrid Quantum-Classical Annealing

Adiabatic quantum computing (AQC) is an equivalent alternative to the gate-based model for quantum computing described in chapter I. It has been shown to be universal by Aharonov et al. in 2004 [109]. However, the two approaches differ a lot: In contrast to the circuit model, where the computation is performed via a sequence of unitary quantum gates, in AQC, the solution of the problem of interest will be encoded in the ground state of some suitable Hamiltonian. Finding this ground state is a computationally hard task in general. The core idea is to evolve the system over time, from the known, unique and easily preparable ground state of some initial Hamiltonian, to the ground state of the desired Hamiltonian. If this evolution is slow enough, the adiabatic theorem guarantees that the system will stay in the instantaneous ground state during all the evolution time and the solution of the problem will be found by just measuring the state of the final Hamiltonian in its eigenbasis. Obviously, the drawback of this approach is the condition to evolve "slow enough". In many cases of interest, satisfying this condition implies an exponential growth of the needed evolution time with respect to the system size. In this chapter, we discuss hybrid quantum-classical annealing, an alternative approach to target this issue. Here, the core idea is to accept diabatic excitations during the sweep due to finite sweep times and to cool the system back to the instantaneous ground state afterwards. As cooling reduces energy, carefully engineered decoherence will be needed to drain the energy out of the system.

Preface

This chapter is based on joint work of many people including me. I spent a long time on the principle ideas how a cooling scheme assisting AQC could work and to find a master equation approach which promised reliable results, as we were interested in a parameter regime where typical approximations are questionable. At the time we knew what to test and how to do the numerics, I went to parental leave and during this time, Lukas S. Theis took over my project (still supported by me) and finished the work on HQCA for a single qubit that resulted in the preprint [110]. Section 9 is based on this preprint and it also appears as a part of the PhD thesis of its first author Lukas S. Theis. The majority of this preprint has been written by him during the time of my parental leave. However, as his work was based on my previous work, it is warrantable to be part of my thesis too. Section 10 is currently unpublished and completely written by me.

8 Introduction to Adiabatic Quantum Computing

In this section, I give a brief overview on the field of adiabatic quantum computing, its promises and drawbacks. In the last years, its development became faster and faster, driven by academic and industrial research [111]. I do not cover all the details here. For further reading, I recommend the elaborate review [12].

8.1 3-SAT

Some of the simplest examples of NP-complete problems come from propositional logic [7]. A *Boolean formula* over the variables u_1, \dots, u_n consists of the variables and the logical operators AND (\wedge), NOT (\neg) and OR (\vee). If φ is a Boolean formula over variables u_1, \dots, u_n and $z \in \{0, 1\}^n$, then $\varphi(z)$ denotes the value of φ when the variables of φ are assigned the values z (where we identify 1 with TRUE and 0 with FALSE). A formula φ is *satisfiable* if there exists some assignment z such that $\varphi(z)$ is TRUE. Otherwise, we say that φ is *unsatisfiable*.

A Boolean formula over variables u_1, \dots, u_n is in *conjunctive normal form*, if it is an AND of OR's of variables or their negations, i. e.

$$\bigwedge_i \bigvee_j v_{ij}, \quad (3.1)$$

where each v_{ij} is either a variable u_k or to its negation $\neg u_k$. The terms v_{ij} are called the *literals* of the formula and the terms

$$C_i := \bigvee_j v_{ij} \quad (3.2)$$

are called its *clauses*. Now, we focus on the following problem:

Is a given formula φ , written in conjunctive normal form in which all clauses contain at most k literals, satisfiable?

This is a standard problem in computer science known as k -SAT. It is proven to be NP-complete for $k \geq 3$. This means, each problem in NP can be mapped to k -SAT and k -SAT \in NP itself [7]. Particularly, 3-SAT is NP-complete.

8.2 Solving 3-SAT by Exploiting Physics

A k -local Hamiltonian is a Hermitian matrix that acts nontrivially on at most k p -state particles [12]. The *k -local Hamiltonian problem* is defined on n qubits with the following input:

- The total Hamiltonian \hat{H} can be written as a sum $\hat{H} = \sum_{i=1}^r \hat{H}_i$, where each \hat{H}_i is k -local, $r = \text{poly}(n)$ and $\|\hat{H}_i\| = \text{poly}(n)$ and its nonzero entries are specified by $\text{poly}(n)$ bits¹.
- There exist two real numbers a and b specified with $\text{poly}(n)$ bits of precision, such that

$$b - a > \frac{1}{\text{poly}(n)}. \quad (3.3)$$

¹The expression " $x = \text{poly}(n)$ " for some left hand side x means that the growth of x with increasing number of qubits n can be bounded by some polynomial function in n .

The output (0 or 1) answers the question: Is the smallest eigenvalue of \hat{H} smaller than a (output is 1), or are all eigenvalues larger than b (output is 0)? Here, we are promised that the ground state eigenvalue is not between a and b .

It is possible to map 3-SAT to the 3-local Hamiltonian problem as follows. For each clause C_i , we define a 3-local projector \hat{H}_i onto all the unsatisfying assignments of C_i . As \hat{H}_i is a projector, it has eigenvalues 0 and 1, where 0 corresponds to satisfying assignments and 1 corresponds to unsatisfying assignments. Hence,

$$\hat{H}|X\rangle = \sum_{i=1}^r \hat{H}_i|X\rangle = q|X\rangle, \quad (3.4)$$

where q is the number of unsatisfied assignments by X . Therefore, 3-SAT can be solved by solving the following 3-local Hamiltonian problem:

Is the smallest eigenvalue of \hat{H} zero (the 3-SAT problem is satisfiable) or it is greater or equal 1 (the 3-SAT problem is unsatisfiable)?

This native mapping from 3-SAT to the 3-local Hamiltonian problem proves the 3-local Hamiltonian problem to be NP-complete¹. Now, one could argue that this observation is not a big deal as we just replaced a computational hard problem by another equivalent computational hard problem. From the point of view of classical computing, this statement is true. However, in contrast to 3-SAT, the 3-local Hamiltonian problem is a problem in *physics*. Therefore, one could imagine to engineer an *analogue device* which is supposed to find the ground state of a 3-local Hamiltonian by the laws of physics rather than brute-force calculating it. Unfortunately, all (known) interactions existing in nature are 2-local and hence, there is no 3-local Hamiltonian in nature which can be used for this task. Hence, the desired 3-local Hamiltonian has to be engineered artificially using 2-local terms. This can be done using *perturbative gadgets* [12, 112, 113, 114, 115, 116]. The goal of the gadget is to approximate the 3-local target Hamiltonian \hat{H}_{target} of n qubits by a 2-local gadget Hamiltonian \hat{H}_{gadget} acting on the same n qubits plus some polynomial number of ancilla qubits. The gadget Hamiltonian \hat{H}_{gadget} can be chosen such that its low-energy eigenspace equals the eigenspace of \hat{H}_{target} up to a weak perturbation and all the "unwanted" states feel an energy penalty. For the details of this construction, we recommend App. E of Ref. [12].

With this, it is possible to map 3-SAT onto finding the ground state of problem Hamiltonians of the form

$$\begin{aligned} \hat{H}_P := & \sum_{(i,j) \in E(\mathcal{G})} J_{ij}^x \hat{\sigma}_i^x \hat{\sigma}_j^x + J_{ij}^y \hat{\sigma}_i^y \hat{\sigma}_j^y + J_{ij}^z \hat{\sigma}_i^z \hat{\sigma}_j^z \\ & + \sum_{i \in V(\mathcal{G})} h_i^x \hat{\sigma}_i^x + h_i^y \hat{\sigma}_i^y + h_i^z \hat{\sigma}_i^z, \end{aligned} \quad (3.5)$$

where $V(\mathcal{G})$ and $E(\mathcal{G})$ denote the vertices and the edges of a graph \mathcal{G} , $\hat{\sigma}_i^\nu$ is the Pauli- ν -operator on the i -th qubit for $\nu \in \{x, y, z\}$ and the coefficients h_i^ν and J_{ij}^ν can all be chosen to be real. Indeed, it is sufficient to focus on a special case of equation (3.5), namely the well-studied Ising spin glass Hamiltonian

$$\hat{H}_{\text{Ising}} := \sum_{(i,j) \in E(\mathcal{G})} J_{ij}^z \hat{\sigma}_i^z \hat{\sigma}_j^z + \sum_{i \in V(\mathcal{G})} h_i^z \hat{\sigma}_i^z. \quad (3.6)$$

¹Alternatively, there is a direct map to graph colouring too.

The problem to solve will be encoded in the coefficients h_i^z and J_{ij}^z . Hence, we are going to discuss how to build an analogue device which is supposed to find the ground states of Ising spin glass Hamiltonians in the following sections.

8.3 Adiabatic Quantum Computing

As we have seen in section 8.2, we can map the NP-complete 3-SAT problem to the problem of finding the ground state of the famous Ising spin glass Hamiltonian defined in equation (3.6) up to a polynomial overhead in the number of qubits n . Hence, if we would be able to build an analogue device which is supposed to find the ground state of such a Hamiltonian, we would be able to solve any problem in NP with it. Now, the question arises how to build such a device in practice. A promising ansatz is the so-called *quantum annealer* which will be discussed in the following.

When the term *adiabatic quantum computing (AQC)* has been introduced, it was focused on optimization [117]. Later on, it has been extended its scope and is now treated as a competing approach to the gate-based model for quantum computing. The original idea of using adiabatic evolution for solving computational problems appeared in Ref. [118]. Here, adiabaticity was proposed to solve classical combinatorial problems. This ansatz was introduced as *quantum stochastic optimization*, but the term *quantum annealing* has been established later on [119] as it is a quantum-improved version of the classical simulated annealing algorithm [120]. Quantum annealing can be implemented to run in the "native instruction set" of an AQC platform [121].

The core idea of AQC relies on the *adiabatic theorem* which appears in various approximate and rigorous versions [12, 122, 123, 124, 125, 126, 127, 128, 129, 130, 131]. Here, we give its simplest as well as one of the oldest traditional versions [12]:

Let $|\epsilon_j(t)\rangle$ ($j \in \mathbb{N} \cup \{0\}$) denote the instantaneous eigenstate of the time-dependent Hamiltonian $\hat{H}(t)$ with energy $\epsilon_j(t)$ such that $\epsilon_j(t) \leq \epsilon_{j+1}(t) \forall j, t$ and $j = 0$ denotes the (possibly degenerate) ground state. We assume that the initial state is prepared in one of the eigenstates $|\epsilon_j(0)\rangle$. Let t_f denote the final time and $s := t/t_f$. The quantum system will remain in the same instantaneous eigenstate $|\epsilon_j(t)\rangle$ (up to a global phase) for all $s \in [0, 1]$ if

$$\frac{1}{t_f} \max_{s \in [0,1]} \frac{|\langle \epsilon_i(s) | \partial_s \hat{H}(s) | \epsilon_j(s) \rangle|}{|\epsilon_i(s) - \epsilon_j(s)|^2} \ll 1 \quad \forall j \neq i. \quad (3.7)$$

The condition (3.7) gives rise to the widely used criterion that the total adiabatic evolution time should be large on the time scale set by the minimum of the square of the inverse spectral gap $\Delta_{ij}(s) := \epsilon_i(s) - \epsilon_j(s)$. In AQC, one is typically interested in the ground state, so that $\Delta_{ij}(s)$ can be replaced by

$$\Delta := \min_{s \in [0,1]} \Delta(s) = \min_{s \in [0,1]} (\epsilon_1(s) - \epsilon_0(s)). \quad (3.8)$$

In other words, if we prepare a quantum system in its instantaneous ground state and evolve the system Hamiltonian slow enough to some target Hamiltonian at $t = t_f$, then the adiabatic theorem guarantees the quantum system to end up in the ground state of this Hamiltonian at $t = t_f$. This observation leads to the original paradigm of AQC:

1. We encode the solution of some computational problem in the ground state of some Hamiltonian \hat{H}_{target} . If it is a computational hard problem, this ground state will be hard to be computed on a classical computer as well.
2. We prepare a quantum system in the well-known and non-degenerate ground state of some easily preparable Hamiltonian \hat{H}_0 .
3. We evolve the system adiabatically from \hat{H}_0 to \hat{H}_{target} . The adiabatic theorem guarantees us to end up in the desired ground state.
4. We measure the ground state of \hat{H}_{target} and we get the solution of the original computational problem.

Usually, the quantum system will consist of n strongly interacting qubits. A typical choice for the Hamiltonians \hat{H}_0 and \hat{H}_{target} is then given by

$$\hat{H}_0 := -\frac{1}{2} \sum_{i=1}^n \Delta_i \hat{\sigma}_i^x \quad \text{and} \quad \hat{H}_{\text{target}} := \hat{H}_{\text{Ising}} = \sum_{\substack{i,j=1 \\ j>i}}^n J_{ij}^z \hat{\sigma}_i^z \hat{\sigma}_j^z + \sum_{i=1}^n h_i^z \hat{\sigma}_i^z. \quad (3.9)$$

The reason behind this choice is manifold. The Hamiltonian \hat{H}_0 has a unique, well-known and easily preparable ground state by applying a strong transversal magnetic field to the n -qubit system. And \hat{H}_{Ising} as written in equation (3.6) is a diagonal matrix with known eigenstates. Nevertheless, finding the ground state of a general Ising spin glass Hamiltonian \hat{H}_{Ising} is NP-complete (even though the eigenstates are known, it is not clear which one of them is the ground state as there are 2^n possibilities). Therefore, even if the problem setting we choose here looks very specific, it is rather general as each computational problem in NP could be solved this way¹.

Now, the question arises how to interpolate between \hat{H}_0 and \hat{H}_{Ising} . The most general *annealing schedule* can be written as

$$\hat{H}(s) := A(s)\hat{H}_0 + B(s)\hat{H}_{\text{cat}} + C(s)\hat{H}_{\text{Ising}}, \quad (3.10)$$

where $A(s)$, $B(s)$ and $C(s)$ are smooth functions satisfying $A(t_f) = B(0) = B(t_f) = C(0) = 0$ and $A(0) = C(t_f) = 1$. The Hamiltonian \hat{H}_{cat} is called the *catalyst Hamiltonian* and can be used to optimize the schedule. In this work, we focus on the linear schedule

$$\hat{H}(s) := (1-s)\hat{H}_0 + s\hat{H}_{\text{Ising}}, \quad (3.11)$$

which is not optimal but the simplest option to study.

So far, we explained the original paradigm of adiabatic quantum computing. Obviously, this approach has a crucial drawback². The gist of the matter is "to evolve the system adiabatically from \hat{H}_0 to \hat{H}_{target} ". What does "adiabatically" mean in this context? How fast are we allowed to sweep? Figure 3.1 targets these questions regarding a qubit undergoing the standard Landau-Zener sweep [132, 133] which serves as a toy model for AQC³. It is the easiest time-dependent problem leading to an avoided crossing and hence, passing through a minimal gap Δ .

¹We do not really expect AQC to efficiently solve NP-complete problems. However, it is worth it to try.

²If life would be that easy, then we could stop all the research programs on quantum computing immediately.

³For the Landau-Zener problem, the time t fulfills $t \in [-t_f, t_f]$ due to historical reasons.

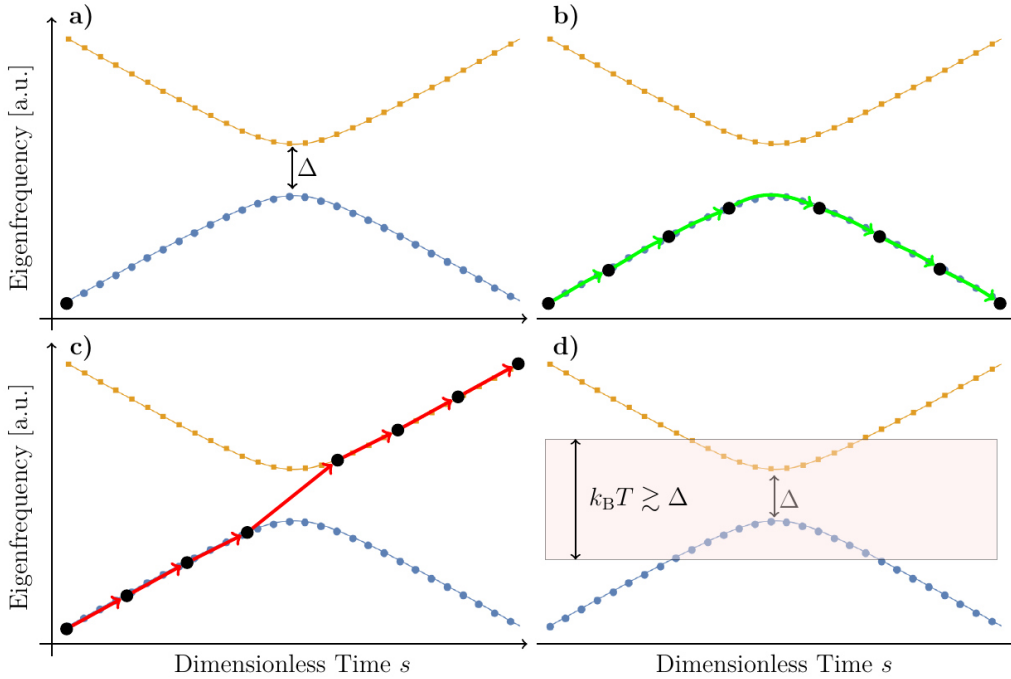


FIGURE 3.1: Landau-Zener physics as a toy model for AQC. **a)** Qubit eigenfrequencies as a function of dimensionless time $s \in [-1, 1]$. The qubit is initialized in the ground state at $s = -1$ (visualized as the black dot) and it is supposed to end up in the ground state at $s = 1$. During the sweep, the qubit will pass through the minimal gap Δ at $s = 0$. **b)** Desired time evolution. If the sweep velocity v is small enough, the qubit will stay in its instantaneous ground state throughout all the sweep time (green path). **c)** Diabatic errors. If the sweep velocity v is too large, the qubit will undergo a diabatic transition to the excited state (red path) and hence, the qubit will be found in the wrong state at the end of the sweep. **d)** Finite temperature effects. If $k_B T \gtrsim \Delta$, then the system can be excited by thermal fluctuations.

The Landau-Zener Hamiltonian $\hat{H}_{\text{LZ}}(t)$ reads

$$\hat{H}_{\text{LZ}}(t) := -\frac{v \cdot t}{2} \hat{\sigma}^z - \frac{\Delta}{2} \hat{\sigma}^x. \quad (3.12)$$

Here, the schedule is linear in t with a constant sweep velocity v . The goal is, starting in the ground state at $t = -t_f$, to end up in the ground state at $t = t_f$. To guarantee success, we have to satisfy the condition (3.7). Hence, the sweep velocity (which is proportional to $1/t_f$) has to be chosen as a function of Δ . The smaller Δ , the larger t_f has to be to avoid diabatic transitions. This is a challenging observation, because it is known that the size of the minimal gap Δ typically becomes tiny for computationally hard problems. In the worst-case scenario, it can decrease exponentially with the number of qubits n [134]. But, an exponentially decreasing gap means an exponentially increasing t_f . On the other hand, if the temperature of the annealer's environment exceeds the minimal gap, the qubit system will thermalize if the sweep is too slow. To add insult to injury, the size of the gap is unknown in general as calculating the gap requires diagonalization of the Hamiltonian [135]. Hence, even if the gap decreases only polynomially with increasing system size, we do not know

how to choose the time t_f to satisfy the condition (3.7) properly. In other words, we are not allowed to go too fast, we are not allowed to go too slow, and we do not know what "fast" and "slow" mean in practice. Hence, we will never be guaranteed to reach the ground state of the target Hamiltonian when we try to solve an unsolved computational problem.

In this regard, we should extend this original paradigm of AQC to target these issues. We tackle this challenge with an approach which we call *hybrid quantum-classical annealing (HQCA)* [110]. This approach is based on *engineered decoherence* which will be used to cool the system to its instantaneous ground state during the sweep. This concept is shown schematically in figure 3.2. Consider the 2^n eigenstates of a given Ising spin glass Hamiltonian of n qubits in some arbitrary order. These states form the discrete configuration space we would like to search for the state of lowest energy. Quantum annealing exploits the quantum mechanical tunnel effect to search the configuration space. This allows to go "through the hills in the energy landscape" which would not be possible in classical optimization. However, pure tunneling is totally coherent. Therefore, energy is conserved. On the other hand, the classical ansatz to use relaxation allows for reducing the energy, but it is exponentially likely to be stuck in some local minimum. The concept of hybrid quantum-classical annealing combines these two strategies: On the one hand, we exploit the tunnel effect to search the configuration space. On the other hand, we carefully engineer some decoherence on top of the pure coherent evolution to cool the system down to the desired ground state. This concept will be discussed in the following sections. We note that HQCA is distinct from the thermally assisted adiabatic quantum computation (TA-AQC) of Ref. [136] as the relaxation is induced by an engineered heat bath rather than using natural thermal fluctuations.

9 Hybrid Quantum-Classical Annealing of a Single Qubit

In section 8.3, we discussed the core idea of hybrid quantum-classical annealing as an advancement of adiabatic quantum computing. The main principle is to accept unavoidable diabatic transitions during the annealing sweep and to cool the system back to its instantaneous ground state using carefully engineered decoherence. Now, we apply this idea to a suitable toy model, namely the dissipative Landau-Zener problem governed by a spin-boson model [137].

9.1 Model and Equations of Motion

We investigate a dissipative Landau-Zener problem, governed by a spin-boson model [137]. The bare system Hamiltonian $\hat{H}_Q(t)$ features a generally time-dependent drive $\epsilon(t) \in \mathbb{R}$ and a constant tunneling amplitude $\Delta > 0$, i.e.

$$\hat{H}_Q(t) := -\frac{\epsilon(t)}{2}\hat{\sigma}^z - \frac{\Delta}{2}\hat{\sigma}^x. \quad (3.13)$$

In the simplest non-trivial model, $\epsilon(t)$ is linear in time with sweep velocity v and y -intercept ϵ_0 , i.e. $\epsilon(t) = v \cdot t + \epsilon_0$. Without loss of generality we will assume $\epsilon_0 = 0$ in the remainder of this work and let the sweep take place within the time interval $[-t_0, t_0]$ with t_0 chosen such that the initial energy splitting is large compared to the gap, i.e. $v \cdot t_0 = 80\Delta$. This serves as a proper toy model, especially if the two eigenstates can

*Section 9 is available as a preprint "L. S. Theis, P. K. Schuhmacher, M. Marthaler and Frank K. Wilhelm", [arXiv:1808.09873](https://arxiv.org/abs/1808.09873) (2018). The majority of the text was written by L. S. Theis.

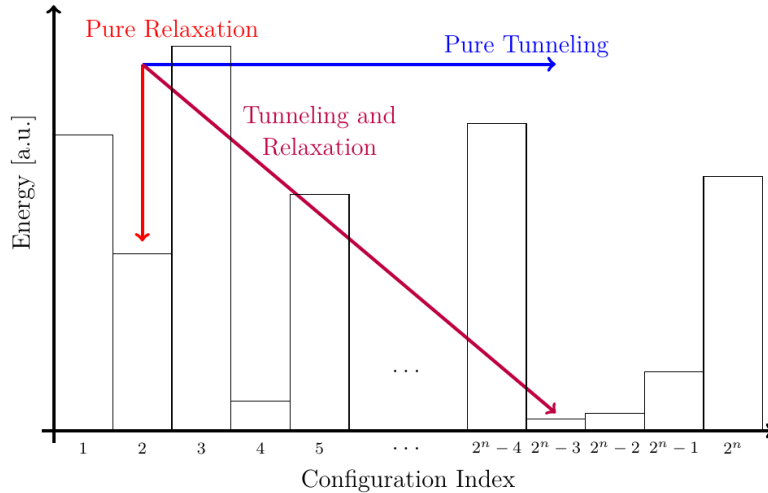


FIGURE 3.2: Hybrid Quantum-Classical Annealing (HQCA). The ultimate goal is to find the configuration which minimizes the energy. Quantum annealing exploits the quantum mechanical tunnel effect to search the configuration space. However, pure tunneling is totally coherent (it conserves energy). Hence, it only allows for going horizontally in the diagram. On the other hand, pure dissipation allows for reducing the energy, but it is exponentially likely to be stuck in some local minimum. Hybrid quantum-classical annealing combines these two principles: We use quantum tunneling to search the configuration space and in addition, we engineer some decoherence to reduce the energy.

be mapped to well-isolated adiabatic states of a larger system. In fact, a system that features such an isolated small gap has been engineered and analyzed with respect to the influence of (thermal) noise [138]. The full Hamiltonian of our system is given by the bare qubit $\hat{H}_Q(t)$, the heat bath \hat{H}_B and the qubit-environment coupling terms \hat{H}_{QB} . We model each heat bath as harmonic oscillators and assume that there are both X - and Z -couplings present, which we will refer to as transverse and longitudinal, respectively. The respective Hamiltonians are then given by

$$\hat{H}_{QB} := \sum_{\nu=x,z} \sum_k \hat{\sigma}^\nu \lambda_k^\nu (\hat{b}_k^\nu + \hat{b}_k^{\nu\dagger}) \quad (3.14)$$

$$\hat{H}_B := \sum_{\nu=x,z} \sum_k \omega_k^\nu \hat{b}_k^{\nu\dagger} \hat{b}_k^\nu. \quad (3.15)$$

Based on previous ideas and experiments [139, 140, 141, 142, 143] we propose a cooling scheme via an additional $\hat{\sigma}^x$ coupling – for instance realized by using a coplanar waveguide (CPW) as an environment, as shown in figure 3.3. The coupling strength to the qubit can be controlled in the fabrication process through the distance d between CPW and qubit. In order to derive an analytic set of equations of motions for the qubit subsystem, we follow the core idea of the standard Bloch-Redfield formalism (see section 3.7). An adequate model to describe the physics of AQC/QA is the spin-boson model [137], which properly characterizes the coupling of some quantum system with an external environment. In order to obtain analytic expressions for the equations of motion in case of generic time-dependent Hamiltonians we apply an appropriate formulation [144, 145] of the Bloch-Redfield theory. Following Refs. [144, 146] we

transform to a frame defined by the time-dependent rotation $\hat{R}(t) := \exp(i\phi(t)\hat{\sigma}^y/2)$ and denote operators in that frame with a tilde, i.e. $\tilde{O}(t) := \hat{R}(t)\hat{O}(t)\hat{R}^\dagger(t)$. Since the transformation is time-dependent the qubit Hamiltonian acquires an additional inertial term, which can be related to non-stoquastic interactions in a multi-qubit scenario [147], so that the Landau-Zener Hamiltonian in the rotating frame reads

$$\tilde{H}_Q(t) = -\frac{E(t)}{2}\hat{\sigma}^x + \frac{\dot{\phi}(t)}{2}\hat{\sigma}^y \quad (3.16)$$

where we use the mixing angle $\phi(t) = \arctan(\epsilon(t)/\Delta)$ and the instantaneous energy splitting $E(t) = \sqrt{\Delta^2 + \epsilon^2(t)}$. For later use we define $\tilde{H}_0(t) := -E(t)\hat{\sigma}^x/2$. Analogously, the qubit-environment coupling becomes

$$\tilde{H}_{\text{QB}}(t) = \sum_{\nu=x,z} \sum_k \tilde{\sigma}^\nu \lambda_k^\nu \left(\hat{b}_k^\nu + \hat{b}_k^{\nu\dagger} \right) \quad (3.17)$$

with $\tilde{\sigma}^\nu$ being the Pauli matrices in the rotating frame. By introducing the weights $f_1(t) := \sin(\phi(t))$ and $f_2(t) := \cos(\phi(t))$ we can express the rotating-frame-matrices as $\tilde{\sigma}^x = -f_1(t)\hat{\sigma}^z + f_2(t)\hat{\sigma}^x$ and $\tilde{\sigma}^z = f_2(t)\hat{\sigma}^z + f_1(t)\hat{\sigma}^x$, respectively. In order to provide closed analytical expressions for the equations of motion, one employs standard Markovian approximations and an additional adiabatic-Markovian approximation [144] (AMA). The latter is inevitable to deal with the interaction picture transformation needed to carry out the time-dependent Bloch-Redfield formalism. For a detailed derivation, please see appendix A.d. The AMA features two important parts: (i) the memory time of the bath τ_{mem} is assumed to be much smaller than any system time scale and (ii) the drive $\epsilon(t)$ approximately acts on time scales much larger than τ_{mem} so that it has no significant contribution to the rates. This, in turn, allows to derive the Bloch equations for the density matrix

$$\tilde{\rho}_Q(t) = \frac{1}{2} \left(\hat{\mathbb{I}} + \sum_n r_n(t) \hat{\sigma}_n \right) \quad (3.18)$$

associated to the qubit subsystem (3.16). The Bloch vector $(r_x, r_y, r_z)^T$ is determined by the set of quantum master equations (QME)

$$\dot{r}_x = \left(\dot{\phi} - \gamma_{xz} \right) r_z - \gamma_r (r_x - \bar{r}_x), \quad (3.19)$$

$$\dot{r}_y = E_t r_z - (\gamma_d + \gamma_r) r_y, \quad (3.20)$$

$$\dot{r}_z = -\dot{\phi} r_x - E_t r_y - \gamma_d r_z - \gamma_{zx} (r_x - \bar{r}_x). \quad (3.21)$$

Here, we used the shorthand notation $E_t := E(t)$ and $\bar{r}_x := \tanh(\beta E_t/2)$. The energy normalization is given by $\beta = 1/k_B T$ with Boltzmann constant k_B and temperature T . Note that we explicitly assume equal temperature for both reservoirs since, in experiments, they will be located in the same cryostat. We also defined the set of

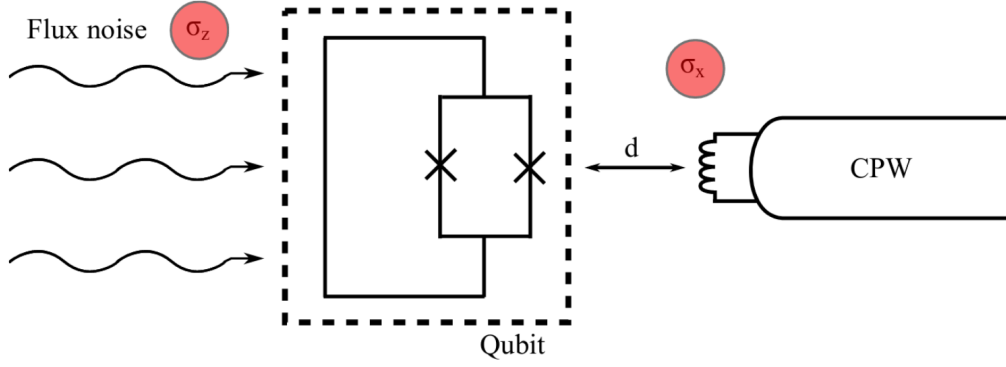


FIGURE 3.3: Schematic circuit diagram to implement both $\hat{\sigma}^x$ and $\hat{\sigma}^z$ coupling to a superconducting flux qubit. While the flux noise $\hat{\sigma}^z$ is always present, we propose to add an additional $\hat{\sigma}^x$ coupling in terms of a coplanar waveguide (CPW) at distance d from the qubit. The $\hat{\sigma}^x$ -coupling strength is set by the distance d .

rates

$$\gamma_r := 2\pi \coth\left(\frac{\beta E_t}{2}\right) (f_1^2 J_x(E_t) + f_2^2 J_z(E_t)), \quad (3.22)$$

$$\gamma_d := 4\pi \lim_{\omega \rightarrow 0} \bar{n}(\omega) (J_z(\omega) + J_x(\omega)), \quad (3.23)$$

$$\gamma_{xz} := 4\pi f_1 f_2 \lim_{\omega \rightarrow 0} \bar{n}(\omega) (J_x(\omega) - J_z(\omega)), \quad (3.24)$$

$$\gamma_{zx} := 2\pi f_1 f_2 \coth\left(\frac{\beta E_t}{2}\right) (J_x(E_t) - J_z(E_t)), \quad (3.25)$$

where $\bar{n}(\omega) = 1/(e^{\beta\omega} - 1)$ is the single particle Bose distribution. Note that the rates depend on the spectral densities $J_\nu(\omega)$ of the respective environments. Relaxation is encoded in γ_r , while γ_d and $\gamma_{xz,zx}$ describe pure dephasing and cross-dephasing, respectively. We stress that the Bloch-type equations (3.58)-(3.60) are based on a proper treatment of external drives. The performed AMA might suggest that the QME are only valid inside the adiabatic regime, i.e. when $v \ll \Delta^2$. However, even for non-adiabatic drives they are still a good approximation. This has been verified numerically for a similar Hamiltonian in Ref. [146] by comparing the numerical solutions of their equivalent of equations (3.58)-(3.60) to a numerically exact solution obtained via the path integral based method QUAPI which we introduced in section 3.13. Furthermore, a detailed analysis of the assumptions that lead to the QME in terms of different time scales has been carried out in Ref. [145].

9.2 Environmental Engineering

In our analysis we restrict ourselves to the case of Ohmic heat baths [148, 149]. That is, the spectral densities $J_\nu(\omega)$ depend linearly on ω . However, this model is only valid up to some high-frequency cutoff ω_C^ν . For our purpose, we choose to work with an exponential cutoff at frequencies $\omega_C^\nu := 10\Delta$ whereby the exact numerical value has an irrelevant impact on the quality of our results. Different coupling strengths are modeled by the parameter α_ν , so that the spectral density is eventually given by

$$J_\nu(\omega) := \alpha_\nu \omega e^{-\omega/\omega_C^\nu}. \quad (3.26)$$

With this explicit form of $J(\omega)$ we compute the limit

$$\lim_{\omega \rightarrow 0} \bar{n}(\omega) J_\nu(\omega) = \frac{\alpha_\nu}{\beta}. \quad (3.27)$$

We simulate the set of quantum master equations (3.19)-(3.21) with initial conditions set up such that the system will always start in the exact ground state of Hamiltonian (3.16). We use the final ground state population p_G after a full Landau-Zener sweep as our figure of merit to evaluate cooling effects.

In figure 3.4a we depict the dependence of p_G on the sweep velocity v , temperature T and for a pure $\hat{\sigma}^z$ coupling with $\alpha_z = 5 \cdot 10^{-3}$. As one expects, thermal excitations heat the system significantly, leading to significant population loss compared to coherent dynamics. If temperatures are not too high, i.e. $k_B T \lesssim 5\Delta$, there is a locally optimal velocity v_0 at which the sum of diabatic errors due to finite sweep length and thermal excitations are minimized [150, 151]. However, since both v_0 and $p_G(v_0)$ strongly depend on α_z and temperature, sweeping with velocity v_0 would be a tradeoff which still features poor performance. Instead, we deduce from figure 3.4b that an additional transversely coupled reservoir with $\alpha_x = \alpha_z$ generally performs significantly better compared to the situation with only longitudinal thermal noise. The relative gain we show in figure 3.4c is defined as $(p_G^{(x,z)} - p_G^z)/p_G^z$ where the superscript indicates the type of couplings in the system. We find that – as long as $k_B T < 30\Delta$ – the relative gain increases with temperature. Finite temperatures in QA applications pose a significant fundamental problem, since ideally the temperature of a quantum annealer should decrease logarithmically (or power law) with its system size [152]. It is therefore important to remark that the benefit of our method rises with temperature. The data in figure 3.4b reveals that there is indication for TA-AQC [136] in the non-adiabatic regime for $v \gtrsim \Delta^2$: We find enhancement of p_G with increasing temperature due to the presence of a thermal environment during open system dynamics. Remarkably, we observe cooling effects even for $\alpha_z > \alpha_x$, noting that the effect is slightly attenuated compared to the situation $\alpha_z \leq \alpha_x$. Aside, we remark that the results for higher temperatures serve as a mock-up for small energy gaps.

In case of pure thermal noise ($\hat{\sigma}^z$), we only observe negligible TA-AQC for reasonable values of α_z in the non-adiabatic regime. Nevertheless, for $\alpha \gtrsim \mathcal{O}(0.001)$, we find appreciable indications for TA-AQC even without an additional transversely coupled reservoir. A detailed numerical study of how the final ground state population depends on α_x and α_z for fixed temperature $k_B T = 5\Delta$ and fixed velocity $v = 0.5\Delta^2$ is depicted in figure 3.5a. Comparing to the behavior of $p_G(\alpha_z)$ for $\alpha_x = 0$, the advantage of an additional $\hat{\sigma}^x$ heat bath becomes clear: as soon as even a small coupling α_x is present, pronounced relaxation after sweeping through the avoided crossing leads to significant cooling of the system. This is apparent from equation (3.22): Contributions to the relaxation rate γ_r are non-negative so that additional transverse coupling amplifies relaxation processes.

Based on the concept of frustrated decoherence [139, 140] one might suspect that excitations into the excited state are effectively blocked due to the non-commutativity of $\hat{\sigma}^x$ and $\hat{\sigma}^z$. However, we do not observe such quantum effects (which are similar to the Zeno blockade [153]) and attribute the efficiency of the cooling scheme solely to enhanced relaxation effects, as illustrated in Appendix B. Hence, the general quantum annealing process is supported by relaxation processes at finite temperatures that must be smaller than $E(t)$ well outside the avoided crossing regime; which is similar to the classical simulated annealing [120] algorithm. We therefore refer to our method as *Hybrid Quantum-Classical Annealing (HQCA)*.

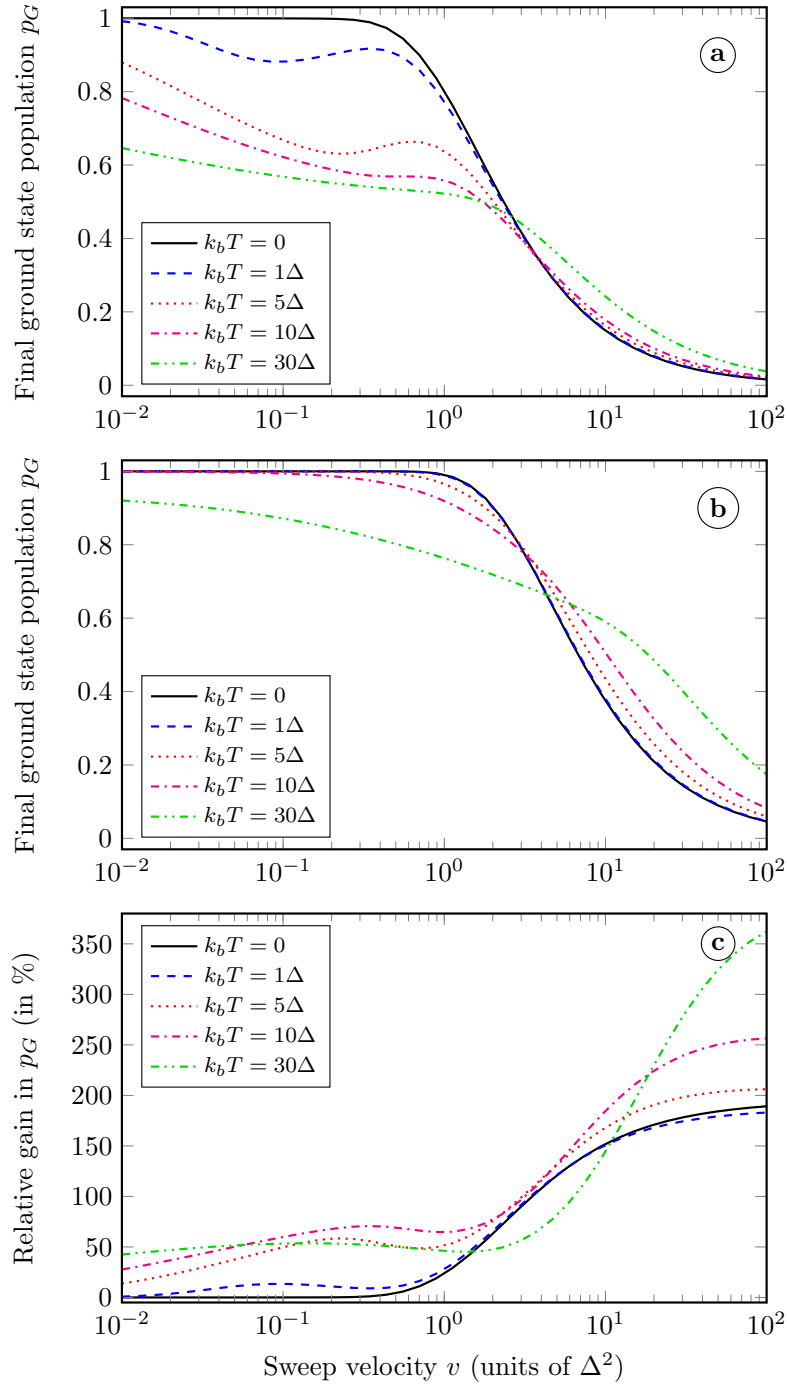


FIGURE 3.4: (a) Final ground state population p_G as a function of the sweep velocity v for a $\hat{\sigma}^z$ -only coupling with coupling strength $\alpha_z = 5 \cdot 10^{-3}$ at different temperatures. Clearly, even for small velocities and small temperatures, a significant amount of population is lost into the excited state owing to heating. (b) Final population p_G if an additional transversely coupled heat bath with coupling strength $\alpha_x = \alpha_z$ is present. We observe significant improvements over the results with only longitudinal couplings. In the non-adiabatic regime we find numerical evidence for TA-AQC, that is better results at higher temperature. (c) Relative improvement of p_G computed from the data in (a) and (b), i.e. we plot $(p_G^{(x,z)} - p_G^z)/p_G^z$ where the superscript indicates the type of couplings in the system. In the adiabatic regime we find improvements of about 50% while the cooling effect in the non-adiabatic regime is even more pronounced with gains of a few hundred percent. Generally, the relative gain increases with temperature, as long as temperature is smaller than the instantaneous splitting $E(t)$ outside the avoided crossing regime.

If the transverse coupling exceeds $\alpha_x \gtrsim 5 \cdot 10^{-3}$, roughly all population has relaxed back to the ground state by the end of the sweep – irrespective of α_z . The value $\alpha_{z,0}$ where the curve $p_G(\alpha_z)$ reaches its minimum decreases with increasing temperature. Note that the non-monotonic behavior of $p_G(\alpha_z)$ for $\alpha_x \lesssim 10^{-4}$ in figure 3.5a can be explained using a key result of Ref. [154], where the authors show how dissipative dynamics merge into semiclassical dynamics if the associated rates exceed a certain temperature-dependent value. In that case, the final ground state population will be approximately given by the result of coherent dynamics – which can be estimated via the Landau-Zener formula $p_G^{LZ}(v) = 1 - e^{-\pi\Delta^2/(2v)}$ [132, 133]. For the parameters in figure 3.5 this corresponds to a semiclassical limit of about 0.95, which is in good agreement to the limit we find for $\alpha_z \approx 1$. We provide the exact dependence of $p_G(\alpha_z)$ for $\alpha_x = 0$ in figure 3.5b and remark that it effectively equals the intersection $p_G(\alpha_z, 10^{-7})$ one can deduce from figure 3.5a.

9.3 Conclusion

In conclusion, we presented a gap-independent cooling scheme for a quantum system affected by $\hat{\sigma}^z$ noise. Our method generally increases the ground state population after sweeping through an avoided crossing at finite temperatures, owing to enhanced relaxation processes induced by an additional transversely coupled heat bath, that can for instance be realized in form of a coplanar waveguide. We find numerical indications for thermally assisted quantum annealing, and numerically demonstrated that the proposed cooling scheme improves ground state populations by up to a few hundred percent. Thereby we developed a method that has the potential to improve the quality of current quantum annealing devices. Recall that parameters are independent of the energy gap, so that the cooling scheme is intrinsically robust against fluctuations of the energy gap.

10 On the Scaling to Larger Qubit Numbers

In section 8, we have presented hybrid quantum-classical annealing (HQCA), an ansatz to enhance the performance of quantum annealing by engineering an artificial heat bath to effectively cool the annealer back to its instantaneous ground state during the annealing sweep. In this spirit, we discussed HQCA of a single qubit in section 9. Here, we enhanced the ground state population of the qubit by attaching an additional Ohmic heat bath coupled via $\hat{\sigma}^x$ to always present longitudinal noise coupled via $\hat{\sigma}^z$. The results appeared to be encouraging (see figure 3.4). Now, the natural question arises how to scale this method up to larger qubit numbers. Unfortunately, there is no obvious way to generalize the procedure and it is still ongoing research to answer this question. Here, we give a brief overview on the approaches we tried, their challenges and we give an outlook what could be tried in the future.

10.1 Cooling Operator Candidates

For a single qubit undergoing a Landau-Zener sweep, we observed a large benefit by attaching an Ohmic heat bath coupled via $\hat{\sigma}^x$ to the qubit (see section 9). This is due to the fact that $\hat{\sigma}^x$ causes transitions in the $\hat{\sigma}^z$ basis. Hence, if the qubit is excited around the end of the sweep (then the qubit eigenstates are close to the eigenstates of $\hat{\sigma}^z$), $\hat{\sigma}^x$ allows for relaxation from the excited state to the ground state. On the other hand, $\hat{\sigma}^x$ commutes with the Hamiltonian (3.13) at the avoided crossing and hence, there are no diabatic transitions at the gap due to the engineered bath. Therefore,

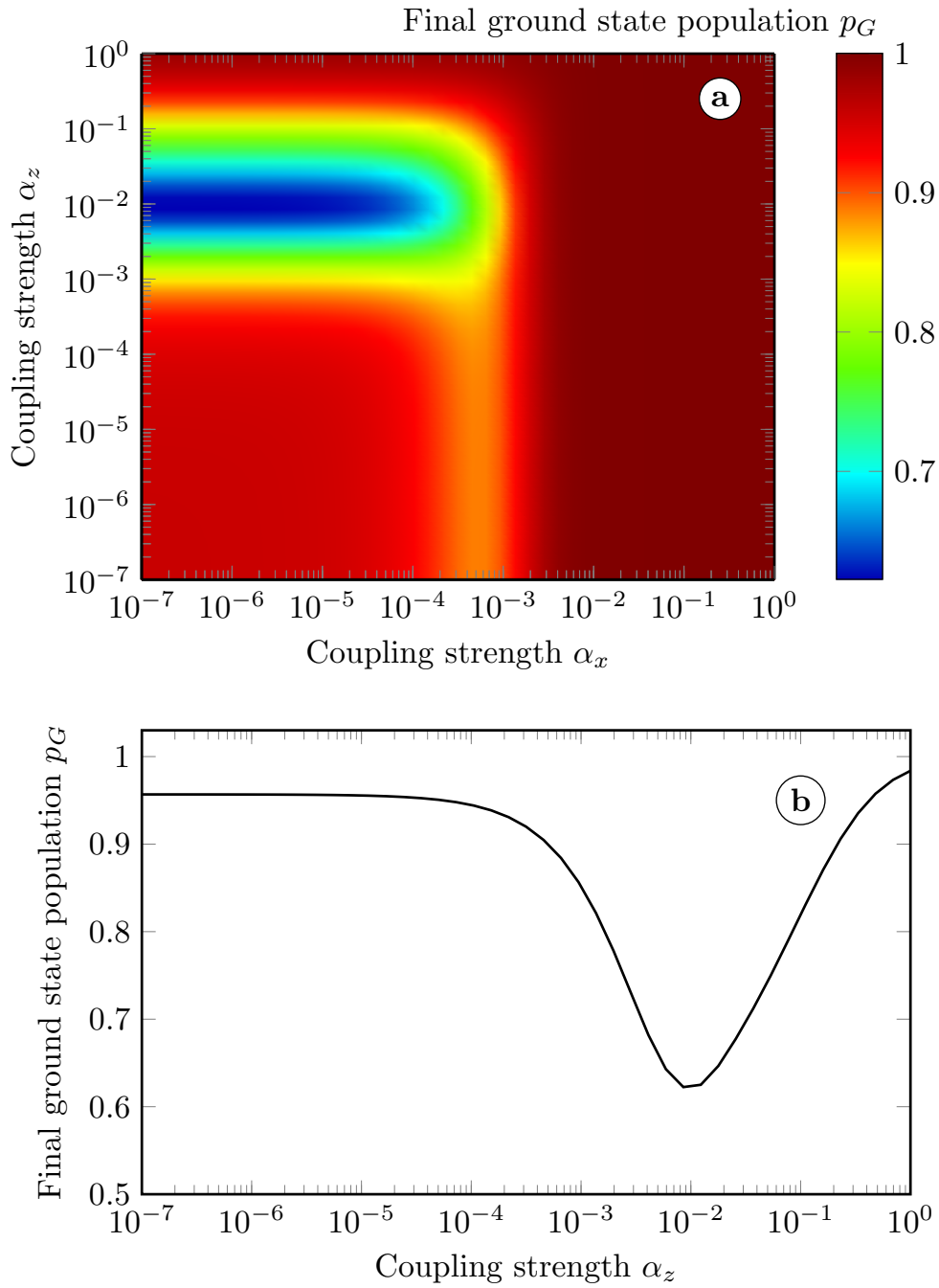


FIGURE 3.5: (a): Dependence of the final ground state population p_G on the coupling strengths α_x and α_z for a temperature of $k_B T = 5\Delta$ at fixed sweep velocity $v = 0.5\Delta^2$. The velocity is chosen such that it corresponds to a local optimum of $p_G(v)$ as extracted from figure 3.4a. (b): Dependence of p_G on α_z without the existence of an additional CPW, i.e. for $\alpha_x = 0$, with identical parameters as in (a). The minimum is reached at $\alpha_{z,o} \approx 0.01$.

as we want to generalize the method to larger qubit numbers, it is desirable to find *cooling operators* satisfying similar properties for the schedule Hamiltonian $\hat{H}(s)$. This is a question related to *shortcuts to adiabaticity* [155, 156, 157, 158, 159] and therefore, the ideal cooling operator \hat{C} will strongly depend on the nature of $\hat{H}(s)$. To make the first baby steps, we focus here on linear schedule Hamiltonians of the form

$$\hat{H}(s) := (1 - s)\hat{H}_0 + s\hat{H}_{\text{target}} \quad (3.28)$$

with

$$\hat{H}_0 := -\frac{1}{2} \sum_{i=1}^n \Delta_i \hat{\sigma}_i^x \quad \text{and} \quad \hat{H}_{\text{target}} := \hat{H}_{\text{Ising}} = \sum_{\substack{i,j=1 \\ j>i}}^n J_{ij} \hat{\sigma}_i^z \hat{\sigma}_j^z + \sum_{i=1}^n h_i \hat{\sigma}_i^z. \quad (3.29)$$

Here, the computational problem to solve is encoded in the couplings J_{ij} and the local fields h_i [12].

We are not aware of any method to compute the desired cooling operator \hat{C} for a given schedule Hamiltonian. Therefore, we are going to test two phenomenological approaches and compare their observed cooling effects in the following.

10.1.1 Approach I: Generalizing $\hat{\sigma}^x$ to Higher Dimensions

Our first ansatz is to use the naïve generalization of $\hat{\sigma}^x$ to higher dimensions. For n qubits, we define

$$\hat{\Sigma}_n^x := \sum_{m=1}^n \hat{\Sigma}_{nm}^x := \sum_{i=1}^n \hat{\sigma}_i^x + \sum_{\substack{i,j=1 \\ j>i}}^n \hat{\sigma}_i^x \hat{\sigma}_j^x + \sum_{\substack{i,j,k=1 \\ k>j>i}}^n \hat{\sigma}_i^x \hat{\sigma}_j^x \hat{\sigma}_k^x + \cdots + \prod_{i=1}^n \hat{\sigma}_i^x. \quad (3.30)$$

Here, $\hat{\Sigma}_{nm}^x$ denotes the m -th term in the sum above read from left to right. In the eigenbasis of \hat{H}_{Ising} the operator $\hat{\Sigma}_n^x$ has the matrix representation

$$\hat{\Sigma}_n^x = \begin{pmatrix} 0 & 1 & 1 & 1 & \cdots & 1 \\ 1 & 0 & 1 & 1 & \cdots & 1 \\ 1 & 1 & 0 & 1 & \cdots & 1 \\ 1 & 1 & 1 & 0 & \cdots & 1 \\ \vdots & \vdots & \vdots & \vdots & \ddots & \vdots \\ 1 & 1 & 1 & 1 & \cdots & 0 \end{pmatrix} \Rightarrow \left(\hat{\Sigma}_n^x \right)_{ij} = 1 - \delta_{ij}. \quad (3.31)$$

Hence, $\hat{\Sigma}_n^x$ couples all the eigenstates of \hat{H}_{Ising} to each other. In other words, if we treat these eigenstates as 2^n vertices of a graph, then $\hat{\Sigma}_n^x$ is the adjacency matrix corresponding to the complete graph.

We treat $\hat{\Sigma}_n^x$ as a promising cooling operator candidate for the following reason: We want to have an operator which causes transitions between all the eigenstates of the target Hamiltonian to its ground state at the end of the sweep as this operator should allow for cooling to the ground state. However, as we do not know the ground state, we should couple every single state to every other single state. As \hat{H}_{Ising} is given as a diagonal matrix, $\hat{\Sigma}_{nm}^x$ should do this job. However, it is obvious that such a cooling operator will never be implemented in an actual physical device, as one would have to implement all the k -local couplings for $1 \leq k \leq n$. Hence, we will also test its restricted contributions $\hat{\Sigma}_{nm}^x$. We expect to reach better cooling behavior the higher the number of couplings we are able to engineer.

10.1.2 Approach II: Schedule Hamiltonian Derived Cooling Operators

The second approach that we are going to test is to use a cooling operator which will be computed as a function of the given schedule Hamiltonian $\hat{H}(s)$. This is a plausible ansatz as a cooling scheme that is adapted on the actual problem rather than defining a cooling operator for all the possible Hamiltonians together should lead to better results.

To find plausible cooling operator candidates, we perform a short derivation following Ref. [160]. The basic idea is to relate the appearance of avoided crossings to the energy level curvature. As already mentioned, we consider schedule Hamiltonians of the form (3.28). Let $|\psi_n(s)\rangle$ denote an instantaneous eigenstate of $\hat{H}(s)$, i.e.

$$\hat{H}(s)|\psi_n(s)\rangle = E_n(s)|\psi_n(s)\rangle. \quad (3.32)$$

Using the Hellmann-Feynman theorem, it is easy to see that

$$\frac{dE_n(s)}{ds} = \left\langle \psi_n(s) \left| \frac{d\hat{H}(s)}{ds} \right| \psi_n(s) \right\rangle. \quad (3.33)$$

If we differentiate equation (3.33) with respect to s again, we get

$$\frac{d^2 E_n(s)}{ds^2} = 2 \sum_{k \neq n} \frac{\left| \left\langle \psi_n(s) \left| \frac{d\hat{H}(s)}{ds} \right| \psi_k(s) \right\rangle \right|^2}{E_n(s) - E_k(s)} + \underbrace{\left\langle \psi_n(s) \left| \frac{d^2 \hat{H}(s)}{ds^2} \right| \psi_n(s) \right\rangle}_{=0 \text{ for the linear schedule}}. \quad (3.34)$$

Equation (3.34) is commonly used to compute the energy level curvature [122, 161]. If we expand the fraction in the sum by $(E_n(s) - E_k(s))^2$ and make use of the identity

$$-i \left\langle \psi_n(s) \left| \frac{d\hat{H}(s)}{ds} \right| \psi_k(s) \right\rangle (E_n(s) - E_k(s)) = -i \left\langle \psi_n(s) \left| \left[\hat{H}(s), \frac{d\hat{H}(s)}{ds} \right] \right| \psi_k(s) \right\rangle \quad (3.35)$$

taken from Ref. [162], we can relate the energy level curvature to the commutator $\left[\hat{H}(s), \frac{d\hat{H}(s)}{ds} \right]$ as

$$\frac{d^2 E_n(s)}{ds^2} = -2 \sum_{k \neq n} \frac{\left| \left\langle \psi_k(s) \left| \left[\hat{H}(s), \frac{d\hat{H}(s)}{ds} \right] \right| \psi_n(s) \right\rangle \right|^2}{(E_n(s) - E_k(s))^3}. \quad (3.36)$$

We deduce from equation (3.36) that the commutator $-i \left[\hat{H}(s), \frac{d\hat{H}(s)}{ds} \right]$ might be a good cooling operator candidate. For the linear schedule (3.28), it reads

$$-i \left[\hat{H}(s), \frac{d\hat{H}(s)}{ds} \right] = -i \left[(1-s)\hat{H}_0 + s\hat{H}_{\text{target}}, \hat{H}_0 + \hat{H}_{\text{target}} \right] = -i \left[\hat{H}_0, \hat{H}_{\text{target}} \right]. \quad (3.37)$$

In addition to this commutator, we test the operator $\frac{d\hat{H}(s)}{ds} = -\hat{H}_0 + \hat{H}_{\text{target}}$ too, as the change of the Hamiltonian over time is the source of diabatic transitions.

10.2 Defining the Toy Model

Our goal is to benchmark the performance of several cooling operator candidates for the linear annealing schedule. To have a fair competition, we need to define a suitable toy model to simulate. As the toy model itself will strongly influence the results (even in a qualitative manner), and the parameter set for the simulation is way to large to explore everything, we define our problem setting in the following way:

- To minimize the number of parameters, we restrict ourselves to a two-qubit system initially prepared in the ground state of \hat{H}_0 undergoing a linear annealing sweep from \hat{H}_0 to \hat{H}_{Ising} . The two qubits are assumed to be identical.
- As in the single-qubit case, our figure of merit is the ground state probability p_G . This quantity will depend on the sweep velocity, or equivalently the total sweep time t_f . Hence, we are going to compute $p_G(t_f)$ for all the cooling operator candidates and reasonable sweep times.
- We try to avoid to rely too much on the chosen schedule Hamiltonian $\hat{H}(s)$. Hence, we are going to create 10 random target Hamiltonians and therefore, 10 random schedule Hamiltonians. Afterwards we average $p_G(t_f)$ over the 10 instances.
- In the spirit of section 9, the qubits are affected by always present longitudinal noise. Hence, the system Hamiltonian $\hat{H}(s)$ is constantly coupled to a heat bath in thermal equilibrium at temperature T through $\hat{\sigma}_1^z + \hat{\sigma}_2^z$. We refer this heat bath to the *natural* bath. In absence of any engineered bath, it defines the base line to benchmark the performance of some engineered cooling operator. All the appearing heat baths are assumed to be Ohmic ($J_b(\omega) = \alpha_b \omega \exp(-\omega/\omega_C)$ for $b \in \{\text{nat}, \text{eng}\}$) and to share the same temperature T . Additionally, we fix $\alpha_{\text{nat}} = \alpha_{\text{eng}}$.
- We are interested in the parameter range $h\nu \lesssim k_B T$, where ν is a typical technical frequency defining the size of the minimal gap. In this regard, we fix the temperature T to equal the typical cryostat temperature $T := 20$ mK. This implies ν lies in the GHz range, which corresponds to a natural time scale measured in nano seconds.
- We fix $\Delta_1 = \Delta_2 := 1$ GHz and hence $\hat{H}_0 = -\frac{1}{2} \sum_{i=1}^n \hat{\sigma}_i^x$ measured in the unit GHz. The parameters for the 10 instances of the Ising Hamiltonian are chosen randomly in the range $0 \text{ GHz} < h_1, h_2, J_{12} \leq 1 \text{ GHz}$.

In summary, a single instance of our toy model is described by the total Hamiltonian

$$\hat{H}_{\text{tot}}(s) := (1-s)\hat{H}_0 + s\hat{H}_{\text{Ising}} + \hat{H}_{\text{B,nat}} + \hat{H}_{\text{B,eng}} + \hat{H}_{\text{int,nat}} + \hat{H}_{\text{int,eng}}. \quad (3.38)$$

As both heat baths in equation (3.38) are assumed to be harmonic (see section 3.12) with Ohmic spectral densities and $\alpha_{\text{nat}} = \alpha_{\text{eng}} =: \alpha$, we can treat them as a single Ohmic heat bath coupled to the system through

$$\hat{H}_{\text{int}} := \alpha \left(\hat{\Sigma}^z + \hat{C} \right), \quad (3.39)$$

where \hat{C} is the engineered cooling operator, $\hat{\Sigma}^z := \hat{\sigma}_1^z + \hat{\sigma}_2^z$ and we fixed $\alpha := 5 \cdot 10^{-3}$ in the spirit of Ref. [110]. In the following, we briefly discuss the methods we tried to simulate the dynamics generated by the Hamiltonian (3.38).

10.3 Methods

The adiabatic theorem states that, if we sweep slowly enough, the system will stay in its instantaneous ground state [12]. Hence, we would not see any cooling effect if we stay inside the adiabatic limit (1.109). Therefore, to benchmark the performance of the cooling operator candidates, we have to leave the adiabatic limit. Unfortunately, the validity of the adiabatic master equation (1.133) derived in Ref. [54] relies exactly on this assumption. This is also the reason why we used this unusual time-dependent Bloch-Redfield master equation in section 9 to simulate the qubit dynamics. This method was shown to be valid to simulate Landau-Zener dynamics [146]. However, we are not aware of a generalization to use it for more than a single qubit. Therefore, we decided to apply the numerically exact path integral method QUAPI [71, 72] instead, which we reviewed in section 3.13. For time-independent Hamiltonians, an open source code written by N. Dattani [73] is available. We applied this code and generalized it to time-dependent Hamiltonians¹. Unfortunately, using QUAPI turned out to be a very bad idea for a non-obvious reason: As already mentioned in section 3.13, the primary memory cost scales like

$$\text{PMC} \propto M^{2(\Delta k+1)}, \quad (3.40)$$

where $M = 4$ is the Hilbert space dimension for two qubits and Δk is the number of previous time-steps used to compute the next time-step for the density matrix of the two-qubit system $\hat{\rho}_S(t)$. Hence, the maximum Δk one can use in practice is strongly limited by computational hardware due to this exponential scaling. This limitation to some maximum Δk implies a minimum size of the time-step δt , because the product

$$\Delta k \cdot \delta t = \tau_B \quad (3.41)$$

has to cover all the bath memory time τ_B at least to not effectively change the simulated physics. This memory time satisfies $\tau_B \propto 1/T$. Therefore, it becomes larger for smaller temperatures, which forces the minimal step size δt to become larger too. The numerical error induced by QUAPI scales like δt^3 . In the end, it turned out that we are not able to reach the desired accuracy for convergence regarding the boundary conditions set by our system of interest².

In conclusion, the months we spent on implementing QUAPI turned out to be wasted time. Hence, we decided to use the adiabatic master equation in Lindblad form (1.133) despite the fact that its validity is not guaranteed for the parameter regime we are interested in. Nevertheless, it turned out to be the only method we are aware of which gave us physically reasonable results. To run the simulations, we used a software tool developed by H. Chen [163].

10.4 The Cooling Operator Championship

In this section, we show the results of the competition between our suggested cooling operator candidates phenomenologically derived in section 10.1. We computed our figure of merit, namely the average ground state probability p_G at $t = t_f$, as a function of the total annealing time for the considered cooling operator candidates by means of the toy model described in section 10.2. At this juncture, we compare two different cooling scenarios: First, we consider a cooling scheme in which the cooling operators

¹Implementing QUAPI is a Sisiphus-like task, because it covers a huge index battle. It took us several months to make it run.

²The numerical error we observed has been that large that we got negative probabilities!

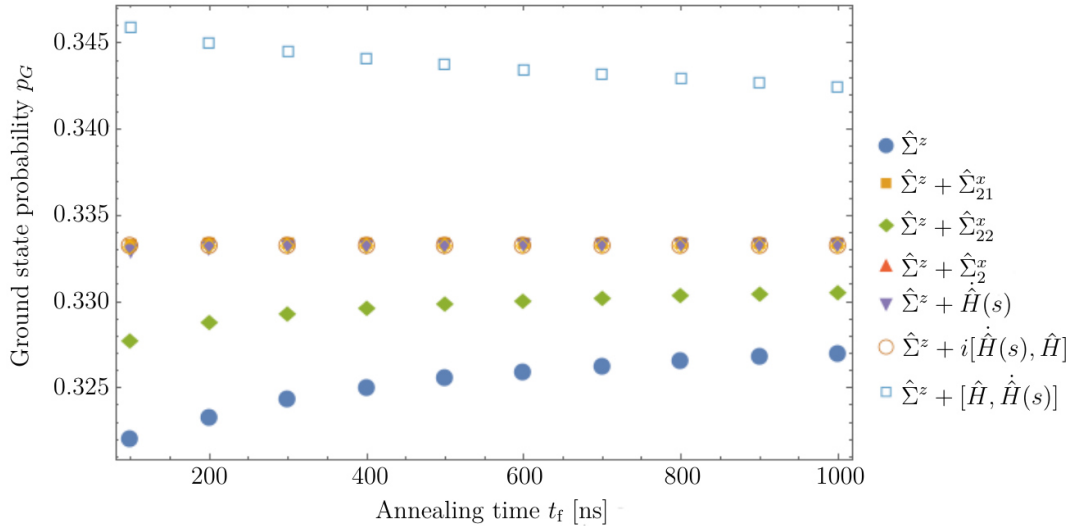


FIGURE 3.6: Average ground state probability p_G as a function of the total annealing time t_f to benchmark the performance of the considered cooling operator candidates, if the engineered heat bath is turned on throughout all the sweep. Here, we assume always present longitudinal noise affecting the two-qubit system through $\hat{\Sigma}^z = \hat{\sigma}_1^z + \hat{\sigma}_2^z$. We show the performance of the bare ground state probability as the reference point for cooling (blue dots). We observe that all the considered cooling operator candidates \hat{C} lead to cooling for all the considered sweep times. However, the effect is rather small (it acts on the second digit after the decimal point). The smallest effect is shown by the cooling operator $\hat{C} = \hat{\Sigma}_{22}^x = \hat{\sigma}_1^x \hat{\sigma}_2^x$. We observe the best performance using the anti-Hermitian cooling operator $\hat{C} = [\hat{H}(s), \dot{\hat{H}}(s)]$. All the other results are that close to each other, such that the points in the plot overlapp.

are chosen to be constant throughout all the sweep time t_f . Second, we compute the position of the minimal gap between ground state and first excited state for each random target Hamiltonian and then, we turn on the engineered cooling operators right after the gap. In practice, the second strategy is not very realistic, because the position of the gap is typically unknown. However, we were interested in its performance compared to the cooling throughout as one should see, if the engineered baths lead to unwanted heating in the beginning of the sweep. The numerical results of the first scenario are shown in figure 3.6. Overall, all the considered cooling operator candidates induce some amount of cooling with respect to the bare case with only natural longitudinal noise. The smallest effect is shown by the cooling operator $\hat{C} = \hat{\Sigma}_{22}^x = \hat{\sigma}_1^x \hat{\sigma}_2^x$. We observe the best performance using the anti-Hermitian cooling operator $\hat{C} = [\hat{H}(s), \dot{\hat{H}}(s)]$ ¹, and hence we refer it to the winner of the cooling operator championship. All the other results are that close to each other, such that the points in the plot overlapp. Unfortunately, the magnitude of the observed gain is too small to improve quantum annealing in a useful way. However, the observed results are interesting in a qualitative manner. As mentioned in section 10.1.1, we expected the performance of the cooling to be better the more eigenstates of \hat{H}_{Ising} will be coupled by the engineered cooling operator. Hence, we expected the performance of $\hat{\Sigma}_{22}^x$ to

¹We computed the performance of this anti-Hermitian operator by accident. In the first run, we just forgot about the imaginary unit in front of the commutator.

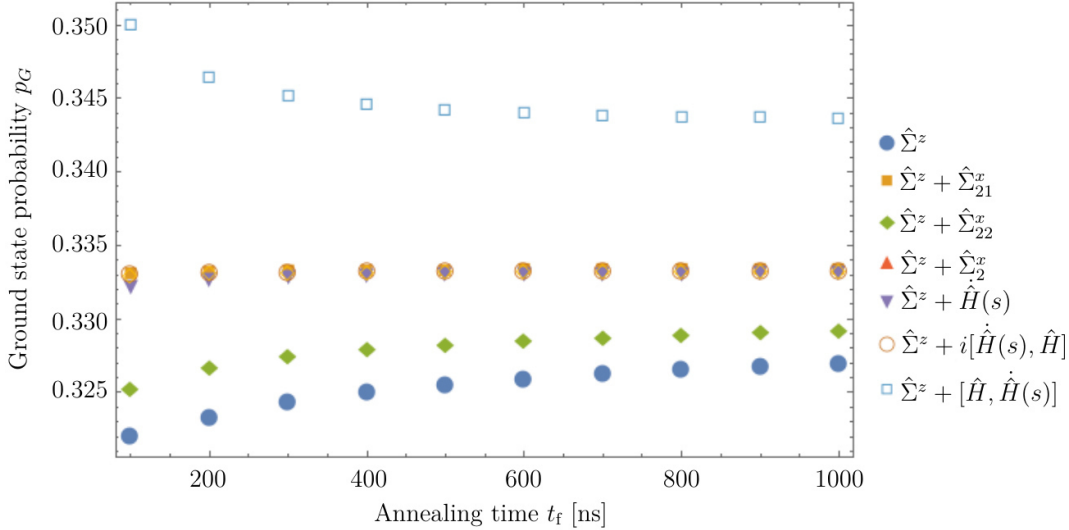


FIGURE 3.7: Average ground state probability p_G as a function of the total annealing time t_f to benchmark the performance of the considered cooling operator candidates, if the engineered heat bath is turned on right after the minimal gap. Here, we assume always present longitudinal noise affecting the two-qubit system through $\hat{\Sigma}^z = \hat{\sigma}_1^z + \hat{\sigma}_2^z$. We show the performance of the bare ground state probability as the reference point for cooling (blue dots). The results do not change much compared to the case with the cooling operators turned on throughout all the sweep. The only improvement occurs for the anti-Hermitian cooling operator $\hat{C} = [\hat{H}(s), \dot{\hat{H}}(s)]$ for small annealing times. All the other values become slightly worse by starting the cooling only after the gap.

be worse than the performance of $\hat{\Sigma}_{21}^x$ and the performance of $\hat{\Sigma}_{21}^x$ to be worse than the performance of $\hat{\Sigma}_2^x$. This is more or less what we observe in figure 3.6 with the exception that the performance of $\hat{\Sigma}_{21}^x$ and $\hat{\Sigma}_2^x$ are too close to be distinguished as we only averaged over ten random instances.

Additionally, we observe that the schedule Hamiltonian derived cooling operators behave as well as $\hat{\Sigma}_{21}^x$ and $\hat{\Sigma}_2^x$. This is encouraging, because implementing the general cooling operator $\hat{\Sigma}_n^x$ of equation (3.30) for n qubits is far outside experimental reach. In contrast, the schedule Hamiltonian derived cooling operators have no need for more than 2-local couplings.

The most interesting observation is that the anti-Hermitian cooling operator $\hat{C} = [\hat{H}(s), \dot{\hat{H}}(s)]$ performs best. On top, it shows an unexpected behavior as a function of the total annealing time: Whereas the performance of all the other considered cooling operators enhances with growing annealing time t_f (which is expected according to the adiabatic theorem), its resulting ground state probability p_G decreases as a function of t_f . This is unexpected and we have to keep it as an open question why this happens. Nevertheless, this is a point for further research which can not be covered in this thesis anymore.

The numerical results of the second scenario are shown in figure 3.7. The results do not change much compared to the case with the cooling operators turned on throughout all the sweep. The only improvement occurs for the anti-Hermitian cooling operator $\hat{C} = [\hat{H}(s), \dot{\hat{H}}(s)]$ for small annealing times. All the other values become slightly worse by starting the cooling only after the gap. Therefore, we conclude that

the engineered cooling effect by implementing one of the considered cooling operators is more relevant to the performance than a possible heating imposed by the additional bath.

10.5 Conclusion and Outlook

In section 10, we tried to find the best cooling operators to translate the approach of *hybrid quantum-classical annealing* developed in Refs. [110, 164] and reviewed in section 9 to larger qubit numbers. We tried two different types of cooling operators: The first type is based on a direct generalization of the $\hat{\sigma}^x$ operator of a single qubit. The second type is phenomenologically derived from the given schedule Hamiltonian itself. Each considered cooling operator candidate indeed shows a small increase of the ground state probability at the end of the annealing sweep and hence, cooling. However, the observed effect is relatively small and hence not yet useful from a practical perspective. Nevertheless, we showed that cooling by engineered decoherence is possible in principle not only for the single-qubit case and therefore, we claim that the potential of HQCA should be explored in more detail. There are plenty ways to move on: The coupling strength of the engineered heat baths to the system could be optimized, the temperature dependence of the performance should be studied and one should explore the reason, why the anti-Hermitian operator $\hat{C} = [\hat{H}(s), \dot{\hat{H}}(s)]$, which we tried by accident, behaves much better than its Hermitian counterpart.

Appendices

A.d Derivation of the quantum master equations

We provide details on the derivation of the quantum master equation. The total Hamiltonian is decomposed as

$$\hat{H}(t) = \hat{H}_Q(t) + \hat{H}_{QB} + \hat{H}_B, \text{ with} \quad (3.42)$$

$$\hat{H}_Q(t) := -\frac{\epsilon(t)}{2}\hat{\sigma}^z - \frac{\Delta}{2}\hat{\sigma}^x \quad (3.43)$$

$$\hat{H}_{QB} := \sum_{\nu=x,z} \sum_k \hat{\sigma}^\nu \lambda_k^\nu \left(\hat{b}_k^\nu + \hat{b}_k^{\nu\dagger} \right) \quad (3.44)$$

$$\hat{H}_B := \sum_{\nu=x,z} \sum_k \omega_k^\nu \hat{b}_k^\nu \hat{b}_k^{\nu\dagger}. \quad (3.45)$$

Following Ref. [144], we move to the rotating frame defined by the transformation $\hat{R}(t) := \exp(i\phi(t)\hat{\sigma}^y/2)$ with $\phi(t) = \arctan(\epsilon(t)/\Delta)$. With the instantaneous energy splitting $E(t) = \sqrt{\epsilon^2(t) + \Delta^2}$ the bare system Hamiltonian and the coupling term become

$$\tilde{H}_Q(t) = -\frac{E(t)}{2}\hat{\sigma}^x + \frac{\dot{\phi}(t)}{2}\hat{\sigma}^y =: \tilde{H}_0(t) + \frac{\dot{\phi}(t)}{2}\hat{\sigma}^y \quad (3.46)$$

$$\tilde{H}_{QB}(t) = \sum_{\nu=x,z} \sum_k \tilde{\sigma}^\nu \lambda_k^\nu \left(\hat{b}_k^\nu + \hat{b}_k^{\nu\dagger} \right). \quad (3.47)$$

By introducing the weights $f_1(t) := \sin(\phi(t))$ and $f_2(t) := \cos(\phi(t))$ we can express the rotating-frame-matrices as $\tilde{\sigma}^x = -f_1(t)\hat{\sigma}^z + f_2(t)\hat{\sigma}^x$ and $\tilde{\sigma}^z = f_2(t)\hat{\sigma}^z + f_1(t)\hat{\sigma}^x$, respectively. Following standard Bloch-Redfield theory (cf. section 3.3 in Ref. [26] or section 3.7) we start in the interaction frame with respect to $\tilde{H}_Q(t)$ and \tilde{H}_B . Hence, the coupling Hamiltonian in the interaction picture is given by

$$\tilde{H}_{QB,I}(t) = \sum_{\nu=x,z} \tilde{U}_Q(t) \tilde{\sigma}^\nu(t) \tilde{U}_Q^\dagger(t) \otimes \hat{B}^\nu(t), \quad \hat{B}^\nu(t) = \sum_k \lambda_k^\nu \left(e^{i\omega_k^\nu t} \hat{b}^\dagger + e^{-i\omega_k^\nu t} \hat{b} \right) \quad (3.48)$$

with some bath operator \hat{B}^ν and the free propagator of the bare qubit $\tilde{U}_Q(t) = \hat{T} \exp\left(-i \int_0^t \tilde{H}_Q(s) ds\right)$. The equation of motion for the density matrix of the reduced qubit subsystem is hence given by

$$\begin{aligned} \dot{\tilde{\rho}}_{Q,I}(t) &= - \int_0^\infty \text{Tr}_B \left[\tilde{H}_{QB,I}(t), \left[\tilde{H}_{QB,I}(s), \tilde{\rho}_{Q,I}(t) \otimes \hat{\rho}_B \right] \right] ds \\ &= - \int_0^\infty \sum_{\nu,\nu'} \left\{ \tilde{\sigma}_I^\nu(t) \tilde{\sigma}_I^{\nu'}(t-s) \tilde{\rho}_{Q,I}(t) \left\langle \hat{B}^\nu(t) \hat{B}^{\nu'}(t-s) \right\rangle \right. \\ &\quad \left. - \tilde{\sigma}_I^{\nu'}(t) \tilde{\rho}_{Q,I}(t) \tilde{\sigma}_I^\nu(t-s) \left\langle \hat{B}^{\nu'}(t-s) \hat{B}^\nu(t) \right\rangle + \text{h.c.} \right\} ds. \end{aligned} \quad (3.49)$$

In the above equation we have already included (i) a weak-coupling approximation (Born approximation), which states that the reservoir is negligibly affected by the system so that we may write the full density matrix as a tensor product $\tilde{\rho}_I(t) = \tilde{\rho}_{Q,I}(t) \otimes \hat{\rho}_B$ and (ii) a Markovian approximation. The latter states that there is no memory, i.e. time evolution of the state depends only on its present value, and is based on the assumption that the correlation functions decay sufficiently fast compared

to the time scale over which the system changes notably. If we choose $\hat{\rho}_B$ to be a stationary state of the reservoir, the correlation functions are homogeneous in time, hence $\langle \hat{B}^\nu(t)\hat{B}^{\nu'}(t-s) \rangle = \langle \hat{B}^\nu(s)\hat{B}^{\nu'}(0) \rangle$. Furthermore we assume that there is no correlation between different baths, i.e. $\langle \hat{B}^\nu(s)\hat{B}^{\nu'}(0) \rangle \propto \delta_{\nu,\nu'}$. We can then write equation (3.49) in the form

$$\dot{\rho}_{Q,I}(t) = - \int_0^\infty \sum_{\nu=x,z} \left\{ [\tilde{\sigma}_I^\nu(t), \tilde{\sigma}_I^\nu(t-s)\tilde{\rho}_{Q,I}(t)] \langle \hat{B}^\nu(s)\hat{B}^{\nu'}(0) \rangle + \text{h.c.} \right\}. \quad (3.50)$$

We are looking for the equation of motion in the Schrödinger picture, that is the evolution of $\tilde{\rho}_Q(t)$, which we obtain by computing

$$\dot{\rho}_Q(t) = \tilde{U}_Q(t)\dot{\rho}_{Q,I}(t)\tilde{U}_Q^\dagger(t) - i [\tilde{H}_Q(t), \tilde{\rho}_Q(t)]. \quad (3.51)$$

A straightforward calculation reveals the sought equation of motion in the Schrödinger picture to be

$$\dot{\tilde{\rho}}_Q(t) = -i [\tilde{H}_Q(t), \tilde{\rho}_Q(t)] - \sum_{\nu=x,z} \left\{ [\tilde{\sigma}^\nu(t), \tilde{S}^\nu(t)\tilde{\rho}_Q(t)] + \text{h.c.} \right\} \quad (3.52)$$

where we introduced the operator

$$\tilde{S}^\nu(t) := \int_0^\infty \tilde{U}_Q(t, t-s)\tilde{\sigma}^\nu(t-s)\tilde{U}_Q^\dagger(t, t-s) \langle \hat{B}^\nu(s)\hat{B}^{\nu'}(0) \rangle ds. \quad (3.53)$$

In order to derive an analytic form for the equation of motion we further need to apply an adiabatic Markovian approximation [144] which amounts to expressing the propagator as

$$\tilde{U}_Q(t, t-s) \approx \exp(-i\tilde{H}_Q(t)s). \quad (3.54)$$

This is sufficiently accurate provided the memory time τ_{mem} of the bath is much smaller than any system time scale, $\tau_{\text{mem}} \ll (t-s)$, and if the drive $\epsilon(t)$ acts on time scales $\tau_\epsilon \gg \tau_{\text{mem}}$ so that it has no significant effect on the rates. The correlation function can be expressed in terms of the spectral density $J_\nu(\omega)$ (see section 3.12)

$$\langle \hat{B}^\nu(s)\hat{B}^{\nu'}(0) \rangle = \int_0^\infty J_\nu(\omega) ((\bar{n}_\nu(\omega) + 1)e^{-i\omega s} + \bar{n}_\nu(\omega)e^{i\omega s}) d\omega \quad (3.55)$$

with the single-particle Bose distribution $\bar{n}_\nu(\omega) = 1/(e^{\beta_\nu\omega} - 1)$. Using the identity $\bar{n}_\nu(-\omega) = -(\bar{n}_\nu(\omega) + 1)$ we can rewrite equation (3.55) as an integral over positive and negative ω , i.e.

$$\langle \hat{B}^\nu(s)\hat{B}^{\nu'}(0) \rangle = \int_{-\infty}^\infty \text{sgn}(\omega) J_\nu(|\omega|)\bar{n}_\nu(\omega)e^{i\omega s} d\omega. \quad (3.56)$$

Inserting equation (3.56) into the definition (3.53) allows us to carry out the integration over s first, which yields terms $\int_0^\infty e^{i\omega s} ds \approx \delta(\omega)$. Note that we here neglect imaginary parts resulting from principal value integrals since they simply manifest themselves as Lamb shifts. Calculating the right hand side of equation (3.52) while

using the Bloch representation

$$\tilde{\rho}_Q(t) = \frac{1}{2} \left(\hat{\mathbb{I}} + \sum_n r_n(t) \hat{\sigma}_n \right) \quad (3.57)$$

we eventually find the quantum master equations presented in section 9.1

$$\dot{r}_x = \left(\dot{\phi} - \gamma_{xz} \right) r_z - \gamma_r (r_x - \bar{r}_x), \quad (3.58)$$

$$\dot{r}_y = E_t r_z - (\gamma_d + \gamma_r) r_y, \quad (3.59)$$

$$\dot{r}_z = -\dot{\phi} r_x - E_t r_y - \gamma_d r_z - \gamma_{zx} (r_x - \bar{r}_x). \quad (3.60)$$

Here, we used the shorthand notation $E_t := E(t)$ and $\bar{r}_x := \tanh(\beta E_t/2)$. The energy normalization is given by $\beta = 1/k_B T$ with Boltzmann constant k_B and temperature T . Note that we explicitly assume equal temperature for both reservoirs since, in experiments, they will be located in the same cryostat. The rates are then given by

$$\gamma_r := 2\pi \coth \left(\frac{\beta E_t}{2} \right) (f_1^2 J_x(E_t) + f_2^2 J_z(E_t)), \quad (3.61)$$

$$\gamma_d := 4\pi \lim_{\omega \rightarrow 0} \bar{n}(\omega) (J_z(\omega) + J_x(\omega)), \quad (3.62)$$

$$\gamma_{xz} := 4\pi f_1 f_2 \lim_{\omega \rightarrow 0} \bar{n}(\omega) (J_x(\omega) - J_z(\omega)), \quad (3.63)$$

$$\gamma_{zx} := 2\pi f_1 f_2 \coth \left(\frac{\beta E_t}{2} \right) (J_x(E_t) - J_z(E_t)). \quad (3.64)$$

A.e Numerical verification of relaxation and cooling

In addition to the graphics shown in section 9, we want to support the statements by providing further numerical data. Our statement that cooling is solely caused by relaxation processes is supported by Fig. 5, which depicts the evolution of ground state population for different parameter settings. If the CPWs transversely coupled to the qubit, excitation out of the ground state is not minimized intermediately. Instead, population relaxes back into the ground state after passing the avoided crossing. We find qualitatively identical dynamics for other parameter regimes as well.

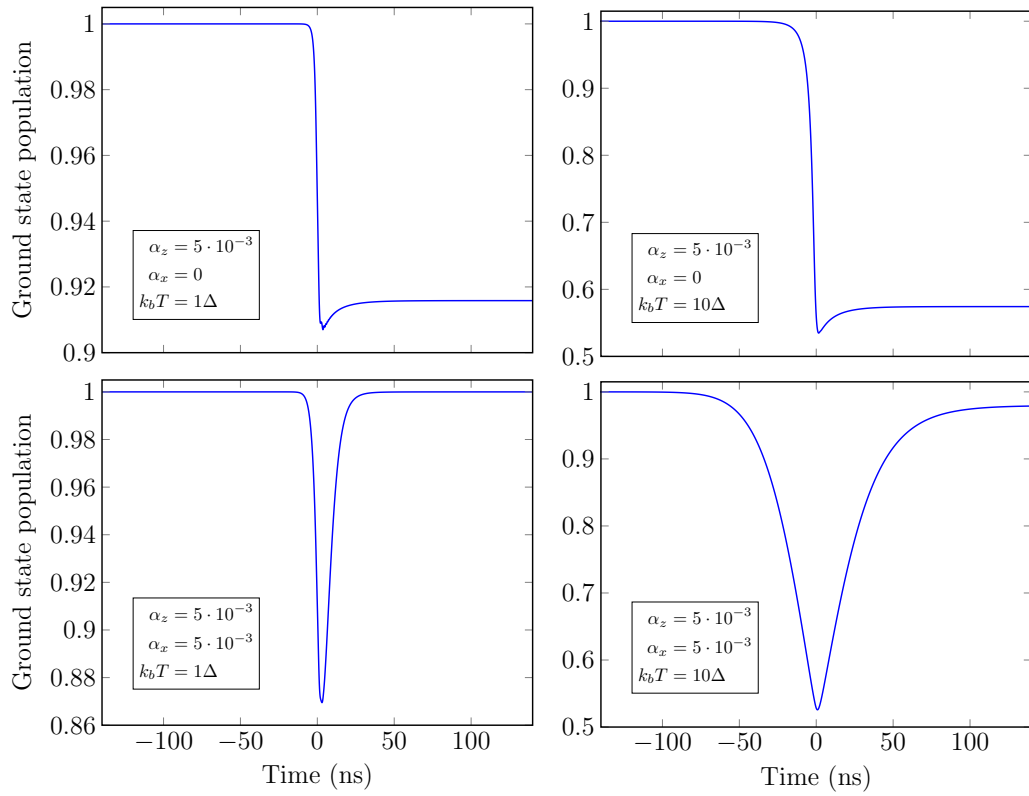


FIGURE 3.8: Population of the ground state as a function of time for different parameter settings with sweep velocity $v = 0.3\Delta^2$. As apparent from the plots, an additional transverse coupling does not reduce intermediate excitations. Cooling into the groundstate is achieved by relaxation back into the ground state.

Conclusion and Outlook

In quantum information theory, physicists, mathematicians, computer scientists and engineers work together as well from hardware-side as from application-side to exploit the counter-intuitive nature of quantum mechanics to solve real-life problems. The main obstacle in this development is decoherence: the process which causes the transition between quantum and classical behavior of a physical system. As decoherence reduces the quantum nature of matter and radiation (i.e. quantum superposition and entanglement) to classical physics, it removes the resource of a quantum computer's advantage with respect to classical computing. Nevertheless, I did not only regard decoherence as a real-life phenomenon we have to deal with in this thesis. On the contrary, I discussed the potential of purposefully engineered decoherence as a resource to improve the performance of specific quantum information applications. Prima facie, treating decoherence itself as a possibly beneficial resource for quantum computing looks like an oxymoron. However, as the time evolution in quantum mechanics of closed systems is unitary, and hence undirected in time, carefully engineered decoherence could allow for a desired directional time evolution, and therefore for hybrid quantum-classical algorithms. In this work, I discussed two examples of such approaches: quantum stochastic walks and hybrid quantum-classical annealing.

This thesis consists of three distinct chapters: Whereas chapter I reviews the basic concepts and methods in quantum information theory and the theory of open quantum systems to set up a solid background, chapter II and chapter III cover new research results.

As mentioned above, chapter I provides an introduction to the field of quantum information theory as well as to the field of open quantum systems. It consists of three sections: After a brief historical overview on the developments of modern computers in section 1, section 2 introduces the main terms and concepts of quantum information theory, which are needed to understand the purposes of the following chapters. Here, after a dense summary of standard quantum mechanics, I introduced the concepts of qubits, quantum algorithms and the famous DiVincenzo criteria, a qualitative summary of the basic ingredients to build a functional quantum computer [27].

Section 3 provides a rather broad introduction to the theory of open quantum systems. In quantum mechanics of closed systems, the system's entropy is preserved for the whole time of quantum evolution predicted by Schrödinger's equation. Hence, decoherence only appears in the context of open quantum systems and therefore, their understanding is crucial for the rest of this thesis. First, I introduced the basic concepts like density matrices, entropy and quantum channels. Afterwards, I assembled a toolbox for the simulation of open quantum system dynamics. There are two fundamentally distinct approaches: quantum master equations and path integral techniques. Both approaches arise with their own benefits and drawbacks, so I tried to give an idea under which conditions one or the other should be used.

Chapter II covers the quantum simulation of *quantum stochastic walks (QSWs)*, which generalize the concept of coherent quantum walks to additional non-unitary evolution [85]. This allows for incoherent movement of the walker, and therefore, directionality. QSWs arise in two distinct versions: continuous-time and discrete-time.

The first version is defined by a specific kind of a Lindblad master equation and is widely used in literature for different computational tasks [83, 87, 88, 89]. In section 5, I presented our results of Ref. [47], in which we have shown how to simulate a restricted class of them on a coherent quantum computer using a trajectory approach. We are not aware of any previous work targeting this problem. The restriction follows from the requirement of conservation of probability. Interestingly, we found the same restriction in Ref. [78] (presented in section 6) when we showed how to simulate a continuous-time QSW by using a discrete-time QSW. However, the quantum simulation of discrete-time QSWs, which we defined as the repetitive application of a quantum stochastic map of the form (2.3), itself is not subject to this restriction. Up to date, we are not aware of any further application of discrete-time QSWs besides the simulation of their continuous counterparts yet. Nevertheless, I am optimistic that they will be used in future as we found that they underly less restrictive conditions to be simulated on a quantum computer than continuous-time QSWs.

Last but not least, chapter III highlights another route to use engineered decoherence as a beneficial tool in quantum computing: *hybrid quantum-classical annealing (HQCA)*. Here, we combined the paradigms of quantum annealing with the classical simulated annealing algorithm. The core idea of this approach is explained in section 8: HQCA uses quantum tunneling to search the energy landscape of a given optimization problem (i.e. finding the ground state of a Ising spin glass Hamiltonian) and a carefully engineered heat bath is supposed to force the system to relax to the desired ground state. In section 9, I presented our results on HQCA of a single qubit which are available as a preprint [110]. Here, we benchmarked the performance of an artificially engineered Ohmic heat bath, which is coupled via $\hat{\sigma}^x$ to a qubit undergoing the standard Landau-Zener sweep in addition to the always present longitudinal noise. We found that this procedure can enhance the final ground state population of the qubit dramatically. However, this encouraging observation only holds for the case of a single qubit so far. It is not clear how to scale HQCA up to larger qubit numbers in a useful way. Particularly, it is not clear which operator should be used to take the role of $\hat{\sigma}^x$ used in the single-qubit case. In this regard, section 10 is a roadmap to further exploration. Here, I presented two phenomenological approaches: generalizing $\hat{\sigma}^x$ to higher dimensions and deriving the desired operator as a function of the schedule. To make a long story short, we observed an enhancement of the final ground state probability, but the effect so far observed is tiny. The reason for this remains unclear and needs to be explored further in future research.

Bibliography

- [1] A. M. Turing, *Proceedings of the London mathematical society* **2**, 230 (1937).
- [2] A. Churchill, S. Biderman, and A. Herrick, “arXiv:1904.09828,” (2019), [arXiv:1904.09828 \[cs.AI\]](#) .
- [3] W. B. Shockley, J. Bardeen, and W. H. Brattain, in *Nobel Prize* (1956).
- [4] S. Kilby Kack, in *Nobel Prize* (2010).
- [5] G. E. Moore, *IEEE Solid-State Circuits Society Newsletter* **11**, 33 (2006).
- [6] M. M. Waldrop, *Nature News* **530**, 144 (2016).
- [7] S. Arora and B. Barak, *Computational Complexity: A Modern Approach*, 1st ed. (Cambridge University Press, USA, 2009).
- [8] M. Nielsen and I. Chuang, *Quantum Computation and Quantum Information* (Cambridge University Press, Cambridge, UK, 2000).
- [9] P. Benioff, *Journal of Statistical Physics* **22**, 563 (1980).
- [10] R. P. Feynman, *International journal of theoretical physics* **21**, 467 (1982).
- [11] F. K. Wilhelm, R. Steinwandt, B. Langenberg, P. J. Liebermann, A. Messinger, P. K. Schuhmacher, and A. Misra-Spieldenner, *BSI Project Number 283* (2018).
- [12] T. Albash and D. A. Lidar, *Rev. Mod. Phys.* **90**, 015002 (2018).
- [13] Y. Aharonov, L. Davidovich, and N. Zagury, *Phys. Rev. A* **48**, 1687 (1993).
- [14] E. Farhi and S. Gutmann, *Physical Review A* **58**, 915 (1998).
- [15] D. Aharonov, A. Ambainis, J. Kempe, and U. Vazirani, in *Proceedings of the thirty-third annual ACM symposium on Theory of computing - STOC '01* (ACM Press, New York, NY, USA, 2001) pp. 50–59.
- [16] A. Ambainis, E. Bach, A. Nayak, A. Vishwanath, and J. Watrous, in *Proceedings of the thirty-third annual ACM symposium on Theory of computing* (ACM, 2001) pp. 37–49.
- [17] A. M. Childs, R. Cleve, E. Deotto, E. Farhi, S. Gutmann, and D. A. Spielman, in *Proceedings of the thirty-fifth ACM symposium on Theory of computing - STOC '03* (ACM Press, New York, New York, USA, 2003) p. 59.
- [18] N. B. Lovett, S. Cooper, M. Everitt, M. Trevers, and V. Kendon, *Phys. Rev. A* **81**, 042330 (2010).
- [19] A. M. Childs, *Phys. Rev. Lett.* **102**, 180501 (2009).
- [20] I. Buluta and F. Nori, *Science* **326**, 108 (2009).

- [21] B. P. Lanyon, J. D. Whitfield, G. G. Gillett, M. E. Goggin, M. P. Almeida, I. Kassal, J. D. Biamonte, M. Mohseni, B. J. Powell, M. Barbieri, A. Aspuru-Guzik, and A. G. White, *Nat Chem* **2**, 106 (2010).
- [22] P. J. J. O'Malley, R. Babbush, I. D. Kivlichan, J. Romero, J. R. McClean, R. Barends, J. Kelly, P. Roushan, A. Tranter, N. Ding, B. Campbell, Y. Chen, Z. Chen, B. Chiaro, A. Dunsworth, A. G. Fowler, E. Jeffrey, A. Megrant, J. Y. Mutus, C. Neill, C. Quintana, D. Sank, A. Vainsencher, J. Wenner, T. C. White, P. V. Coveney, P. J. Love, H. Neven, A. Aspuru-Guzik, and J. M. Martinis, "Scalable Quantum Simulation of Molecular Energies," (2015), arXiv:1512.06860, arXiv:1512.06860 .
- [23] V. Kendon, *Electronic Proceedings in Theoretical Computer Science* **315**, 1–17 (2020).
- [24] A. Ciani, B. M. Terhal, and D. P. DiVincenzo, *Quantum Science and Technology* **4**, 035002 (2019).
- [25] M. L. Baez, M. Goihl, J. Haferkamp, J. Bermejo-Vega, M. Gluza, and J. Eisert, *Proceedings of the National Academy of Sciences* **117**, 26123 (2020), <https://www.pnas.org/content/117/42/26123.full.pdf> .
- [26] H.-P. Breuer and F. Petruccione, *The Theory of Open Quantum Systems* (Oxford University Press, 2006).
- [27] D. P. DiVincenzo, *Fortschritte der Physik: Progress of Physics* **48**, 771 (2000).
- [28] C. Cohen-Tannoudji, B. Diu, and F. Laloe, *Quantum Mechanics*, Quantum Mechanics No. Bd. 1 (Wiley, 1991).
- [29] D. Griffiths, *Introduction to Quantum Mechanics*, Bd. 1 (Cambridge University Press, 2017).
- [30] V. B. Braginsky and F. Y. Khalili, *Quantum measurement* (Cambridge University Press, 1992).
- [31] A. Einstein, B. Podolsky, and N. Rosen, *Phys. Rev.* **47**, 777 (1935).
- [32] J. S. Bell and A. Aspect, *Speakable and Unspeakable in Quantum Mechanics: Collected Papers on Quantum Philosophy*, 2nd ed. (Cambridge University Press, 2004).
- [33] B. G. Christensen, K. T. McCusker, J. B. Altepeter, B. Calkins, T. Gerrits, A. E. Lita, A. Miller, L. K. Shalm, Y. Zhang, S. W. Nam, N. Brunner, C. C. W. Lim, N. Gisin, and P. G. Kwiat, *Phys. Rev. Lett.* **111**, 130406 (2013).
- [34] G. Carvacho, J. Cariñe, G. Saavedra, A. Cuevas, J. Fuenzalida, F. Toledo, M. Figueroa, A. Cabello, J.-A. Larsson, P. Mataloni, G. Lima, and G. B. Xavier, *Phys. Rev. Lett.* **115**, 030503 (2015).
- [35] M.-H. Li, C. Wu, Y. Zhang, W.-Z. Liu, B. Bai, Y. Liu, W. Zhang, Q. Zhao, H. Li, Z. Wang, L. You, W. J. Munro, J. Yin, J. Zhang, C.-Z. Peng, X. Ma, Q. Zhang, J. Fan, and J.-W. Pan, *Phys. Rev. Lett.* **121**, 080404 (2018).
- [36] T. Sleator and H. Weinfurter, *Phys. Rev. Lett.* **74**, 4087 (1995).

- [37] S. Boixo, S. V. Isakov, V. N. Smelyanskiy, R. Babbush, N. Ding, Z. Jiang, M. J. Bremner, J. M. Martinis, and H. Neven, *Nature Physics* **14**, 595 (2018).
- [38] F. Arute, K. Arya, R. Babbush, D. Bacon, J. C. Bardin, R. Barends, R. Biswas, S. Boixo, F. G. S. L. Brandao, D. A. Buell, B. Burkett, Y. Chen, Z. Chen, B. Chiaro, R. Collins, W. Courtney, A. Dunsworth, E. Farhi, B. Foxen, A. Fowler, C. Gidney, M. Giustina, R. Graff, K. Guerin, S. Habegger, M. P. Harrigan, M. J. Hartmann, A. Ho, M. Hoffmann, T. Huang, T. S. Humble, S. V. Isakov, E. Jeffrey, Z. Jiang, D. Kafri, K. Kechedzhi, J. Kelly, P. V. Klimov, S. Knysh, A. Korotkov, F. Kostritsa, D. Landhuis, M. Lindmark, E. Lucero, D. Lyakh, S. Mandrà, J. R. McClean, M. McEwen, A. Megrant, X. Mi, K. Michielsen, M. Mohseni, J. Mutus, O. Naaman, M. Neeley, C. Neill, M. Y. Niu, E. Ostby, A. Petukhov, J. C. Platt, C. Quintana, E. G. Rieffel, P. Roushan, N. C. Rubin, D. Sank, K. J. Satzinger, V. Smelyanskiy, K. J. Sung, M. D. Trevithick, A. Vainsencher, B. Villalonga, T. White, Z. J. Yao, P. Yeh, A. Zalcman, H. Neven, and J. M. Martinis, *Nature* **574**, 505 (2019).
- [39] P. W. Shor, *SIAM J. Comp.* **26**, 1484 (1997).
- [40] L. Grover, 28th STOC , 212 (1996).
- [41] H. G. Katzgraber, H. Bombin, and M. A. Martin-Delgado, *Phys. Rev. Lett.* **103**, 090501 (2009).
- [42] A. G. Fowler, M. Mariantoni, J. M. Martinis, and A. N. Cleland, *Phys. Rev. A* **86**, 032324 (2012).
- [43] J. M. Chow, J. M. Gambetta, E. Magesan, D. W. Abraham, A. W. Cross, B. Johnson, N. A. Masluk, C. A. Ryan, J. A. Smolin, S. J. Srinivasan, *et al.*, *Nature communications* **5**, 4015 (2014).
- [44] J. Preskill, *Quantum* **2**, 79 (2018).
- [45] P.-L. Dallaire-Demers and F. K. Wilhelm, *Phys. Rev. A* **93**, 032303 (2016).
- [46] P.-L. Dallaire-Demers and F. K. Wilhelm, *Phys. Rev. A* **94**, 062304 (2016).
- [47] L. C. G. Govia, B. G. Taketani, P. K. Schuhmacher, and F. K. Wilhelm, *Quantum Science and Technology* **2**, 015002 (2017).
- [48] M. Reiher, N. Wiebe, K. M. Svore, D. Wecker, and M. Troyer, *Proceedings of the National Academy of Sciences* **114**, 7555 (2017).
- [49] R. Babbush, C. Gidney, D. W. Berry, N. Wiebe, J. McClean, A. Paler, A. Fowler, and H. Neven, *Phys. Rev. X* **8**, 041015 (2018).
- [50] H.-P. Breuer and F. Petruccione, *The Theory of Open Quantum Systems* (Oxford University Press, 2010).
- [51] D. W. Kribs, *Linear Algebra and its Applications* **400**, 147 (2005).
- [52] G. Lindblad, *Communications in Mathematical Physics* **48**, 119 (1976).
- [53] A. G. Redfield, *IBM Journal of Research and Development* **1**, 19 (1957).
- [54] T. Albash, S. Boixo, D. A. Lidar, and P. Zanardi, *New Journal of Physics* **14**, 123016 (2012).

- [55] M. Fox, *Quantum Optics: An Introduction*, Oxford Master Series in Physics (OUP Oxford, 2006).
- [56] C. Fleming, N. I. Cummings, C. Anastopoulos, and B. L. Hu, *Journal of Physics A: Mathematical and Theoretical* **43**, 405304 (2010).
- [57] A. A. Buchheit and G. Morigi, *Phys. Rev. A* **94**, 042111 (2016).
- [58] F. K. Wilhelm, M. J. Storcz, U. Hartmann, and M. R. Geller, in *Manipulating Quantum Coherence in Solid State Systems*, edited by M. E. Flatté and I. Tifrea (Springer Netherlands, Dordrecht, 2007) pp. 195–232.
- [59] M. Toda, R. Kubo, N. Saitō, N. Hashitsume, *et al.*, *Statistical physics II: nonequilibrium statistical mechanics*, Vol. 2 (Springer Science & Business Media, 1991).
- [60] W. Rossmann, *Lie Groups: An Introduction Through Linear Groups*, Oxford graduate texts in mathematics (Oxford University Press, 2006).
- [61] R. P. Feynman, A. R. Hibbs, and D. F. Styer, *Quantum mechanics and path integrals* (Courier Corporation, 2010).
- [62] K. Binder and D. Heermann, *Monte Carlo Simulation in Statistical Physics: An Introduction*, Graduate Texts in Physics (Springer Berlin Heidelberg, 2010).
- [63] M. Newman and G. Barkema, *Monte Carlo Methods in Statistical Physics* (Clarendon Press, 1999).
- [64] R. Egger, L. Mühlbacher, and C. H. Mak, *Phys. Rev. E* **61**, 5961 (2000).
- [65] L. Mühlbacher and E. Rabani, *Phys. Rev. Lett.* **100**, 176403 (2008).
- [66] T. Albash, G. Wagenbreth, and I. Hen, *Phys. Rev. E* **96**, 063309 (2017).
- [67] F. Alet, K. Damle, and S. Pujari, *Phys. Rev. Lett.* **117**, 197203 (2016).
- [68] A. Honecker, S. Wessel, R. Kerkdyk, T. Pruschke, F. Mila, and B. Normand, *Phys. Rev. B* **93**, 054408 (2016).
- [69] K. Okunishi and K. Harada, *Phys. Rev. B* **89**, 134422 (2014).
- [70] I. Hen, *Phys. Rev. E* **99**, 033306 (2019).
- [71] N. Makri, *Chemical Physics Letters* **193**, 435 (1992).
- [72] N. Makri, *Journal of Mathematical Physics* **36**, 2430 (1995).
- [73] N. S. Dattani, *Computer Physics Communications* **184**, 2828 (2013).
- [74] D. Segal, A. J. Millis, and D. R. Reichman, *Phys. Rev. B* **82**, 205323 (2010).
- [75] N. Hatano and M. Suzuki, “Finding exponential product formulas of higher orders,” in *Quantum Annealing and Other Optimization Methods*, edited by A. Das and B. K. Chakrabarti (Springer Berlin Heidelberg, Berlin, Heidelberg, 2005) pp. 37–68.
- [76] R. Feynman and F. Vernon, *Annals of Physics* **281**, 547 (2000).
- [77] N. Makri, *J. Phys. Chem. B* **103**, 2823 (1999).

- [78] P. K. Schuhmacher, L. C. G. Govia, B. G. Taketani, and F. K. Wilhelm, “Quantum simulation of a discrete-time quantum stochastic walk,” (2020), [arXiv:2004.06151 \[quant-ph\]](#) .
- [79] J. Kempe, *Contemporary Physics* **44**, 307 (2003).
- [80] M. Schuld, I. Sinayskiy, and F. Petruccione, *Physical Review A* **89**, 032333 (2014), [arXiv:1404.0159](#) .
- [81] P. Rebentrost, M. Mohseni, and S. Lloyd, *Phys. Rev. Lett.* **113**, 130503 (2014).
- [82] N. Shenvi, J. Kempe, and K. B. Whaley, *Phys. Rev. A* **67**, 052307 (2003).
- [83] M. Mohseni, P. Rebentrost, S. Lloyd, and A. Aspuru-Guzik, *The Journal of chemical physics* **129**, 174106 (2008), [arXiv:0805.2741](#) .
- [84] M. Walschaers, J. F.-d.-C. Diaz, R. Mulet, and A. Buchleitner, *Phys. Rev. Lett.* **111**, 180601 (2013).
- [85] J. D. Whitfield, C. A. Rodríguez-Rosario, and A. Aspuru-Guzik, *Phys. Rev. A* **81**, 022323 (2010).
- [86] D. Lu, J. D. Biamonte, J. Li, H. Li, T. H. Johnson, V. Bergholm, M. Faccin, Z. Zimborás, R. Laflamme, J. Baugh, and S. Lloyd, *Phys. Rev. A* **93**, 042302 (2016).
- [87] H. J. Briegel and G. De las Cuevas, *Scientific reports* **2** (2012).
- [88] G. D. Paparo, V. Dunjko, A. Makmal, M. A. Martin-Delgado, and H. J. Briegel, *Phys. Rev. X* **4**, 031002 (2014).
- [89] Z. Zimborás, M. Faccin, Z. Kádár, J. D. Whitfield, B. P. Lanyon, and J. Biamonte, *Scientific Reports* **3**, 2361 EP (2013).
- [90] S. Attal, F. Petruccione, C. Sabot, and I. Sinayskiy, *Journal of Statistical Physics* **147**, 832 (2012).
- [91] I. Sinayskiy and F. Petruccione, *Journal of Physics: Conference Series* **442**, 012003 (2013).
- [92] B. G. Taketani, L. C. G. Govia, and F. K. Wilhelm, *Phys. Rev. A* **97**, 052132 (2018).
- [93] H. Weimer, M. Muller, I. Lesanovsky, P. Zoller, and H. P. Buchler, *Nat Phys* **6**, 382 (2010).
- [94] K. W. Murch, U. Vool, D. Zhou, S. J. Weber, S. M. Girvin, and I. Siddiqi, *Phys. Rev. Lett.* **109**, 183602 (2012).
- [95] T. Fogarty, E. Kajari, B. G. Taketani, T. Busch, and G. Morigi, *Physical Review A* **87**, 050304 (2013).
- [96] L. C. G. Govia and F. K. Wilhelm, *Phys. Rev. Applied* **4**, 054001 (2015).
- [97] L. G. Mourokh and F. Nori, *Phys. Rev. E* **92**, 052720 (2015).
- [98] A. Metelmann and A. A. Clerk, *Phys. Rev. X* **5**, 021025 (2015).

- [99] H. Wiseman and G. Milburn, *Quantum Measurement and Control* (Cambridge University Press, 2010).
- [100] K. Jacobs and D. A. Steck, *Contemporary Physics* **47**, 279 (2006), <http://dx.doi.org/10.1080/00107510601101934> .
- [101] C. W. Gardiner and P. Zoller, *Quantum Noise* (Springer Complexity, Heidelberg, 2004).
- [102] F. Caruso, *New Journal of Physics* **16**, 055015 (2014).
- [103] S. Viciani, M. Lima, M. Bellini, and F. Caruso, *Phys. Rev. Lett.* **115**, 083601 (2015).
- [104] F. Caruso, A. Crespi, A. G. Ciriolo, F. Sciarrino, and R. Osellame, *Nat Commun* **7** (2016).
- [105] H. Park, N. Heldman, P. Reberntrost, L. Abbondanza, A. Iagatti, A. Alessi, B. Patrizi, M. Salvalaggio, L. Bussotti, M. Mohseni, F. Caruso, H. C. Johnsen, R. Fusco, P. Foggi, P. F. Scudo, S. Lloyd, and A. M. Belcher, *Nat Mater* **15**, 211 (2016).
- [106] J. Casanova, L. Lamata, I. L. Egusquiza, R. Gerritsma, C. F. Roos, J. J. García-Ripoll, and E. Solano, *Phys. Rev. Lett.* **107**, 260501 (2011).
- [107] I. Bengtsson and K. Życzkowski, *Geometry of Quantum States: An Introduction to Quantum Entanglement* (Cambridge University Press, New York, NY, USA, 2006).
- [108] R. Sweke, M. Sanz, I. Sinayskiy, F. Petruccione, and E. Solano, *Phys. Rev. A* **94**, 022317 (2016).
- [109] D. Aharonov, W. Van Dam, J. Kempe, Z. Lamda, S. Lloyd, and O. Regev, in *Proceedings of the 45th IEEE Symposium on Foundations of Computer Science, Rome, Italy* , 42 (2004).
- [110] L. S. Theis, P. K. Schuhmacher, M. Marthaler, and F. K. Wilhelm, “Gap-independent cooling and hybrid quantum-classical annealing,” (2018), [arXiv:1808.09873 \[quant-ph\]](https://arxiv.org/abs/1808.09873) .
- [111] Office of the Director of National Intelligence, *Quantum Enhanced Optimization (QEO)* (visited on: 2020-08-10).
- [112] J. Kempe, A. Kitaev, and O. Regev, *SIAM Journal on Computing* **35**, 1070 (2006).
- [113] J. D. Biamonte and P. J. Love, *Phys. Rev. A* **78**, 012352 (2008).
- [114] S. Bravyi, D. P. DiVincenzo, D. Loss, and B. M. Terhal, *Phys. Rev. Lett.* **101**, 070503 (2008).
- [115] Y. Cao, R. Babbush, J. Biamonte, and S. Kais, *Phys. Rev. A* **91**, 012315 (2015).
- [116] M. Schöndorf and F. Wilhelm, *Phys. Rev. Applied* **12**, 064026 (2019).
- [117] W. van Dam, M. Mosca, and U. Vazirani, in *Proceedings 42nd IEEE Symposium on Foundations of Computer Science* (2001) pp. 279–287.

- [118] B. Apolloni, C. Carvalho, and D. De Falco, *Stochastic Processes and their Applications* **33**, 233 (1989).
- [119] B. Apolloni, D. De Falco, and N. Cesa-Bianchi, *A numerical implementation of "quantum annealing"*, Tech. Rep. (1988).
- [120] S. Kirkpatrick, C. D. Gelatt, and M. P. Vecchi, *Science* **220**, 671 (1983).
- [121] C. C. McGeoch, *Synthesis Lectures on Quantum Computing* **5**, 1 (2014).
- [122] M. H. S. Amin, *Phys. Rev. Lett.* **102**, 220401 (2009).
- [123] T. Kato, *Journal of the Physical Society of Japan* **5**, 435 (1950).
- [124] G. Nenciu, *Communications in mathematical physics* **152**, 479 (1993).
- [125] J. E. Avron and A. Elgart, *Communications in mathematical physics* **203**, 445 (1999).
- [126] G. A. Hagedorn and A. Joye, *Journal of Mathematical Analysis and Applications* **267**, 235 (2002).
- [127] S. Jansen, M.-B. Ruskai, and R. Seiler, *Journal of Mathematical Physics* **48**, 102111 (2007), <https://doi.org/10.1063/1.2798382> .
- [128] M. J. O'Hara and D. P. O'Leary, *Phys. Rev. A* **77**, 042319 (2008).
- [129] D. A. Lidar, A. T. Rezakhani, and A. Hamma, *Journal of Mathematical Physics* **50**, 102106 (2009), <https://doi.org/10.1063/1.3236685> .
- [130] D. Cheung, P. Høyer, and N. Wiebe, *Journal of Physics A: Mathematical and Theoretical* **44**, 415302 (2011).
- [131] Y. Ge, A. Molnár, and J. I. Cirac, *Phys. Rev. Lett.* **116**, 080503 (2016).
- [132] L. Landau, *Physikalische Zeitschrift der Sowjetunion* **2**, 46 (1932).
- [133] C. Zener and R. H. Fowler, *Proceedings of the Royal Society of London. Series A, Containing Papers of a Mathematical and Physical Character* **137**, 696 (1932).
- [134] E. Farhi, J. Goldstone, S. Gutmann, and M. Sipser (2000).
- [135] S. Ashhab, J. R. Johansson, and F. Nori, *Phys. Rev. A* **74**, 052330 (2006).
- [136] M. H. S. Amin, P. J. Love, and C. J. S. Truncik, *Phys. Rev. Lett.* **100**, 060503 (2008).
- [137] U. Weiss, *Quantum Dissipative Systems*, Series in modern condensed matter physics (World Scientific, 2008).
- [138] N. G. Dickson, M. W. Johnson, M. H. Amin, R. Harris, F. Altomare, A. J. Berkley, P. Bunyk, J. Cai, E. M. Chapple, P. Chavez, F. Cioata, T. Cirip, P. deBuen, M. Drew-Brook, C. Enderud, S. Gildert, F. Hamze, J. P. Hilton, E. Hoskinson, K. Karimi, E. Ladizinsky, N. Ladizinsky, T. Lanting, T. Mahon, R. Neufeld, T. Oh, I. Perminov, C. Petroff, A. Przybysz, C. Rich, P. Spear, A. Tcaciuc, M. C. Thom, E. Tolkacheva, S. Uchaikin, J. Wang, A. B. Wilson, Z. Merali, and G. Rose, *Nature Communications* **4**, 1903 (2013).

- [139] E. Novais, A. H. Castro Neto, L. Borda, I. Affleck, and G. Zarand, *Phys. Rev. B* **72**, 014417 (2005).
- [140] H. Kohler and F. Sols, *Phys. Rev. B* **72**, 180404 (2005).
- [141] K. Saito, M. Wubs, S. Kohler, Y. Kayanuma, and P. Hänggi, *Phys. Rev. B* **75**, 214308 (2007).
- [142] R. Harris, T. Lanting, A. J. Berkley, J. Johansson, M. W. Johnson, P. Bunyk, E. Ladizinsky, N. Ladizinsky, T. Oh, and S. Han, *Phys. Rev. B* **80**, 052506 (2009).
- [143] P.-Q. Jin, M. Marthaler, A. Shnirman, and G. Schön, *Phys. Rev. Lett.* **108**, 190506 (2012).
- [144] P. Nalbach, *Phys. Rev. A* **90**, 042112 (2014).
- [145] M. Yamaguchi, T. Yuge, and T. Ogawa, *Phys. Rev. E* **95**, 012136 (2017).
- [146] L. Arceci, S. Barbarino, R. Fazio, and G. E. Santoro, *Phys. Rev. B* **96**, 054301 (2017).
- [147] W. Vinci and D. A. Lidar, *npj Quantum Information* **3**, 38 (2017).
- [148] A. J. Leggett, S. Chakravarty, A. T. Dorsey, M. P. A. Fisher, A. Garg, and W. Zwerger, *Rev. Mod. Phys.* **59**, 1 (1987).
- [149] A. Shnirman, Y. Makhlin, Y. Makhlin, G. Schön, and G. Schön, *Physica Scripta* **T102**, 147 (2002).
- [150] M. Keck, S. Montangero, G. E. Santoro, R. Fazio, and D. Rossini, *New Journal of Physics* **19**, 113029 (2017).
- [151] L. Arceci, S. Barbarino, D. Rossini, and G. E. Santoro, *Phys. Rev. B* **98**, 064307 (2018).
- [152] T. Albash, V. Martin-Mayor, and I. Hen, *Phys. Rev. Lett.* **119**, 110502 (2017).
- [153] K. Kraus, *Foundations of Physics* **11**, 547 (1981).
- [154] M. H. S. Amin and D. V. Averin, *Phys. Rev. Lett.* **100**, 197001 (2008).
- [155] M. Demiralp and S. A. Rice, *J. Phys. Chem. A* **107**, 9937 (2003).
- [156] M. V. Berry, *Journal of Physics A: Mathematical and Theoretical* **42**, 365303 (2009).
- [157] D. Sels and A. Polkovnikov, *Proceedings of the National Academy of Sciences* **114**, E3909 (2017).
- [158] D. Guéry-Odelin, A. Ruschhaupt, A. Kiely, E. Torrontegui, S. Martínez-Garaot, and J. G. Muga, *Rev. Mod. Phys.* **91**, 045001 (2019).
- [159] H. Zhou, Y. Ji, X. Nie, X. Yang, X. Chen, J. Bian, and X. Peng, *Phys. Rev. Applied* **13**, 044059 (2020).
- [160] S. Bedkihal and M. Canturk, “Notes on curvature operator,” (2020).
- [161] A. Maksymov, P. Sierant, and J. Zakrzewski, *Phys. Rev. B* **99**, 224202 (2019).

-
- [162] K. Nakamura and M. Lakshmanan, *Phys. Rev. Lett.* **57**, 1661 (1986).
- [163] H. Chen and D. A. Lidar, “Hoqst: Hamiltonian open quantum system toolkit,” (2020), [arXiv:2011.14046 \[quant-ph\]](#) .
- [164] L. S. Theis, “Enhancing the performance of quantum computers,” (2018).